Sixth National Image-Guided Therapy Workshop

March 21-23, 2013
Washington, DC

www.ncigt.org

Workshop Chairs
Ferenc Jolesz, MD
Clare Tempany, MD
Kevin Cleary, PhD
Andreas Melzer, MD
Michael Marohn, MD

Program Chairs
Tina Kapur, PhD
Raj Shekhar, PhD
Keyvan Farahani, PhD
Steven Krosnick, MD

Table of Contents

Welcome

Welcome to the Sixth Image-Guided Therapy workshop sponsored by the National Center for Image Guided Therapy (NCIGT, P41EB015898), the Neuroimage Analysis Center (NAC, P41EB015902), the National Institutes of Health (NIH), the International Society for Minimally Invasive Therapy (SMIT), and the Children's National Medical Center (CNMC). The overall goal of this workshop series is to assess the current needs and opportunities in the field of image-guided therapy and the role of NCIGT as a national center serving the greater IGT community. The focus for this year's workshop is **Interventional applications for a changing healthcare environment.**

The program for this workshop includes a single track of scientific talks, as well as a poster session. The talks are divided into sessions that focus on cardiovascular interventions, pelvic interventions, robotics, intra-operative (optical and fluorescence) imaging, medical image computation, emerging technologies for minimally invasive interventions, and high intensity focused ultrasound.

Similar to previous workshops in this series, we are honored to have in attendance our colleagues from academia, industry, as well as the National Institutes of Health. We hope that you continue to contribute to the success of this workshop by your participation.

Sincerely,
Members of the Program Committee

Workshop Chairs

Ferenc Jolesz, MD
Clare Tempany, MD
Kevin Cleary, PhD
Andreas Melzer, MD
Michael Marohn, MD

Program Chairs

Tina Kapur, PhD
Raj Shekhar, PhD
Keyvan Farahani, PhD
Steven Krosnick, MD

Program Committee

Ron Kikinis, MD
William M. Wells, PhD
Alexandra Golby, MD
Noby Hata, PhD
Bruno Madore, PhD
Ehud Schmidt, PhD
Nathan McDannold, PhD
Andriy Fedorov, PhD
Marius Linguraru, PhD
Ziv Yaniv, PhD

ORAL PROGRAM, THURSDAY, MARCH 21, 2013

9:00-10:00 AM	**Registration and Coffee**	
10:00-10:10 AM	Opening Remarks	Ferenc Jolesz, MD Harvard Medical School
10:10-10:30AM	A Novel Multimodal Nanoparticle Platform for Combined Diagnostic and Intraoperative Cancer Imaging	Moritz Kircher, MD, PhD Memorial Sloan Kettering Cancer Center
10:30AM -12:00PM **NCIGT Session 1: Cardiac** **Session Chair: Ehud Schmidt, PhD**	MRI-guided Atrial-Fibrillation Radio-Frequency Ablation in humans: What's accomplished & hurdles that remain towards practical procedures	Ehud Schmidt, PhD Harvard Medical School
	Accelerated MRI Acquisition and Reconstruction for Cardiovascular Interventions	Michael Hansen, PhD NHLBI Intramural
	Utility of MRI for complex VT ablations	Saman Nazarian, MD, PhD Johns Hopkins
	MRI-guided Cardiovascular Interventions: The NIH Experience	Anthony Faranesh, PhD NHLBI Intramural
	Challenges and Promises of CMR Roadmap for Electrophysiology	Reza Nazafat, PhD Harvard Medical School
	Endovascular Catheter for Magnetic Navigation under MRI Guidance: Evaluation of Safety In Vivo at 1.5T	Steven Hetts, MD University of California San Francisco
12:00-1:30 PM	**Lunch and Poster Session**	
1:30-2:45 PM **NCIGT Session 2: Pelvis** **Session Chair: Clare Tempany, MD**	3T MR-guided Prostate Interventions at Brigham and Women's Hospital	Clare Tempany, MD Harvard Medical School
	MR/US Fusion Biopsy of the Prostate	Peter Choyke, MD NIH
	In vivo Acoustic Radiation Force Impulse (ARFI) Elasticity Imaging of Prostate	Kathy Nightingale, PhD Duke University
	A PET-directed, 3D ultrasound-guided Biopsy System	Fei Baowei, PhD Emory
	Real-time Catheter Tracking and Visualization in 3-T MR-Guided Brachytherapy	Akila Viswanathan, MD Brigham and Women's Hospital
2:45-3:30 PM	**Break and Poster Session**	
3:30-5:00 PM **NCIGT Session 3: Robotics** **Session Chair: Noby Hata, PhD**	Clinical Implementation of a Smart Template for 3T MRI-guided Transperineal Targeted Prostate Biopsy	Noby Hata, PhD Harvard Medical School
	Medical Robotics and Computer-Integrated Interventional Medicine	Russ Taylor, PhD Johns Hopkins University
	Towards Robot-Assisted Neurosurgery Under Continuous MRI	Jaydev Desai, PhD University of Maryland
	Advanced biophotonics for robotic image-guidance of brain surgery phantoms	Eric Siebel, PhD University of Washington
	Image-guided Robotic Surgery Inside the Beating Heart	Pierre Dupont, PhD Childrens Hospital, Boston
	Integrated 3D tracked ultrasound image guided steerable needle directionally-conformable therapeutic ultrasound minimally-invasive interventional therapy	Clif Burdette, PhD Acoustic Medical Inc.
5:30-7:30 PM	**Dinner and Poster Session**	

ORAL PROGRAM, FRIDAY, MARCH 22, 2013

7:30-8:00 AM	**Breakfast**	
8:00-8:30 AM **NCIGT Session 4: NIH (NCI, NIBIB) Programs Directions**	NCI Initiatives in Image-Guided Interventions	Keyvan Farahani, PhD, NCI
	NIBIB Directions	Steve Krosnick, MD, NIBIB
8:30-10:30 AM **NCIGT Session 5: Intra-Operative, Optical, Fluorescent Imaging** **Session Chair: Alexandra Golby, MD**	Fluorescence Image-Guided Surgery of Nerves	Christina Tan Hehir, PhD GE Research,
	In-situ Augmentation for Image-Guided Microsurgery	John Galeotti, PhD & George Stetten, MD, PhD Carnegie Mellon University
	Quantitative Endoscopy for High Accuracy Navigation	Greg Hager, PhD Johns Hopkins University,
	Improved MR Thermometry Processing for MR-guided FUS in the Brain	Kim Butts Pauly, PhD Stanford University,
	Ultrasound Registration and Visualization for Neuronavigation	Matthew Toews, PhD Brigham and Women's Hospital,
	Motion-tracked thermometry and relaxometry using a US-MRI hybrid acquisition	Bruno Madore, PhD Brigham and Women's Hospital
10:30-11:00 AM	**Break**	
11:00AM- 12:00PM **NCIGT Session 6: Medical Image Computing** **Session Chair: Ron Kikinis, MD**	Prototyping clinical applications with the Public Library for Ultrasound (PLUS) toolkit and 3D Slicer	Gabor Fichtinger, PhD, Queens University
	Neuroimage Analysis for Intra-Procedural Imaging	Steve Pieper, PhD, Isomics, Inc.
	Emerging CT-imaging Technology and Its Implications to Image-guided Therapy	Xiaochun Pan, PhD, Chicago Cancer Center
12:00-1:30 PM	**Lunch and Poster Session**	

ORAL PROGRAM
FRIDAY AFTERNOON, MARCH 22, 2013

1:30-3:30 PM **SMIT 25th Anniversary Opening Session:** **Emerging Technologies for Minimally Invasive Interventions**	Improving Surgical Outcomes	Paul Wetter, MD Society of Laparondoscopic Surgeons
	Innovations in Information-Intensive Interventions: MRI-guided Procedures	Jonathan Lewin, MD Johns Hopkins University
	Advanced Mapping for Cardiac Interventions	Marek Orban, MD ICRC Brno. Czech Republic & TBN, Mayo Clinic Rochester
	Ultrasound-Guided Interventions	Purang Abolmaesumi, PhD, University of British Columbia, Canada
	Navigation and Ultrasound Guided Therapy	Thomas Lango, PhD Trondheim,
	Imaging Robotics	Gernot Kronreif, PhD Austrian Center for Medically Innovative Technology,
3:30-4:00 PM	**Break**	
4:00-6:00 PM **SMIT Session II: High Intensity Focused Ultrasound**	State of the Art of Brain FUS	Neal Kassell, MD University of Virginia, Focused Ultrasound Foundation
	Novel Clinical Applications	Arik Hananel, MD Focused Ultrasound Foundation
	HIFU Potential for Pediatrics	Peter Kim, MD Children's National Medical Center
	FUS Mediated Targeted Drug Delivery	Brad Wood, MD NIH Clinical Center
	FUS and Beyond	Andreas Melzer, MD University of Dundee
6:00 PM	**Optional Self-Pay Group Dinner in Crystal City**	

SATURDAY, MARCH 23, 2013

8: 30AM-1:30PM Tours at Children's National Medical Center

POSTER PROGRAM

Thursday: 12-1:30PM; 2:45-3:30PM; 5:30-7:30PM
Friday: 12-1:30PM

GROUP A: ABDOMEN

1. INTRAVENOUS CHEMOTHERAPY FILTER (CHEMOFILTER): PROTOTYPE AND IN-VITRO PROOF-OF-CONCEPT OF A NOVEL DEVICE FOR HIGH DOSE INTRA-ARTERIAL CHEMOTHERAPY DELIVERY. ANAND S. PATEL, ERIN J. YEE, AARON D. LOSEY, PRASHEEL V. LILLANEY, MARK W. WILSON AND STEVEN W. HETTS

2. SEMI-AUTOMATIC KIDNEY QUANTIFICATION FOR SURGICAL DECISION MAKING IN HYDRONEPHROSIS. CARLOS MENDOZA, XIN KANG, NABILE SAFDAR, CRAIG PETERS AND MARIUS GEORGE LINGURARU

3. METHODS FOR ASSISTING NEEDLE ANGLE SELECTION DURING CT-GUIDED BIOPSIES. CHENG WILLIAM HONG, SHENG XU, ANKUR KAPOOR, NADINE ABI-JAOUDEH, KIMBERLY L IMBESI, CHARISSE GARCIA, ARADHANA M VENKATESAN, ELLIOT LEVY, RICHARD CHANG AND BRADFORD J WOOD

4. *IN VIVO* TREATMENT OF PIG LIVER USING STEERABLE NEEDLE THERAPEUTIC ULTRASOUND WITH COMBINED IMAGING AND ELECTROMAGNETIC TRACKING SYSTEM. GOUTAM GHOSHAL, TAMAS HEFFTER, EMERY WILLIAMS, CORINNE BROMFIELD, VASANT SALGAONKAR, LAURIE RUND, JOHN M. EHRHARDT, CHRIS J. DIEDERICH AND E. CLIF BURDETTE

5. TOWARDS A FRAMEWORK FOR ROBOTICALLY ASSISTED URETEROSCOPY. RAHUL KHARE, KEVIN CLEARY, LINAN ZHANG, EMMANUEL WILSON, PATRICK CHENG AND CRAIG PETERS

6. PROOF OF CONCEPT OF WIRELESS TISSUE PALPATION IN ABDOMINAL SURGERY. MARCO BECCANI, CHRISTIAN DI NATALI, MARK RENTSCHLER AND PIETRO VALDASTRI

7. MR-GUIDED FOCUSED ULTRASOUND SYSTEM FOR CONTINUOUS BREATHING LIVER ABLATION. ANDREW HOLBROOK, PEJMAN GHANOUNI, JUAN SANTOS, CHARLES DUMOULIN, YOAV MEDAN AND KIM BUTTS PAULY

GROUP B: BRAIN, HEAD AND NECK, EYE

8. MR-GUIDED EPISCLERAL PLAQUE BRACHYTHERAPY FOR UVEAL MELANOMA. JACQUELINE ESTHAPPAN, YANLE HU AND PERRY GRIGSBY

9. INTRAARTERIAL MR PERFUSION IMAGING OF MENINGIOMAS: COMPARISON TO DIGITAL SUBTRACTION ANGIOGRAPHY. STEVEN HETTS, ALASTAIR MARTIN, CHRISTOPHER DOWD, VAN HALBACH, RANDALL HIGASHIDA, MICHAEL MCDERMOTT AND DAVID SALONER

10. SYSTEMATIC INVESTIGATION OF CONVECTION-ENHANCED DELIVERY INFUSION PROTOCOLS AND CATHETERS USING REAL-TIME MRI. BENJAMIN GRABOW, RAGHU RAGHAVAN, MARTIN BRADY, KEN KUBOTA, CHRIS ROSS, ETHAN BRODSKY, JAMES RASCHKE, ANDREW ALEXANDER AND WALTER BLOCK

11. SINGLE VS. MULTIPLE TENSOR DIFFUSION TRACTOGRAPHY: WHICH IS BETTER CORRELATED WITH FUNCTION? LAUREN J. O'DONNELL, JIAOLONG CUI, NEELAN MARIANAYAGAM, KELLY DOOLIN, ISAIAH NORTON, YANMEI TIE, LAURA RIGOLO AND ALEXANDRA J. GOLBY

12. SUBMINUTE DEFORMABLE IMAGE REGISTRATION FOR IMAGE-GUIDED RADIATION THERAPY. WEN LI, WILLIAM PLISHKER, JUNGHOON LEE, JOHN WONG AND RAJ SHEKHAR

GROUP C: CARDIOVASCULAR

13. DEVELOPMENT OF A NOVEL VASCULAR PHANTOM FOR NAVIGATION TESTING IN INTERVENTIONAL MRI. AARON D. LOSEY, ALASTAIR J. MARTIN, PRASHEEL LILLANEY, ERIN J. YEE, MARK W. WILSON, MAYTHEM SAEED, LOI DO AND STEVEN W. HETTS

14. AN EVALUATION OF RF HEATING IN A NITINOL BRAIDED ENDOVASCULAR CATHETER AT 1.5T AND 3T. AARON D. LOSEY, PRASHEEL LILLANEY, ALASTAIR J. MARTIN, MARK W. WILSON, MAYTHEM SAEED, ERIN J. YEE AND STEVEN W. HETTS.

15. IMAGE-BASED COMPUTATIONAL SIMULATIONS FOR PATIENT-SPECIFIC FONTAN SURGERY PLANNING. CHRISTOPHER M. HAGGERTY, MARIA RESTREPO, KIRK R. KANTER, TIMOTHY C. SLESNICK, JAREK ROSSIGNAC, THOMAS L. SPRAY, MARK A. FOGEL AND AJIT P. YOGANATHAN

16. INTRA-ARTERIAL MRA BASED ROADMAPPING FOR MAGNETICALLY-ASSISTED REMOTE CONTROL CATHETER TRACKING. ALASTAIR J. MARTIN, PRASHEEL LILLANEY, FABIO SETTECASE, LEE EVANS, MARK WILSON AND STEVEN HETTS

17. CATHETERS FOR INTERVENTIONAL MR: FABRICATION OF MICRO-COILS FOR CATHETER TIP DEFLECTION. PRASHEEL LILLANEY, VINCENT MALBA, LELANDE EVANS, ANTHONY BERNHARDT, MARK WILSON, TIMOTHY ROBERTS, ALASTAIR MARTIN, MAYTHEM SAEED, RONALD ARENSON AND STEVEN HETTS

18. FEATURE TRACKING FOR IMAGE-GUIDED MITRAL VALVE REPAIR. MARTIN RAJCHL, FENG P. LI, JOHN MOORE, CHRIS WEDLAKE, USAF ALADL AND TERRY M. PETERS

19. CT-ENHANCED ULTRASOUND FOR GUIDANCE OF OFF-PUMP BEATING HEART INTERVENTIONS. FENG P. LI, MARTIN RAJCHL, JOHN MOORE, CHRIS WEDLAKE AND TERRY M. PETERS

GROUP D: MUSCOSKELETAL

20. INTERACTIVE REAL-TIME SEGMENTATION FOR VERTEBRAL BODIES AND INTERVERTEBRAL DISCS IN SAGITTAL PLANES. JAN EGGER, TINA KAPUR, BERND FREISLEBEN AND CHRISTOPHER NIMSKY

21. OSTEOCHODRITIS DISSECANS OF THE KNEE; MRI GUIDED RETROGRADE DRILLING AT 1.5 T AND FIRST CLINICAL OUTCOMES IN PEDIATRIC PATIENTS. ROBERTO BLANCO SEQUEIROS, MATTI VAHAKARI, RISTO OJALA, PEKKA KERIMAA, JUSSI KORHONEN, JUHA J. SINIKUMPU AND OSMO TERVONEN

22. *IN VIVO* TREATMENT OF SPINE TUMORS USING NEEDLE BASED THERAPEUTIC ULTRASOUND UNDER IMAGE GUIDANCE WITH 3D ELECTROMAGNETIC TRACKING. GOUTAM GHOSHAL, TAMAS HEFFTER, EMERY WILLIAMS, CORINNE BROMFIELD, SERENA SCOTT, LAURIE RUND, JOHN M. EHRHARDT, CHRIS J. DIEDERICH AND EVERETTE CLIF BURDETTE

23. AN INTEGRATED ULTRASOUND-GUIDED, MAGNETIC-TRACKED, SPINE NEEDLE SYSTEM. ELVIS C.S. CHEN AND TERRY M. PETERS

24. THE PERK TUTOR TRAINING PLATFORM INTEGRATED WITH SIMULATED ULTRASOUND.
LAURA BARTHA, ANDRAS LASSO, CSABA PINTER, TAMAS UNGI AND GABOR FICHTINGER

25. MOBILE IMAGE OVERLAY SYSTEM FOR IMAGE GUIDED INTERVENTIONS.
MANJUNATH ANAND, TAMAS UNGI, ANDRAS LASSO, PAWEENA U-THAINUAL, JAGADEESAN JAYENDER, JAN FRITZ, JOHN CARRINO, FERENC JOLESZ AND GABOR FICHTINGER

GROUP E: PELVIS

26. DEFORMABLE REGISTRATION OF PROSTATE MRI USING STATISTICAL DEFORMATION MODELING. AMIR TAHMASEBI, REZA SHARIFI, HARSH AGARWAL, BARIS TURKBEY, M BERNARDO, PETER CHOYKE, PETER PINTO, BRAD WOOD AND JOCHEN KRUECKER

27. PROSPECTIVE EVALUATION OF SIMULTANEOUS PET/MRI AND PET/CT IN CERVICAL CANCER. PERRY GRIGSBY, KATIE FOWLER, BARRY SIEGEL AND FARROKH DEHDASHTI

28. REAL-TIME 3D NEEDLE SHAPE TRACKING USING FIBER BRAGG GRATING SENSORS FOR PROSTATE PERCUTANEOUS INTERVENTIONS. REZA SEIFABADI, ESTEBAN ESCOBAR GOMEZ, FERESHTEH AALAMIFAR, GABOR FICHTINGER AND IULIAN IORDACHITA

29. TRANSPERINEAL PROSTATE BIOPSY: UPDATE ON MULTIREADER, MULTIPARAMETRIC NAVIGATED INTERVENTIONS. TOBIAS PENZKOFER, KEMAL TUNCALI, ANDRIY FEDOROV, JUNICHI TOKUDA, SANG-EUN SONG, FIONA FENNESSY, NOBUHIKO HATA AND CLARE TEMPANY

30. PRELIMINARY EXPERIENCE WITH A SOFTWARE SYSTEM TO ENABLE MR-GUIDED ADAPTIVE BRACHYTHERAPY OF THE PELVIS. ROBERT CORMACK, Clif BURDETTE, P NEUBAUER, Tamas HEFTER, NOBUHIKO HATA, SANG-EUN SONG, JUNICHI TOKUDA, PAUL NGUYEN AND CLARE TEMPANY

GROUP F: ROBOTICS

32. DEVELOPMENT OF A PASSIVE MASTER-SLAVE SYSTEM FOR MRI-GUIDED INTERVENTIONS. SANTHI ELAYAPERUMAL, MARK CUTKOSKY AND BRUCE DANIEL

33. EVALUATION OF FORCE, TORQUE, AND RANGE OF MOTION EXHIBITED DURING ABDOMINAL ULTRASOUND EXAM OF PHANTOM AND HUMAN SUBJECTS TO SET REQUIREMENTS FOR ROBOT-ASSISTED ULTRASOUND. JAMES GOLDIE, KRISTEN LEROY, BRENDAN LABRECQUE, KEVIN CLEARY, EMMANUEL WILSON, KATHERINE DAVENPORT AND DANIEL SWERDLOW

34. INTEGRATED AND TELEOPERATED SYSTEM FOR WIRELESS ROBOTIC NATURAL ORIFICE TRANSLUMINAL ENDOSCOPIC SURGERY (R-NOTES). BAMSHAD AZIZI KOUTENAEI, RISTO KOJCEV, EMMANUEL WILSON, KEVIN A. GARY, NASSIR NAVAB AND KEVIN CLEARY

35. NEW DEVELOPMENTS IN ROBOTIC NAVIGATION AND GUIDANCE FOR IMAGEGUIDED INTERVENTIONS. YILUN KOETHE, SHENG XU, GNANASEKAR VELUSAMY, BRADFORD WOOD AND ARADHANA VENKATESAN

36. PRELIMINARY OBSERVATIONS ON MRI-GUIDED TARGETED PROSTATE BIOPSY USING A SMART TEMPLATE. SANG-EUN SONG, KEMAL TUNCALI, JUNICHI TOKUDA, ANDRIY FEDOROV, TOBIAS PENZKOFER, CLARE TEMPANY AND NOBUHIKO HATA

37. SMART TISSUE ANASTOMOSIS ROBOT (STAR). SIMON LEONARD, YONJAE KIM, CAROLYN COCHENOUR, KYLE WU, PETER KIM AND AXEL KRIEGER

GROUP G: COMPUTATION

38. INTERACTIVE INITIALIZATION FOR 2D/3D INTRA-OPERATIVE REGISTRATION USING THE MICROSOFT KINECT. REN HUI GONG, ÖZGÜR GÜLER AND ZIV YANIV

39. DYNAMIC TRACKING WITH ELECTROMAGNETIC SYSTEMS USING PARTICLE FILTERS. HASAN TUTKUN SEN AND PETER KAZANZIDES

40. PROTOTYPING IMAGE-GUIDED THERAPY APPLICATIONS USING THE SLICER IGT PLATFORM . TAMAS UNGI, JUNICHI TOKUDA, ADAM RANKIN, ANDRAS LASSO, GABOR FICHTINGER

Abstracts for Oral Presentations

MRI-guided Atrial-Fibrillation Radio-Frequency Ablation in humans: What's accomplished & hurdles that remain towards practical procedures

Ehud J. Schmidt[1], Zion Tse[2], Charles L Dumoulin[3], Ronald Watkins[4], Israel Byrd[5], Jeffrey Schweitzer[5], Raymond Y. Kwong[1], Gregory F. Michaud[1], William G. Stevenson[1].

[1]Brigham&Women's Hospital Radiology and Cardiology, [2]University of Georgia Engineering, [3]Cincinnati Children's Hospital Medical Center Radiology, [4]Stanford University Radiology, [5]St Jude Medical Cardiac Ablations.

We present the BWH experience with MRI-guided radio-frequency ablation (RFA) of patients with Atrial Fibrillation (AF) recurrence. In these "touch up" procedures, MRI identified RFA-lesion gaps from prior procedures and allowed for improved treatment. Despite the clear advantages of MRI-guidance, which are recognized in the electrophysiology (EP) clinical community, several hurtles remain for time- and cost-efficient procedures. We present some of the tissue characterization, device and systems issues, that if resolved could lead to cheaper and faster procedures, possibly leading to broad adoption in the global clinical community. We then present and critically discuss some of our attempts to resolve specific issues. We focus on improving the physiological monitoring of patients inside the MRI scanner, and on improving transfer efficiency between MRI and other modalities used in a state-of-the-art integrated EP suite.

Acknowledgments: NIH U41-RR019703, NIH SBIR-1 R43-HL110427-01, NIH R03 EB013873-01, AHA 10SDG261039,

Accelerated MRI Acquisition and Reconstruction for Cardiovascular Interventions

Michael S. Hansen, PhD
National Heart, Lung, and Blood Institute, NIH

Magnetic Resonance Imaging (MRI) guided cardiovascular interventions require relatively high frame-rate real-time imaging. Since modern MRI scanners have reached physiological limits in terms of hardware performance (gradient performance), most of recent improvements in imaging speed have come from techniques that use non-standard sampling schemes, receive arrays, and high degrees of under-sampling. Such techniques shift the much of the burden of image formation onto the reconstruction software.

Interventional procedures rely on low latency imaging and complicated reconstruction procedures represent a significant challenge. Specifically, there are numerous real-time imaging techniques that employ non-Cartesian sampling schemes and parallel imaging, but traditional reconstruction implementations (hardware and software) would be prohibitively slow for use in an interventional setting.

In this presentation, we will review several these promising real-time imaging techniques that are now becoming feasible to use in an interventional setting. The primary driver of these applications is the availability of cheap parallel computing resources in the form of Graphical Processing Units (GPUs). We will also describe an open source image reconstruction framework, the Gadgetron (Hansen MS and Sorensen TS, Magn Reson Med. 2012 Jul 12), which provides implementations of these algorithms in a form that can be deployed in an interventional setting.

Funding: This work was supported by the Division of Intramural Research, National Heart, Lung, and Blood Institute, National Institutes of Health.

Utility of MRI for complex VT ablations

Saman Nazarian, MD, PhD, Johns Hopkins University

The talk will summarize work on quantification of associations between scar/viable tissue anatomy and electrogram characteristics and late gadolinium enhanced (LGE) cardiac magnetic resonance (CMR) image characteristics of tissues and critical sites that support postinfarct ventricular tachycardia (VT). The results were largely obtained from 23 patients with ischemic cardiomyopathy that underwent VT ablation after undergoing LGE-CMR. Left ventricular wall thickness and postinfarct scar thickness were measured in each of 20 sectors per LGE-CMR short-axis plane. Electroanatomic mapping points were retrospectively registered to the corresponding LGE-CMR images. Multivariable regression analysis, clustered by patient, revealed significant associations among left ventricular wall thickness, postinfarct scar thickness, and intramural scar location on LGE-CMR, and local endocardial electrogram bipolar/unipolar voltage, duration, and deflections on electroanatomic mapping. Anteroposterior and septal/lateral scar localization was also associated with bipolar and unipolar voltage. Antiarrhythmic drug use was associated with electrogram duration. Critical sites of postinfarct VT were associated with >25% scar transmurality, and slow conduction sites with >40 ms stimulus-QRS time were associated with >75% scar transmurality. Additional unpublished results regarding parallel work in a group of patients with non-ischemic cardiomyopathy will also be presented.

Funding: NIH grant K23HL089333 to Nazarian.

MRI-guided Cardiovascular Interventions: The NIH Experience

Anthony Z. Faranesh, PhD
National Heart, Lung, and Blood Institute, NIH

Cardiovascular interventional procedures guided by X-ray fluoroscopy are used to treat a large array of diseases without direct surgical access. As an alternative to X-ray fluoroscopy, magnetic resonance imaging (MRI) may be used to guide minimally invasive catheter-based procedures, with the advantages of providing excellent soft-tissue visualization and sparing exposure to ionizing radiation. This comes at the cost of reduced spatial and temporal resolution and a lack of commercially available MRI compatible devices. We believe these costs are justified, however, to enable the development of completely novel minimally invasive procedures and to spare radiation for complex and pediatric cases.

Our laboratory develops pre-clinical and clinical applications of interventional cardiovascular magnetic resonance (iCMR). In this presentation we will discuss our experience in developing the necessary infrastructure to conduct iCMR procedures, production of MRI-safe interventional devices, and pre-clinical and clinical applications of iCMR.

Funding: This work was supported by the Division of Intramural Research, National Heart, Lung, and Blood Institute, National Institutes of Health.

Cardiac MR Roadmaps for Cardiac Electrophysiology: Challenges and Opportunities

Reza Nezafat, Ph.D.
Department of Medicine (Cardiovascular Division),
Beth Israel Deaconess Medical Center,
Harvard Medical School, Boston, MA
rnrezafat@bidmc.harvard.edu

The field of cardiac electrophysiology (EP) has emerged over the past three decades as a highly successful, albeit imperfect treatment for various cardiac arrhythmias. With ability of cardiac MR (CMR) in assessment of cardiac anatomy, left ventricular function, and scar, there has been an enormous interest from both cardiac MR scientific communities as well as electrophysiologists to integrate CMR in evaluation, guidance and assessment of various EP treatments. While in several procedures, CMR evaluation has been integrated into the clinical management of EP patient, the impact of CMR has been limited to a hand-full of academic hospitals and for limited indications. In addition, the impact of performing CMR exam in downstream cost and management of patients undergoing EP procedure has been very limited. In this talk, I will discuss the promises and challenges of CMR in evaluation, guidance and prognosis of the patients undergoing various EP procedures.

Acknowledgements: R01EB008743-01 from National Institute of Health, NIBIB

Endovascular Catheter for Magnetic Navigation under MRI Guidance: Evaluation of Safety *In Vivo* at 1.5T

Hetts, Steven W.[1]; Saeed, Maythem[1]; Martin, Alastair J.[1]; Evans, Leland[1]; Bernhardt, Anthony F. [1]; Malba, Vincent[1]; Settecase, Fabio[2]; Yee, Erin J. [1]; Losey, Aaron D.[1]; Lillaney, Prasheel V.[1]; Sincic, Ryan S.[1]; Do, Loi[1]; Roy, Shuvo[1]; Arenson, Ronald L.[1]; Wilson, Mark W.[1]

University of California San Francisco, San Francisco, CA[1], University of Toronto, Toronto, Canada[2]

Purpose: Current catheter guidance techniques used in endovascular procedures face multiple challenges including difficulty navigating tortuous vessels. This can be improved by a magnetically assisted remote controlled microcatheter (MARC) system with current-carrying wires at the distal tip. A small magnetic moment generated by current at the microcatheter tip aligns with the magnetic field of an MR scanner allowing controlled deflection. Because resistive heating is a product of current application, thermal damage of vessel walls is a possible side effect. The purpose of this study was to determine a maximum level of applied current safely useable in this MARC system at 1.5T.

Methods: Copper solenoid coils were hand-wound onto alumina tubes (Figure 1) and attached to commercially-available microcatheters (Figure 2). Catheters were tested in the carotid arteries of 8 pigs. Using X-ray fluoroscopy and MRI, catheters were advanced to the external carotid artery (ECA). Current up to 700mA was applied over time intervals ranging from 0.5 to 10 minutes during imaging to assess potential thermal damage. Current was activated at 6 or 7 locations in the carotids beginning at the proximal ECA 1 cm distal to the origin of the ascending pharyngeal artery. To assess possible RF heating and mechanical damage, experiments with no applied current were examined during MR imaging. Imaging was performed with a SSFP sequence with real-time imaging.

To conduct pairwise comparisons on the likelihood of vessel wall damage, variables examined included normal carotid arterial flow versus arterial stasis, amount of current to the catheter tip (≤ 300 mA versus >300 mA), duration of current catheter tip activation (≤1 minute versus >1 minute), and rate of guide catheter saline drip.

Carotids were sectioned and stained with hematoxylin and eosin staining, Masson's trichrome, and cleaved caspase 3 to assess vessel damage. Histological damage was analyzed with STATA version 10 using case control odds ratios, 2-sided Fisher's exact tests, and Wilcoxon log-rank sum tests.

Results: Several heat mitigation techniques demonstrated negligible vascular damage compared to control arteries. Coil currents ≤300 mA resulted in no damage (0/58 samples) compared to 9/36 (25%) for >300 mA activations ($p<0.0001$). Coil activation ≤1 minute and carotid guide catheter saline drip >2 mL/minute had nonsignificantly lower likelihood of vascular damage. For catheter tip coil activations ≤300 mA for ≤1 minute in normal carotid flow, 0/43 samples had tissue damage.

Conclusion: Low current used to activate copper coils at the tip of microcatheters in 1.5T MR scanners can be applied without causing significant damage to blood vessel walls in a controlled experimental setting. Further optimization of catheter design and procedure protocols are necessary for safe remote control magnetic catheter guidance.

Figure 1. Hand-wound solenoid coil

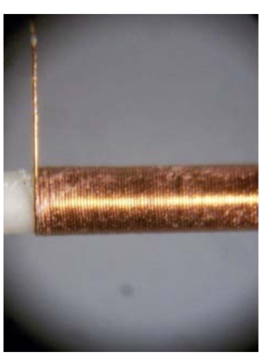

Figure 2. Magnetically Assisted Remote Control (MARC) System

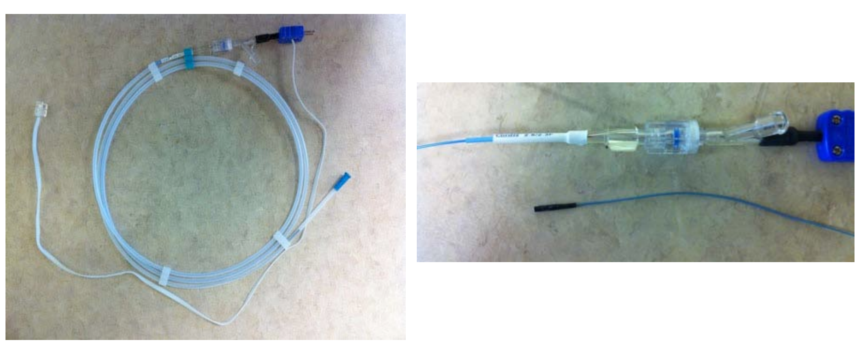

3T MR-guided Prostate Interventions at Brigham and Women's Hospital

Clare Tempany MD and the Prostate Core
National Center for Image Guided Therapy, Brigham and Women's Hospital, Harvard Medical School, Boston

Introduction: This talk will review the current program, aims, results and future plans of the prostate core. We focus on mpMRI (Techniques, acquisition, analysis and validation), prostate interventions (workflow, navigation and enabling technologies-both in the magnet and operating room) and quantitative MR for treatment planning and assessment of treatment response.

Methods: Our focus has to date been exclusively on MR's role in all aspects of our aims. These 3 aims focus specifically on 1) Prostate Biopsy, 2) prostatectomy and 3) radiation therapy. We perform mpMRI prior to and during MR guided transperineal prostate biopsy. This is performed in the wide bore 3T Verio system in our integrated interventional MRI suite (AMIGO). Results of the most recent series of biopsy cases with pathological results will be presented. We will also review the current approaches to provide 3D visualization of the prostate, sub structure including the external urethral sphincter and tumor/NVB relationships for robotic (da Vinci) guided surgery. Radiation and hormonal therapies are changing and there is increasing need to understand the *in vivo* profile of tumor foci and response to therapy using DWI, DCE and T2W images we quantify and correlate the changes.

Conclusion: As we increasingly recognize the importance of molecular imaging and molecular pathology we are expanding our investigation into PET and molecular genetics, specifically mutational profiling.

Acknowledgements. This work was supported in part by National Institutes of Health under Grants P41EB015898/P41RR019703.

MR/US fusion biopsy of the prostate

Peter Choyke, Brad Wood, Baris Turkbey, Peter Pinto, National Cancer Institute, Bethesda MD
Supported by intramural grant ZIA BC 010655

A major problem with random biopsies of the prostate performed under ultrasound guidance is that they detect many inconsequential tumors while missing clinically significant tumors. This is because, while the biopsy is ostensibly "image guided" it is, in fact, blind to the location of lesions. Multiparametric MRI of the prostate has proven to be far more sensitive for the detection of prostate cancer than any other modality. It is particularly important in identifying prostate cancers located anteriorly within the gland, a site that is not routinely biopsied. However, MRI image guided biopsies are cumbersome and expensive. The patient must often be in an uncomfortable position and in most scanners the patient must be positioned prone. However, by fusing the MRI image, pre annotated for suspicious lesions, with a real time ultrasound device, the advantages of MRI (high detection rate for cancer) can be combined with the advantages of ultrasound (real time, portable). MR/US fusion is currently implemented by using a GPS system on the ultrasound. The 3D model of the prostate based on axial, coronal and sagittal T2 weighted MRI is fused with a similar 3D model of the prostate based on real time ultrasound. Once the fusion is complete, it is locked in so that movement of the ultrasound probe results in commensurate movement of the MRI. In this manner highly accurate placement of the needle biopsy can be performed. In our experience with over 800 such biopsies, this method has proven to be highly time efficient and accurate. The average procedure takes about 15 minutes of room time and the patient is positioned in a routine lateral decubitus position with full access to medical staff. Biopsies obtained in this manner can be carefully analyzed to ascertain the extent of the lesion. After focal therapies, the same region can be rebiopsied to verify continued response. Thus, MRI/US fusion biopsy of the prostate integrates easily into current Urology workflows yet provides a much more targeted biopsy that avoids detecting incidental low grade lesions while accurately detecting clinically aggressive lesions, thus reducing morbidity and cost.

In vivo Acoustic Radiation Force Impulse (ARFI) Elasticity Imaging of Prostate

Kathryn Nightingale[1], Stephen Rosenzweig[1], Mark Palmeri[1], Samantha Lipman[1], Rajan Gupta[2], Christopher Kauffman[2], Kirema Garcia[2], Evan Kulbacki[3], Amy Lark[3], Andrew Buckman[3], John Madden[3], Thomas Polascik[4]

[1]Duke University Department of Biomedical Engineering
[2]Duke University Medical Center Department of Radiology
[3]Duke University Medical Center Department of Pathology
[4]Duke University Medical Center Department of Urology

Purpose: We are developing a 3D acoustic radiation force impulse (ARFI) ultrasonic elasticity imaging system for prostate imaging. The goal of this study is to present a comparison of structures portrayed in *in vivo* ARFI, B-mode ultrasound (US), and MR images obtained prior to radical prostatectomy with whole mount histology data in order to determine what structures are portrayed by this new imaging modality.

Methods: Data from over 20 patients have been acquired to date under an ongoing IRB-approved study. Preoperative prostate MR images (T1, T2, and DCE and DWI techniques), and 3D ARFI and B-mode US images were obtained immediately preceding radical prostatectomy with a side fire (ER7B) endorectal array controlled by an external rotation stage and a modified Siemens SC2000 scanner. The excised specimens were fixed in formalin for 48 hours; sectioned and processed using whole mount techniques; and digitized. Images were segmented using ITKsnap, and aligned using non-rigid registration with ANTS. The registered images were evaluated for co-localization of pathology in all modalities.

Results: *In vivo* ARFI images delineate anatomic zones of the prostate with higher contrast than the B-mode US images. Additionally, many cancers have been identified as asymmetrical stiffer regions in coronal prostate imaging planes, which have shown concordance with histologic regions of cancer. In many patients, regions identified by radiologists as suspicious for PCa in the MR image volumes have demonstrated correlation with regions of increased stiffness in ARFI. Atrophy of prostate tissue can be a confounding factor for both ARFI and MR images in identifying regions of suspicion for cancer.

Conclusion: Using diffeomorphic image registration methods, confirmed PCa pathology was found to align with similarly suspicious regions in both ARFI and MR images. The high contrast of some PCa lesions and the structural detail of the ARFI images appear promising for biopsy targeting and focal therapy guidance.

Funding Source: NIH R01 CA142824

A PET-directed, 3D ultrasound-guided Biopsy System

Baowei Fei [1,2,3,4 *], Peter Nieh [5], David Schuster [1], Viraj Master [5]

[1] Department of Radiology and Imaging Sciences, Emory University School of Medicine
[2] Department of Biomedical Engineering, Emory University and Georgia Institute of Technology
[3] Department of Mathematics and Computer Science, Emory University
[4] Winship Cancer Institute, Emory University, Atlanta, GA
[5] Department of Urology, Emory University, Atlanta, GA
* E-mail: bfei@emory.edu, Web: www.feilab.org

Prostate cancer affects 1 in 6 men in the USA. Systematic transrectal ultrasound (TRUS)-guided biopsy is the standard method for a definitive diagnosis of prostate cancer. More than 1.2 million prostate biopsies are performed annually and the medical cost is more than two billion dollars each year. However, this technique has a significant sampling error and is characterized by low sensitivity (24-52%). This *"blind"* biopsy approach can miss up to 30% of prostate cancers. As a negative biopsy does not preclude the possibility of a missed cancer, both the physicians and patients face challenges in making treatment decisions. Due to the increasing number of men with potentially early and curable prostate cancer, this problem must be addressed in order to improve cancer detection rate. At our NIH/NCI-supported Emory Molecular and Translational Imaging Center, positron emission tomography (PET) with a new molecular imaging tracer FACBC has shown very promising results for prostate cancer detection in human patients. We have developed a PET molecular image-directed, 3D ultrasound-guided system for targeted biopsy of the prostate. The system consists of a 3D mechanical localization system and software workstation for image segmentation, registration, and biopsy planning. In order to plan biopsy in a 3D prostate, we developed an automatic segmentation method based wavelet transform. In order to incorporate PET/CT images into ultrasound-guided biopsy, we developed image registration methods to fuse TRUS and PET/CT images. The segmentation results from 40 TRUS image volumes of 20 patients show that the DICE overlap ratio is 90.3% ± 2.3%. The complete biopsy system has been tested in prostate phantoms and a small number of human patients. We are planning an early phase clinical trial on this PET molecular image-directed, 3D ultrasound-guided biopsy technology.

Acknowledgement: This project is supported by NIH grant R01CA156775 (PI: Fei).

Real-time Catheter Tracking and Visualization in 3-T MR-Guided Brachytherapy

Wei Wang[1,2], Alireza Mehrtash[1], Junichi Tokuda[1], Jagadeesan Jayender[1], Ravi T. Seethamraju[4], Tina Kapur[1], Akila N. Viswanathan[2], Robert A. Cormack[2], and Ehud J. Schmidt[1]

[1]Radiology, [2]Radiation Oncology , Brigham and Women's Hospital, Harvard Medical School, Boston, MA, United States; [3]MR R&D, Siemens Healthcare, Boston, MA, United States

Purpose: Interstitial radiation therapy (brachytherapy) is used for treatment of gynecologic malignancies that are unsuitable for standard intracavitary brachytherapy[1]. The placement of multiple interstitial catheters in close proximity to tumor tissue is critical to treatment outcome. Magnetic resonance (MR) imaging is increasingly used, instead of X-ray or ultrasound guidance, due to its improved visualization of the tumor and its surroundings. However, the metallic interstitial catheters are less visible on MR images than on X-ray, which makes the passive tracking of catheters time consuming. The active tracking of such catheters is complicated by (a) the metallic makeup of the brachytherapy needles, and (b) the presence of 10-20 needles in close proximity, leading to static (B_0) and radio-frequency (B_1) magnetic field inhomogeneities[2].The purpose of the present work was to evaluate active tracking of the tip of the interstitial catheters during manipulation inside the body. This will provide the clinician with real-time (>10 frames-per-second) feedback that enables more efficient targeting of the needles.

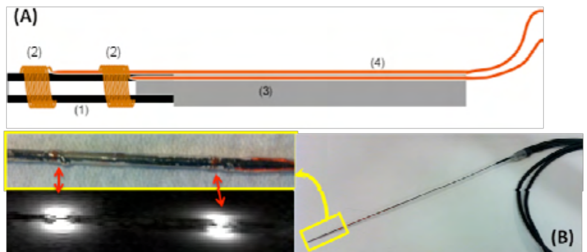

Fig. 1: (A) Schematic of the custom-built brachytherapy needle: (1) carbon fiber tube, (2) microcoils (3) alloy needle (4) micro-coaxial cable. (B) Enlarged view of distal catheter along with an MR image of the two microcoils.

Methods: An actively tracked interstitial catheter was built by modifying commercial MRI-conditional tungsten alloy needle (Fig. 1). The distal end (~ 3 cm) of the needle was replaced with a carbon-fiber tube, on which two 5-mm long solenoid microcoils were mounted. Carbon fiber is diamagnetic, minimal susceptibility artifacts, and has far lower electrical conductivity than metal, making it suitable for placement of tracking coils. This hybrid structure also maintained the stiffness required to perforate tissue. The microcoils were connected to an 8-channel interface for the Siemens Verio scanner. An MR-tracking sequence was implemented with the ability to use the zero-phase-reference or Hadamard multiplexing schemes[3]. The main tracking parameters were: $\alpha = 5°$; resolution $=0.6 \times 0.6 \times 0.6$ mm^3; frame rate = 40 Hz. Phase-field dithering was integrated by adding multiple orthogonal dephasing gradients in order to reduce B_0 and B_1 artifacts[4].

A needle placement procedure was conducted in a cleaned dead chicken. A high-resolution 3D IR-GRE MR scan of the entire chicken was acquired prior to tracking and was loaded into the 3D Slicer workstation in order to serve as a navigational roadmap. The MR-tracking sequence was then performed continuously during navigation, with the tip position and catheter orientation vector calculated in the scanner's reconstruction engine, based on the positions of the two tracking coils. The data was then transferred to the workstation in real time via the OpenIGTLink interface. To remove unwanted rapid "jitter", a first order low-pass filter was applied, providing a smoother temporal visualization during navigation. The catheter tip was visualized on a 3D model, as well as on sagittal, coronal and axial projections. The 3D Slicer Volume-Reslice-Driver module was applied, updating the slices displayed in the three orthogonal views in accordance with the catheter movement.

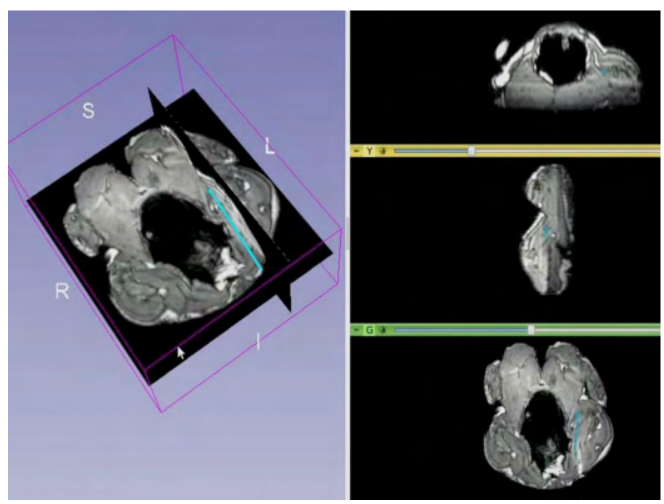

Fig. 2: A screenshot of the catheter (in cyan color) during real-time tracking and visualization in 3D Slicer. The needle tip position and orientation were overlaid on pre-acquired high-resolution 3D images.

Results: The experiments were performed on a 3T Siemens Verio scanner. Fig. 2 shows a visualization of the catheter tip and orientation overlaid on the pre-acquired 3D images. The use of the phase-dithering feature was required for artifact reduction, reducing tracking rate to ~15 fps. 3D Slicer provided real-time visualization and tracking of the catheter tip position and orientation.

Conclusions: We demonstrated the feasibility of active catheter tracking and visualization in MR-guided brachytherapy. This will facilitate catheter placement by providing an accurate and time efficient identification of catheter position and insertion path, as well as target volume and the organs at risk.

Reference: 1.Nag S et al., Gynecol Oncol 1998; 70:27-32. 2. Wang W et al., ISMRM 2013. 3. Dumoulin et al. Magn Reson Med 1993; 29:411-15. 4. Dumoulin et al. Magn Reson Med 2010; 63:1398-1403.

Clinical Implementation of a Smart Template for 3T MRI-guided Transperineal Targeted Prostate Biopsy

Nobuhiko Hata, Junichi Tokuda, Kemal Tuncali, Clare Tempany, Sang-Eun Song

National Center for Image Guided Therapy, Brigham and Women's Hospital, Harvard Medical School, Boston, Massachusetts 02115, USA, hata@bwh.harvard.edu

Introduction. To overcome the limited utility and accuracy of a conventional needle guidance template in MRI-guided prostate interventions, we developed a motorized MRI-compatible needle guidance template "Smart Template" that al-lows automated needle guidance without position restriction in a 3-Tesla MRI scanner. The aim of this study was to validate clinical feasibility and safety of the Smart Template.

Methods. The Smart Template employs a two-degrees-of-freedom (2-DOF) motorized needle guide consisting of vertical and horizontal bars that are positioned by a lead screw and nut mechanism driven by two ultrasonic motors with integrated optical encoders. Smart Template is controlled by a Linux-based control computer via approximately 15 m long electrical cables allowing the control computer located outside the scanner room. For registration, an MR marker-based registration block (Z-frame) that is used to register the conventional template to the MRI coordinate system is affixed to Smart Template. A customized 3D Slicer, an open-source surgical navigation software, with the ProstateNav module, is used as the navigation software to calibrate the robot to images, plan needle placement to targets, monitor position of inserted needles, and to remotely control Smart Template. The navigation software allows a clinician to define targets on either preprocedural or intraprocedural MR images. We performed initial clinical studies to assess the safety and feasibility of Smart Template. Ten men (age range: 60-72 years; weight range: 71-112kg) underwent targeted core biopsy of the prostate in the wide-bore 3T MRI scanner (MAGNETOM Verio, Siemens Healthcare, Erlangen, Germany). The study protocol was approved by hospital's Institutional Review Board prior to patient enrollment and was HIPAA compliant. Informed consent explaining the nature of the procedure and the potential hazards was obtained from each subject.

Results. All procedures were performed successfully without severe adverse events. Tissue samples were collected from targeted lesions in all cases without intraprocedural or postprocedural pain. No major complication was observed. Nine of the 34 sampled specimens were positive for malignant tissue (26.5%), resulting in prostate cancer diagnoses for 70% (N = 7) of the patients. An average of 3.4 ± 1.7 targets was preprocedurally selected per procedure and 2.6 ± 0.9 tissue samples were obtained from each target. An average of 1.8 ± 0.4 needle insertion was performed to obtain a tissue sample with an average biopsy time of 9 ± 1 minutes per sample. The mean procedural time was 124 ± 19 min including 57 ± 15 min of in-MRI preparation time.

Discussions. Early clinical trials demonstrate that Smart Template is acceptable and integrates easily into the procedural workflow of the existing MRI-guided prostate biopsy procedure. Needle placement inaccuracy due to the prostate and patient motion resulting repeated reinsertion remains as a major problem. The automated targeting, however, eliminated human error in target information communication between navigation software and in-bore insertion site, and unrestricted targeting within the prostate provided greater utility.

Acknowledgements. This work was supported in part by National Institutes of Health under Grants 1R01CA111288, R01CA124377, 5R01CA138586, 5P01CA067165, P41EB015898, and P41RR019703.

Medical Robotics and Computer-Integrated Interventional Medicine

Russell H. Taylor
The Johns Hopkins University

This talk will discuss ongoing research at the JHU Engineering Research Center for Computer-Integrated Surgical Systems and Technology (CISST ERC) to develop computer-integrated interventional systems (CIIS) that combine innovative algorithms, robotic devices, imaging systems, sensors, and human-machine interfaces to work cooperatively with surgeons in the planning and execution of surgery and other interventional procedures. The impact of CIIS on medicine in the next 20 years will be as great as that of Computer-Integrated Manufacturing on industrial production over the past 20 years. A novel partnership between human surgeons and machines, made possible by advances in computing and engineering technology, will overcome many of the limitations of traditional surgery. By extending human surgeons' ability to plan and carry out surgical interventions more accurately and less invasively, CIIS systems will address a vital need to greatly reduce costs, improve clinical outcomes, and improve the efficiency of health care delivery.

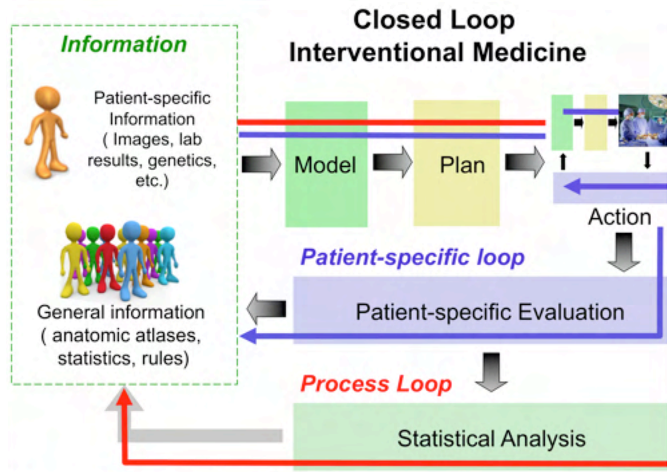

Fig. 1. Information Flow in CIIS

The overall structure of CIIS is illustrated in **Fig. 1**. These systems combine images and other information about an individual patient with "atlas" information about human anatomy to help clinicians plan how to treat the patient. In the operating room, the patient-specific plan and model are updated using images and other real-time information. The system has a variety of means, including robots and "augmented reality" displays to assist the surgeon in carrying out the procedure safely and accurately. The same technology will be used to assist in subsequent patient follow-up and in enabling statistical quality control to help improve the overall efficacy and safety of surgery and interventions.

This talk will describe past and emerging research themes and illustrate them with examples drawn from our current research activities in medical robotics and computer-integrated interventional systems.

Biography

Russell H. Taylor received his Ph.D. in Computer Science from Stanford in 1976. He joined IBM Research in 1976, where he developed the AML robot language and managed the Automation Technology Department and (later) the Computer-Assisted Surgery Group before moving in 1995 to Johns Hopkins, where he is the John C. Malone Professor of Computer Science with joint appointments in Mechanical Engineering, Radiology, and Surgery and is also Director of the Engineering Research Center for Computer-Integrated Surgical Systems and Technology (CISST ERC). He is the author of over 300 peer-reviewed publications, a Fellow of the IEEE, of the AIMBE, of the MICCAI Society, and of the Engineering School of the University of Tokyo. He is also a recipient of numerous awards, including the IEEE Robotics Pioneer Award, the MICCAI Society Enduring Impact Award, and the Maurice Müller Award for Excellence in Computer-Assisted Orthopaedic Surgery.

Towards Robot-Assisted Neurosurgery Under Continuous MRI

Jaydev Desai, PhD
University of Maryland, College Park

Brain tumors are among the most feared complications of cancer occurring in 20–40% of adult cancer patients. Though there have been significant advances in treatment, the prognosis for these patients is poor. Whether there is a primary malignancy or a secondary malignancy, whenever the brain of the cancer patient is involved in treatment, there is a significant impact on their overall quality of life. While the most optimal treatment currently for most brain tumors involves primary surgical resection, many patients may not be able to undergo that treatment plan due to either their poor general health or an unfavorable location (either deep inside the brain or inaccessibility of the tumor) of the lesion.

Magnetic resonance imaging (MRI) provides excellent soft tissue contrast and has become a standard imaging modality for physicians in several image-guided interventions. However, the nature of MR imaging imposes several constraints on the development of a robotic system. These challenges include actuator choice, sensor choice, material choice, size of the robot, etc., to name a few.

In this talk, we will discuss our progress on the development of MINIR: Minimally Invasive Neurosurgical Intracranial Robot, and identify the challenges in the development of this meso-scale robotic system operated under MRI guidance.

Research reported in this publication was supported by the National Institute Of Biomedical Imaging And Bioengineering of the National Institutes of Health under Award Numbers R21EB008796 and R01EB015870. The content is solely the responsibility of the author and does not necessarily represent the official views of the National Institutes of Health.

Advanced biophotonics for robotic image-guidance of brain surgery phantoms

Eric J. Seibel, Research Associate Professor, Dept. Mechanical Engineering, University of Washington

Timothy D. Soper, Research Scientist, Dept. Mechanical Engineering, University of Washington

Sina N. Kosari, Graduate Student, Dept. Electrical Engineering, University of Washington

Vivian W. Hou, Undergraduate Student, Biology Dept., University of Washington

Chenying Yang, Graduate Student, Dept. Bioengineering, University of Washington

Yuanzheng (Louis) Gong, Graduate Student, Dept. Mechanical Engineering, University of Washington

Danying Hu, Graduate Student, Dept. Electrical Engineering, University of Washington

Blake Hannaford, Professor, Dept. of Electrical Engineering, University of Washington

Complete resection of tumor tissue remains one of the most important factors for survival in patients with cancer. Surgical removal is the most common front-line cancer therapy for cancer therapies. Tumor resection in the brain is exceptionally difficult because leaving residual tumor tissue leads to decreased survival and removing normal healthy brain tissue leads to life-long neurological deficits. Brain surgery requires a very high degree of dexterity, accurate navigation, and micro-precision cutting over long durations; thus it is an ideal candidate for robotically assisted surgery. However, tumor resection is compounded by the need to make a small opening (keyhole) in the skull, and the difficulty of distinguishing normal from diseased tissue in an intra-operative setting. A minimally-invasive robotic system that allows surgeons to directly visualize and accurately discriminate neoplastic (cancer) from non-neoplastic tissue in a real-time intra-operative setting is currently not available.

We propose to overcome two major limitations affecting robotically-assisted surgery in a team approach: inability to (1) automatically and (2) optically guide treatments in a minimally-invasive intraoperative environment with advanced photonics and new cancer biomarkers. A single robot arm will hold a standard surgical tool for resecting/removing tumor, and the multimodal fluorescence and reflectance endoscopic imaging system will provide the advanced photonics in an ultra-small size. This presentation will cover the initial steps of integrating the multimodal robotic imaging of brain surgery phantoms that have residual fluorescence-labeled cancer cells in the margins of a tumor resection.

Acknowledgment of funding from NIH NIBIB R01 EB016457 “NRI-Small: Advanced biophotonics for image-guided robotic surgery,” PI – Seibel.

Image-guided Robotic Surgery Inside the Beating Heart

Pierre E. Dupont
Children's Hospital Boston, Harvard Medical School

Image-guided minimally invasive surgery has revolutionized the standard of care throughout the body. The use of catheters in cardiology, for example, has substantially reduced the risk and trauma for the patient in comparison to open-heart surgery. Many intracardiac repairs, however, require manipulating tissue in ways that cannot be achieved by catheters and so still require open surgery. In this talk, I will describe a robotic technology and surgical tool set that my group is developing to convert these intracardiac repairs to percutaneous, beating-heart interventions. The robotic technology is based on concentrically combining pre-curved elastic tubes. Coordinated motorized control of individual tube rotations and translations enables the robot to be navigated through the vasculature and into the heart. Once the surgical site is reached, the distal sections of the robot can deploy and manipulate tools to perform the repair. The robot forms a slender curve comparable in cross section to a catheter, but with a substantially higher tip stiffness. We have developed tools for the fundamental surgical tasks of tissue removal and tissue approximation. Our surgical tools are manufactured using a metal MEMS process that produces fully assembled, millimeter-scale devices with micron-scale features. Creating and operating the robots requires multiple imaging modalities. These include MRI for robot design, 3D ultrasound for robot navigation and fluoroscopy for tissue interaction. Our current challenges will be illustrated through ex vivo and in vivo experimental results.

This work was supported by the National Institutes of Health under grants R01HL073647 and R01HL087797.

Integrated 3D tracked ultrasound image guided steerable needle directionally-conformable therapeutic ultrasound minimally-invasive interventional therapy

E. Clif Burdette[a], Goutam Ghoshal[a], Tamas Heffter[a,f], Emery Williams[a], Corinne Bromfield[b], Serena Scott[c], Vasant Salgaonkar[c], Punit Prakash[c], Tamas Ungi[f], Emad Boctor[d] , Michael Choti[d], Robert Webster[e] , Laurie Rund[b], Gabor Fichtinger[f], John M. Ehrhardt[b], Chris J. Diederich[c]

[a]Acoustic MedSystems, Inc., Savoy, IL, USA
[b]Department of Animal Sciences, College of Veterinary Medicine, University of Illinois, Urbana, IL, USA
[c]Department of Radiation Oncology, University of California, San Francisco, CA USA
[d]Departments of Radiology and Surgery, Johns Hopkins University, Baltimore, MD USA
[e]Department of Mechanical Engineering, Vanderbilt University, Nashville, TN USA
[f]School of Computing, Queen's University, Kingston, ON Canada

Purpose: The availability of integrated technologies for image-guided spatially-tracked targeting of minimally invasive interventional procedures in a low-cost implementation could be a significant tool for management of several diseases, including liver, kidney, spine, prostate, as well as other disease sites. While surgery remains the gold standard, the availability of effective image-guided minimally invasive tools offer multiple advantages for treatment of localized disease, including minimal complications, shorter recovery, and lower cost. Significant strides have been made in image-guided interventions; however, a truly effective, low-cost, accurate, real-time, system and methods for achieving reproducible positive results is not yet available outside of research centers. The primary objective of the work described is to develop a platform with a realistic probability of achieving these goals, and which can be available in various configurations for treatment of multiple anatomical sites. Specifically, liver and kidney are now treated with radiofrequency ablation (RFA), but is limited because heat is transferred mainly through thermal conduction to tissue near the applicator and by lack of control over where heat is deposited. RFA and high intensity focused ultrasound (HIFU) are also used for treating bone metastases with similar limitations as in other tissues. HIFU can be aimed more precisely at small targets, but is limited in that it must be applied externally and cannot traverse paths that are blocked by gas or other bones. Overlapping beam entry/exit regions can lead to undesired thermal dose in areas which need to be protected. Interstitial ultrasound applicators have an advantage in that they are placed directly into the tissue to be ablated, can achieve high-intensity power deposition, and can be sectored for directional control. Success of a minimally invasive procedure depends on accurately targeting the desired region and guiding the entire procedure. The purpose of this study is to use a combined ultrasound imaging and tracking system to accurately place a steerable acoustic needle ablator and multiple temperature sensors *in vivo*.

Methods: 3D acoustic and biothermal transient finite element models were developed to simulate temperature and thermal dose distributions during 7 MHz catheter-cooled interstitial ultrasound ablation. Interstitial ultrasound applicators of center frequency of 6-7 MHz were used to ablate *in vivo* pig liver and tissue adjacent/within spinal vertebral body without damaging nearby structures. Temperature sensors were placed to estimate thermal distribution in the three-dimensional treated volume. A SonixTouch (Ultrasonix, Richmond, BC) and L14-5/38 GPS probe were combined with EM tracking and robotic needle insertion control. An in-house software architecture and interface was developed to communicate with the hardware, ultrasound imaging and tracking system, and for generator treatment control.

Results: During therapy, maximum temperature of 60-70 °C and dose of 10^5-10^6 TEM43°C was observed at radial distances10-20 mm from the center of the ablation transducer depending upon treatment time (5-9 minutes). Dose distribution was analyzed and compared with the gross pathology of the treated region. Accurate placement of acoustic applicator and sensors were achieved using the combined image-guidance and the tracking system. Control of energy direction was used to avoid damaging surrounding structures.

Conclusions: The experimental results demonstrated that the directionality and shape of the ablation zone can be controlled using the proposed technology of angularly-sectored ultrasound transducers. This preliminary study shows the feasibility of ablating tissue near the vertebrae and in vertebral body successfully without damaging the spinal cord. Desired ablation patterns were created in liver without damaging the nearby vein/vessels in the tissue verified from gross pathology inspection. These results suggest that tracked targeting coupled with directionality and shape of the ablated region could accurately control ablation zones using the proposed technology.

This work supported by NIH Grant R44CA134169 and NIH Grant R44CA112852.

Fluorescence Image-Guided Surgery of Nerves

Cristina Tan Hehir, Siavash Yazdanfar, Victoria Cotero, Anshika Bajaj, Tiberiu Siclovan, Evgenia Kim

Diagnostics and Biomedical Technologies
General Electric Global Research
Niskayuna, NY 12309

In many lifesaving surgical procedures, inadvertent nerve injury occurs, resulting in complications that affect patient's quality of life, such as loss of function and sensation, chronic pain, and erectile dysfunction. Despite the use of techniques to avoid or minimize nerve damage, the risk remains high in a wide array of surgeries such as radical prostatectomy, lymph node dissection and thyroid surgery. Nerve-sparing techniques primarily rely on anatomical landmark identification and are highly dependent on the surgeon's skills and experience. Precise localization of nerves is challenging due to variation in the anatomical location in each individual, their size, and their intricacy. Thus, improving the visualization of nerves intraoperatively remains a large unmet clinical need. Fluorescence imaging with targeted contrast agents could address this need by allowing direct, specific, and real-time visualization for image-guided surgery of nerves.

We have recently designed a series of fluorescent compounds for selectively targeting nerve. Coupled with the development of compact and low-cost open and minimally invasive surgical instrumentation, fluorescence imaging offers a potentially disrupting approach to highlighting nerves intraoperatively.

Supported by: NIH grant R01-EB011872

In-Situ Augmentation for Image Guided Microsurgery

John Galeotti, Ph.D., Carnegie Mellon University; George Stetten, M.D., Ph.D., University of Pittsburgh; John Galeotti, Carnegie Mellon University; Samantha Horvath, University of Pittsburgh; Roberta Klatzky, Carnegie Mellon University; Bing Wu, Arizona State University; Vikas Shivaprabhu, University of Pittsburgh; Randy Lee, University of Pittsburgh; Jihang Wang, University of Pittsburgh; Tejas Mathai, Carnegie Mellon University; Mel Siegel, Carnegie Mellon University; George Stetten, University of Pittsburgh

Medical imaging is generally defined to include modalities that scan beneath the surface of the patient. Whereas human vision is generally not included in this list, it may actually be thought of as the original "medical imaging" modality. Confining the display of CT, MR, ultrasound, and such modalities to conventional screens forces the clinician to look away from the patient to interpret these images, losing direct anatomical context. Maintaining a direct view of the actual patient is especially crucial during interventional procedures, but is usually sacrificed to see these other images during image-guided intervention. We have developed new techniques for displaying images directly within the patient, using semi-transparent mirrors and holographic optical elements. Such displays permit a clinician to aim a needle or a scalpel directly at the image in-situ within the patient, aided by familiar visual landmarks on the patient's exterior as well as the tool itself and the clinician's own hand. We have given the clinician, in effect, an augmented sense of vision to see through the skin, without any tracking apparatus or head-mounted display as previously required by augmented reality displays. Our original method involved ultrasound, resulting in a device we call the Sonic Flashlight, which can be used during procedures such as vascular access, biopsy, nerve blocks, guidance in open surgery, etc. More recently, we have adapted the concept to the guidance of surgery under a stereomicroscope using OCT, primarily for eye surgery. Our custom OCT scanner developed in collaboration with Physical Sciences, Inc., is a unique apparatus specifically suited to the needs of in-situ image guidance. We report here on several generations of prototypes in which design constraints have been identified and addressed. These constraints include image brightness, resolution, stereo perception, preservation of an effective surgical space, 3D scanning/visualization, multi-GPU throughput and computation speed, wavelength choice and its affects on scanning depth and speed. In related research, we are also augmenting the surgeon's sense of touch while using an interventional tool by sensing forces at the tool's tip and delivering magnified forces through the handle to the operator's hand. Unlike previous systems based on freestanding robotic arms, our device is completely hand-held, and thus less restricted in its movements. Taken together with the in-situ display, augmented forces may enhance hand-eye coordination in an intuitive and non-intrusive manner, improving the safety and effectiveness of image guided microsurgery.

NIH Funding: R01EY021641, R21 EB007721, R01 EB000860, R01 HL074285

Quantitative Endoscopy for High Accuracy Navigation

Gregory D. Hager, PhD

Computational Interaction and Robotics Lab, Laboratory for Computational Sensing and Robotics, Johns Hopkins University, Baltimore, USA

The advent of widespread high definition video microscopy and endoscopy in the operating room offers new opportunities for computer vision in interventional medicine. In particular, endoscopes can now be used as devices for quantitative measurement, assessment, and feedback to surgeons, thus improving the safety, quality, and consistency of interventions with no extra cost or additional equipment. In this talk, I will illustrate the potential for quantitative endoscopy by describing a method for video-CT registration in skull-base surgery. I will present our preliminary results showing that video-CT registration produces higher accuracy than currently available commercial platforms, and I will describe ongoing work aimed at translating these results into a practical tool for surgical navigation.

Biography: Gregory D. Hager is a Professor and Chair of Computer Science at Johns Hopkins University and the Deputy Director of the NSF Engineering Research Center for Computer Integrated Surgical Systems and Technology. His research interests include time-series analysis of image data, image-guided robotics, medical applications of image analysis and robotics, and human-computer interaction. He is the author of more than 250 peer-reviewed research articles and books in the area of robotics and computer vision. Professor Hager received his PhD in 1988 from the University of Pennsylvania. He spent a year as a Fulbright Professor at the Fraunhofer IITB in Karlsruhe, Germany, and was on the faculty at Yale University from 1991-1999. In 2006, Prof. Hager was elected a fellow of the IEEE for his contributions in Vision-Based Robotics.

Improved MR Thermometry Processing for MR-guided FUS in the Brain

Kim Butts Pauly[1,2,3] Viola Rieke[4], Ronnie Instrella[3], Will Grissom[5], Beat Werner[6], and Ernst Martin[6]

[1]Departments of Radiology, [2]Bioengineering, and [3]Electrical Engineering, Stanford University, [4]Department of Radiology and Biomedical Imaging, UCSF, [5]Department of Biomedical Engineering, Vanderbilt University, [6]MR Center, University Children's Hospital Zurich

Purpose MR-guided focused ultrasound is promising for the non-invasive treatment of a variety of brain disorders including neuropathic pain (1), essential tremor (2), and Parkinsonian tremor. While single slice MR-thermometry with single baseline subtraction processing is adequate to guide these treatments, the method can be corrupted by motion of the brain and tongue and respiratory motion. While respiratory and/or cardiac gating are options to reduce these artifacts, they constrain the acquisition and inevitably increase acquisition times.

The purpose of this work was to investigate the improvements to be found through processing the MR thermometry data with a hybrid multibaseline/referenceless (MB/R) algorithm and to further develop guidelines as the size of the required baseline library. The multibaseline component of the algorithm requires the acquisition of a baseline library acquired continuously, without gating, thereby sampling different points in the cardiac and respiratory cycles. The referenceless component to the algorithm compensates for the effects of non-repetitive motion, such as tongue motion.

Methods MR thermometry images from five sonications in five patients who were treated in Zurich (1), and from three additional volunteers were processed with single baseline subtraction, multibaseline subtraction, and hybrid MB/R processing with one baseline image. The volunteer data was additionally processed with hybrid MB/R processing with 30 baseline images. Absolute temperature error and temporal temperature uncertainty of the different reconstruction methods were analyzed and compared.

In a subsequent study, we analyzed three volunteer datasets to determine how many baseline images are needed to provide 90% of the gain seen with the full 30 baseline library. Temporal standard deviations across the whole head and in ROIs were found. Additionally, a singular value decomposition analysis was performed to determine how many baseline images were sufficiently different from each other to warrant inclusion in the baseline library.

Results Absolute temperature errors and temporal temperature uncertainty were highest with single baseline subtraction and lowest with hybrid multibaseline/referenceless reconstruction in all areas of the brain.

Both the analysis of the temporal standard deviations and the SVD analysis lead to the conclusion that a baseline library of 12-15 images is sufficient to obtain 90% of the improvement seen with a larger library size of 30 images.

Conclusions The results of this study indicate that significant gains in MR thermometry image quality can be achieved through the hybrid MB/R algorithm, with no changes to the acquisition during heating. While a baseline library of 15 is suggested, the baseline library takes less than one minute to acquire and can be reused for each sonication obtained in the same scan plane.

Acknowledgements
PO1 CA159992, General Electric

References

1. Martin E, et al. Ann Neurol. 2009 Dec;66(6):858-61
2. Elias J, et al. Congress of Neurological Surgeons, 2011

Ultrasound Registration and Visualization for Neuronavigation

Matthew Toews[1], Isaiah Norton[1], Alexandra Golby[1], Stephen Aylward[2], Andrei State[3], Tamas Ungi[4], William Wells III[1]
[1]*Harvard Medical School, Brigham and Women's Hospital, Boston, MA* [2]*Kitware, Carrboro, NC*
[3]*InnerOptic Technology, Inc., Hillsborough, NC* [4]*Laboratory for Percutaneous Surgery, Queen's University, ON*

Purpose: B-mode ultrasound (US) is a safe, cheap and portable imaging modality for image-guided medical procedures, for example image-guided neurosurgery. Neuronavigation systems are capable of tracking the rigid 3D position of the US probe relative to the patient, thereby allowing the surgeon to visualize 2D US image data together with pre-operative diagnostic information and image data such as magnetic resonance (MR) volumes used in surgical planning.

The rigid transform relating intra-operative US images to pre-operative patient data can degrade substantially over the course of surgery, impairing visualization. Degradation can be caused by tissue deformation, e.g. brain shift due to resection, invalidating the assumption of a globally rigid probe-to-patient transform. Furthermore, the probe-to-patient transform may not be available due to tracking failure, calibration error, loss of line-of-sight for optical tracking systems, etc.

Methods: We propose to improve visualization in the case where the rigid probe-to-patient transform is insufficient to relate intra- and pre-operative image data, using a novel image registration strategy. Prior to major resection, a *US image appearance model* of the patient anatomy is generated from a dense set of US scans, and aligned to pre-operative image data using a combination of probe tracking information and rigid image registration. This model is then fit to deformed intra-operative US data via image registration, thereby relating pre- and intra-operative image data directly without the use of external tracking information.

The primary technological advancement is an efficient slice-to-model alignment technique, based on robust correspondence of image patches [1]. Local image patches or features arising from distinctive image structure are automatically extracted in all US image data. Feature-to-feature correspondences are then identified between pre- and post-resection US data using a robust matching technique similar to the Hough transform. Individual correspondences provide conditionally independent hypotheses as to the geometry of pre-operatively labeled structures of interest in the intra-operative US. When overlayed upon the intra-operative US, these hypotheses are used to predict and visualize the geometry of structures of interest, e.g. a tumor boundary, in addition to its uncertainty, see Fig 1).

Results and Conclusion: Correspondences can be robustly computed between distinctive anatomical structure despite a high degree of missing or unrecognizable image content, e.g. due to missing tissue or surgical implements. Real time performance should be possible with optimization on standard PC hardware. Further work will investigate optimal visualization techniques and deformable registration.

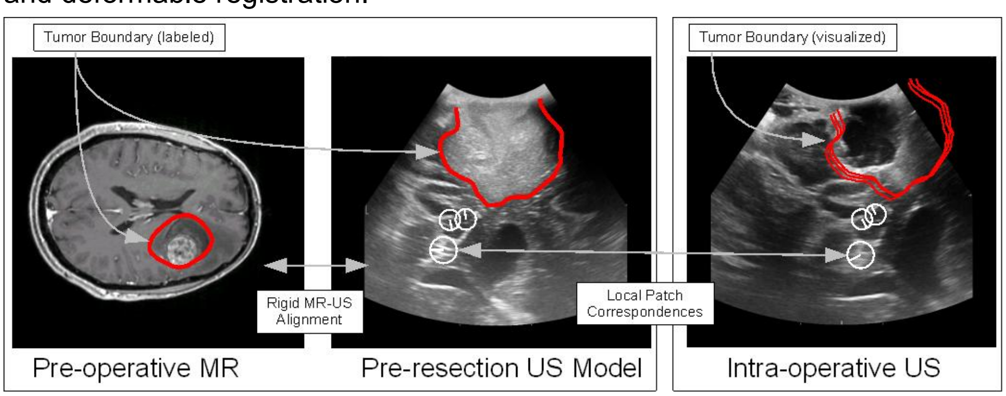

Fig. 1: Left: preoperative MR and a US model slice with tumor labels. Right: an intra-operative US slice following tumor resection. Feature correspondences (circles) are identified and used to predict the tumor boundary.

References and Acknowledgements: [1] Toews and Wells III, IPMI 2009. Funding was received from NIH grants U41RR019703, P41EB015898, R01CA138419.

Motion-tracked thermometry and relaxometry using a US-MRI hybrid acquisition

Bruno Madore, Chang-Sheng Mei, Renxin Chu, Matthew Toews, Scott W. Hoge,
Benjamin M. Schwartz, Lawrence P. Panych
Harvard Medical School, Brigham and Women's Hospital, Department of Radiology, Boston, MA

Introduction: An IRB-approved imaging setup was developed whereby a single-element ultrasound (US) transducer emits and receives signals in an MR environment (see Fig. 1), during MR scanning [1]. While MR images provide good spatial resolution, the US signals provide additional temporal resolution for enhanced feature tracking using a dual pathway PSIF-FISP sequence [2] that is suitable for both temperature and T_2 mapping.

Fig. 1: *The experimental setup includes a US transducer and a (Lego-built) safety device.*

Methods and Results: On a 3T GE HDxt system, 2D images were acquired at a rate of 1.6 frames per second (fps) while US data were gathered at a rate of 156 fps (Fig. 2). The FISP and PSIF images have very different contrast, and the fact that blood vessels tend to be bright in FISP images and dark in PSIF images (Fig. 3) facilitates the task of finding and tracking these vessels. Blood vessels were tracked across MR time frames using a fast landmark-based registration algorithm. A particle filter was used to identify the frames where US data were most similar to those at the current time point. Vessel locations (along with target location) could then be estimated for the current time point via bilinear interpolation at an enhanced rate of about 20 measurements per s.

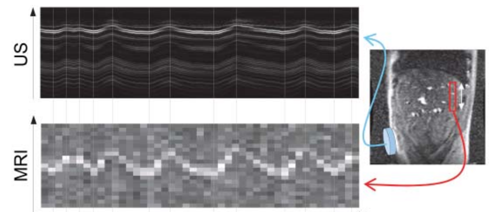

Fig. 2: *US and MRI data were acquired in a synchronized manner, at 1.6 fps and 156 fps, respectively.*

Both the FISP and PSIF images are temperature sensitive, and both can be used together to help optimize temperature-to-noise-ratio (TNR). Because of relaxation time differences, kidney tissues ($T_1/T_2 \approx 1100/76$ ms, red arrow in Fig. 3) tend to appear much brighter in PSIF images than surrounding liver tissues ($T_1/T_2 \approx 810/34$ ms, blue arrow in Fig. 3). For this reason, the benefits and TNR boost obtained from acquiring a PSIF image in addition to a FISP image are more substantial for renal than for hepatic applications. In addition to temperature imaging, a multi-echo version of the same sequence can enable T_2 mapping. A 3T Siemens Trio system was used to acquire the images in Fig. 4, which include temperature as well as R_2 ($= 1/T_2$) overlays. R_2 was calculated from the FISP (S^+) and PSIF (S^-) signals using the equations: $|S^+| \propto \exp\{-TE_{FISP} \times (R_2+R_2')\}$ and $|S^-| \propto \exp\{-TE_{PSIF} \times (R_2-R_2')\} \times \exp\{-TR \times (R_2+R_2')\}$, where $(R_2+R_2') \equiv 1/T_2^*$. Because R_2' appears with different signs in the two equations, it can be discriminated from R_2. The black circle in Fig. 4a is the region where thermal dose exceeded the 240 CEM43 threshold for tissue damage. The mean T_2 value over the square region in Fig. 4b was 44.4±2.5ms, which is consistent with the 47ms value expected for muscle. It is anticipated that T_2 values, along with temperature dose, will help detect temperature-induced tissue damage [3].

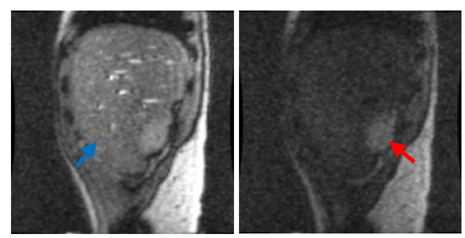

Fig. 3: *Example of FISP (left) and PSIF (right) images, red/blue arrow points to the kidney/liver.*

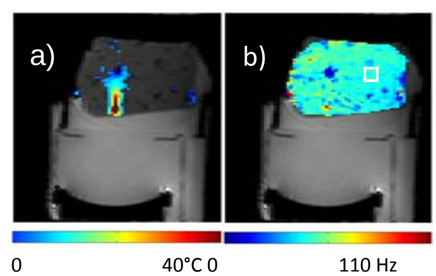

Fig. 4: *Temperature (a) and R_2 (b) map for the time frame with peak temperature, in muscle tissues.*

Conclusion: A motion-tracked US-MRI hybrid method is being developed for temperature and T_2 mapping, to better detect tissue damage during thermal ablation procedures.

References: [1] Schwartz et al. doi: 10.1002/mrm.24336. [2] Madore et al. MRM 2011;66:658. [3] Anzai et al, JMRI 1991;1:553. Support from R01CA149342 and P41EB015898 is acknowledged.

Prototyping clinical applications with the Public Library for Ultrasound (PLUS) toolkit and 3D Slicer

Andras Lasso, Tamas Heffter, Csaba Pinter, Adam Rankin, Tamas Ungi, and Gabor Fichtinger

Ultrasound (US) is becoming an increasingly potent imaging modality in the guidance of medical interventions and a variety of advanced image analysis methods have been under development for US-guided interventions. Unfortunately, the transition from an image analysis algorithm to clinical feasibility trials as part of an intervention system is a long and arduous process. The development of US-guided intervention systems involves the integration of many components, such as imaging and tracking devices, data processing algorithms, and visualization software. This process consumes a great deal of time, money and software engineering effort, which often overwhelms research groups and forces them to abandon their image analysis research before achieving clinical trials. The objective of our work therefore is to provide a freely available open-source software platform - PLUS: Public software Library for Ultrasound - to facilitate rapid prototyping of US-guided intervention systems for translational clinical research. PLUS intends to pave the way for advanced US image analysis methods to be integrated interventional applications ready for clinical trials. PLUS provides a variety of methods for interventional tool pose and ultrasound image acquisition from a wide range of tracking and imaging devices, spatial and temporal calibration, volume reconstruction, and live streaming of the acquired data. Clinical applications can be rapidly and conveniently prototyped by using PLUS from within the 3D Slicer (www.slicer.org) environment via OpenIGTLink. The resulting application prototyping environment is the SlicerIGT, which has been used in a variety scenarios, such as for US-guided lumbar punctures, pedicle screw placements, and nephrostomy. This talk introduces PLUS, explains its functionality and architecture, and presents a handful of its typical uses in US-guided intervention systems in the SlicerIGT environment. These examples will demonstrate that PLUS fulfills the essential requirements for the development of US-guided intervention systems and, coupled with SlicerIGT, it aspires to become a widely used translational research prototyping platform. PLUS and SlicerIGT are freely available as open source under BSD license, the code and documentation are available atwww.plustoolkit.org and www.slicerigt.org.

GRANT ACKNOWLEDGEMENTS: This work was supported through the Applied Cancer Research Unit program of Cancer Care Ontario with funds provided by the Ontario Ministry of Health and Long-Term Care. Gabor Fichtinger was funded as a Cancer Ontario Research Chair. Tamas Ungi was supported as a Queen's University–Ontario Ministry of Research and Innovation Postdoctoral Fellow.

Neuroimage Analysis for Intra-Procedural Imaging

Steve Pieper[1], Alexandra Golby[2], Isaiah Norton[2], James V. Miller[3], Allen Tannenbaum[4], Ron Kikinis[2]

[1]Isomics, Inc., Cambridge MA USA, [2]Brigham and Women's Hospital, Boston, MA USA, [3]General Electric Research, Niskayuna, NY, USA, [4]Boston University, Boston, MA USA

Purpose: Images acquired during a procedure must be analyzed and displayed within a clinically relevant timeframe if they are to help guide decision-making. Yet many algorithms for segmentation and registration of neuroimages have been developed in the context of neuroscience research, where run times of 24 hours are acceptable and not uncommon. In addition, intra-procedural images are often acquired quickly, and may suffer from distortion or noise that complicates automated analysis. Our goal is to develop neuroimage analysis tools that provide the needed clinical information within the time available during the procedure.
Methods: We reviewed the workflow of image guided neurosurgical procedures performed in the AMIGO suite, an OR with 3T MR imaging available, to determine where intra-procedural analysis would have the greatest impact. We surveyed existing techniques for processing this data to identify gaps in the ability of the clinical team to extract maximum value from the acquired images within the available time.
Results: In this clinical scenario, we identified a time window of approximately 15 minutes during which the patient is re-prepped for surgery after the images have been acquired. During this window the surgeon must evaluate the extent of any residual tumor as revealed by the new images and decide what, if any, further resection is required. Neuroimage analysis tasks during this timeframe include: (1) segmentation of residual tumor, typically performed using manual segmentation; (2) registration of intra-procedural images to pre-procedural images, for which automated registration can fail requiring the use of manual techniques; and (3) visualization comparison of resection cavity to diagnostic images and pre-procedure plans, which can sometimes only be performed piecemeal using the navigation system, the PACS workstation, and the scanner console. In addition, we found that during this time window it is increasingly important to be able to perform additional acquisition-specific analysis, such as visualization of intra-procedural diffusion MRI to assess the resection with respect to white matter. We found that the analysis demands are likely to increase as new data collection techniques are introduced and the available time window for neuroimage analysis is likely to shorten as the intra-procedural acquisition process is streamlined.
Conclusions: Based on our analysis we applied for and received funding to develop an integrated set of interactive segmentation, registration, and visualization tools as part of the upcoming renewal period of the Neuroimage Analysis Center which begins June 1, 2013. Our plans call for us to develop tools that provide real-time visualization of intermediate algorithm results and expose control interfaces that allow the clinical team to "steer" the tools to improve speed and accuracy. To optimize performance, we will investigate hardware-accelerated algorithms, such as those implemented to use GPU computing. These tools will be developed as modules in the 3D Slicer application and will be made freely available. In our preliminary work we have implemented a steered version of the GrowCut tool that can run on a GPU.
Acknowledgements: This work is funded as part of the Neuroimaging Analysis Center (NAC), grant number P41EB015902, in collaboration with the National Center for Image Guided Therapy (NCIGT), grant number P41EB015898, from the NIH's National Institute of Biomedical Imaging and Bioengineering (NIBIB).

Emerging CT-imaging Technology and Its Implications to Image-guided Therapy

Xiaochuan Pan, PhD

Computed tomography (CT) remains one of the most widely used tomographic imaging techniques for diagnosis of diseases, and for assessment of treatment responses. There also exists a rapidly increasing effort in exploiting CT technology for guiding minimally invasive surgical procedures and radiation therapy. In the last decade or so, advances in both CT hardware and algorithms allow the development of emerging CT technology tailored to specific clinical tasks, including image-guided interventional procedures. In particular, the enhanced spatial/contrast resolution, fast-imaging capability, and high degrees of imaging flexibility offered by emerging CT-imaging approaches has opened ample opportunities for establishing imaging protocols with considerably lowed radiation dose and contrast-agent load, and with potentially optimized workflow, in guiding innovative procedures in surgery and radiation therapy. In the presentation, I will discuss some of the recent advances in CT technology and their potential applications to guiding surgical and radiation-therapeutic procedures. An emphasis will be placed on illustrating, by use of real-data examples, of possible low-dose, sparse-view, and/or limited-angular-range CT imaging enabled by the recent advances in CT technology, and on discussing its implications to image-guided surgery and radiation therapy.

Biography: Xiaochuan Pan received his Ph.D. degree in Physics at The University of Chicago under the guidance of Professor Ugo Fano and then performed his post-doc research in medical imaging. He is a full Professor in the Departments of Radiology and Radiation & Cellular Oncology, the College, the Committee on Medical Physics, and the Comprehensive Cancer Center at The University of Chicago. His research interest centers on systems, physics, algorithms, and applications of tomographic imaging. Awards received by Dr. Pan include IEEE NPSS Early Achievement Award and IEEE EMBS Technical Award for his contributions to medical imaging. He is a Fellow of AAPM, AIMBE, IEEE, OSA, and SPIE. Dr. Pan has served as the chair, a charter member, and/or a grant reviewer for review panels of funding agencies and foundations such as NIH, NSF, and NSFC, and is currently an associate editor, or an editorial board member, for a number of journals in the field, including IEEE Trans. Med. Imaging, IEEE Trans. Biomed Eng., and Phys. Biol. Med. He has served as a chair or member of numerous technical committees of professional organizations such as IEEE and RSNA, and as a chair of programs, themes, and sessions, or as a technical or a scientific committee chair or member, for conferences such as IEEE EMBC, IEEE MIC, RSNA, and AAPM.

Poster Abstracts

Intravenous Chemotherapy Filter (ChemoFilter): Prototype and In-vitro Proof-of-Concept of a Novel Device for High Dose Intra-arterial Chemotherapy Delivery

Anand S. Patel, MD; Erin J. Yee, BS; Aaron D. Losey, BS; Prasheel V. Lillaney, PhD; Mark W. Wilson, MD; and Steven W. Hetts, MD
Department of Radiology, IR Research Lab, University of California, San Francisco, USA

Purpose:

Primary liver cancer is the 3rd leading cause of cancer death worldwide and is not surgically curable in 80% of cases. Conventional IV chemotherapy is limited by systemic toxicity. A common chemotherapeutic used for a variety of tumors is doxorubicin (Dox), whose toxicities include bone marrow suppression, GI damage, and most seriously irreversible cardiac failure. Intra-arterial chemotherapy (IAC) increases tumoral chemotherapy dose while minimizing systemic toxicity. Nonetheless, up to 50% of injected doxorubicin (Dox) passes directly through hepatic tumors into the systemic circulation and causes toxicity. To further increase tumor dose and limit systemic exposure, we have developed ChemoFilter – an intravenous chemotherapy filter catheter, which through simple central venous access via ultrasound would be guided fluoroscopically into the veins draining the target organ undergoing IAC, and bind escaping chemotherapy. ChemoFilter is a non-implantable disposable catheter that would be inserted at the time of the procedure and removed after infusion.

Methods:

A benchtop flow model simulating in-vivo renal/hepatic IAC with matching physiologic serum pH, electrolytes, temperature, venous dimensions, and flow rates was designed. Based on chemical properties, 15 activated carbons and 19 ion-exchange polymeric resins were obtained to test drug binding capacity and kinetics for a concentrated solution of Dox (0.05 mg/ml). Selected adsorbent material with volume equal to a cone in the renal or hepatic vein (2.5 ml) was placed in the circuit segment, simulating device deployment within the vein. Dox concentrations were measured until equilibrium via UV spectrophotometry. Given interest in rapid high capacity drug binding, we propose a metric, the TACE Factor (TF), defined as *total mg Dox bound during initial 10 minutes* per *ml of adsorbent*. A goal TF is >10 given a 2.5 ml constraint and aim to bind half the administered Dox during standard TACE (25 mg).

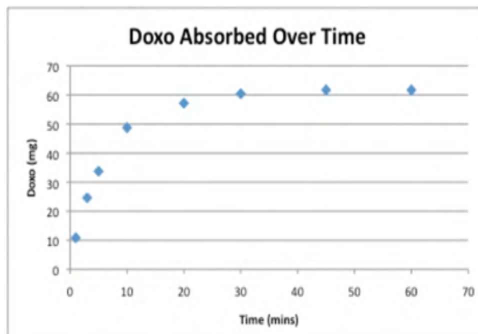

Fig 1. Dox kinetic curve for hydrophilic strong-acid cation exchange resin.

Results:

An activated carbon with pore size and physical properties customized for doxorubicin absorption demonstrated a TF of 8, binding 20 mg of Dox in 10 minutes. Four strong-acid cation exchange resins with a hydrophilic polyvinyl backbone, demonstrated excellent results binding up to 50 mg of Dox in 10 minutes, representing TFs of 15-20, and rapid time to equilibrium at 20-25 minutes (Fig. 1). Several prototype catheter devices were constructed (Fig. 2).

Fig 2. Prototype temporary catheter-based venous filter device. Boston-Scientific Wallflex stent is adapted with resin material (orange) sandwiched between two 200-micron mesh filters

Conclusions:

Proof-of-concept for rapid high capacity Dox binding and feasibility of a novel intravenous chemotherapy filter device was successfully demonstrated using ion-exchange resin and activated carbon filtration mechanisms in an IAC flow model, which has not been described before. Prototype catheter devices will be tested in animal swine studies, which are underway to demonstrate safety, reduced toxicity profile, and high-dose chemotherapy feasibility. Specific filter inserts could be developed for any intra-arterial drug combination, both oncologic and non-oncologic. ChemoFilter could serve as a platform for targeted drug therapy in interventional oncology, a rapidly growing field in cancer treatment.

Semi-Automatic Kidney Quantification for Surgical Decision Making in Hydronephrosis

Carlos S. Mendoza[1;2], Xin Kang[1], Nabile Safdar[1], Craig A. Peters[1;3], Marius George Linguraru[1]

[1] Sheikh Zayed Institute for Pediatric Surgical Innovation, Children's National Medical Center, Washington DC, USA
[2] Signal Processing Department, University of Sevilla, Spain
[3] Department of Urology, Children's National Medical Center, Washington DC, USA

Purpose

The size and geometry of the kidney parenchyma and collecting system are indicators of renal function and drainage. We propose to develop a semi-automatic method to quantify renal size from ultrasound (US) image data for surgical decision making in hydronephrosis.

Methods

A clinical tool was developed to segment kidneys from 111 two-dimensional (2D) pediatric US studies. There were 77 normal kidneys and 34 cases with hydronephrosis (dilation of the collecting system). Data were acquired on scanners from different manufacturers. An expert radiologist selected the largest 2D longitudinal kidney section from each US sequence and manually segmented the kidney to establish the ground truth. The semi-automatic segmentation was initialized from two points at both ends of the major axis of the kidney. Subsequently, the segmentation used active shape models (ASM) combined with a genetic algorithm and models of the kidney contour profiles that take into account the orientation of the organ relative to the US probe. Accuracy was computed in terms of symmetric volumetric overlap (VO), relative area difference (AD) and average perimeter distance (PD) between manual and semi-automatic segmentations.

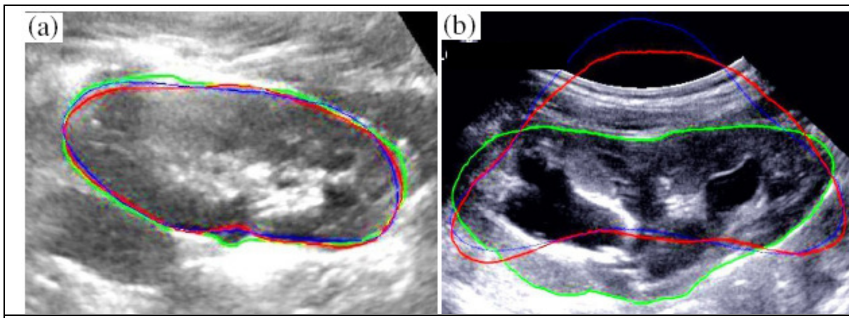

Figure 1. Two examples of kidney segmentation (a) Best segmentation with VO = 96.4%. (b) Worst segmentation with VO = 69.1%. Ground truth is shown in green and the result of our method is shown in red. The initialization of the segmentation produced by the genetic algorithm is shown in blue.

Results

The clinical tool was robust to segmenting normal and hydronephrotic kidneys and in the presence of morphological changes. Results indicate significant improvements ($p < 0.05$, Wilcoxon paired sign test) of median VO from 88.6% to 90.2%, median AD from 13.9% to 10.8%, and median PD from 13.8 to 11.5 pixels for using a classic ASM vs. the proposed method, respectively. Similarly, a reduction of variance was observed for the segmentation results obtained using the clinical tool.

Conclusion

Computer-aided analysis of renal ultrasonic images can robustly quantify the size and geometry of kidneys with various conditions of hydronephrosis. Renal quantification has the potential to support surgical decisions in the management of cases with hydronephrosis

Methods for assisting needle angle selection during CT-guided biopsies

Cheng William Hong BS[1,2], Sheng Xu PhD[1], Ankur Kapoor PhD[3], Nadine Abi-Jaoudeh MD[1], Kimberly L Imbesi BS[4], Charisse Garcia RN[1], Aradhana M Venkatesan MD[1], Elliot Levy MD[1], Richard Chang MD[1], Bradford J Wood MD[1]

[1]National Institutes of Health, Center for Interventional Oncology, Bethesda, MD, USA
[2]Lerner College of Medicine, Cleveland Clinic, Cleveland, OH, USA
[3]Siemens Corporate Research, Princeton, NJ, USA
[4]Duke University School of Medicine, Durham, NC 27705, USA

Purpose: The safety and diagnostic yield of CT-guided biopsies are dependent on accurate needle insertion. This clinical study (NCT01218854) compares potential first-pass needle alignment accuracy to freehand needle alignment using two different angle selection methods. A laser-assisted needle angle selection system (L-NASS) which aligns a laser pointer to the planned insertion axis, and a hypoallergenic plastic block (Ultem ®), with pre-cut holes (B-NASS) at various specified angles were tested.

Methods: Subjects undergoing clinically indicated CT-guided biopsies were recruited and randomized to one of the angle selection systems vs. freehand. A custom electromagnetic (EM) tracking system was used to calculate the distance error associated with each of the angle selection methods vs. freehand. Distance error was defined as the difference between the planned trajectory and the projected needle trajectory. Angle error was measured automatically by the EM tracking system in degrees and needle trajectory error was defined as the minimum distance between the target and the actual vector. This was done to avoid repeated needle insertions. The physician selected the needle trajectory using a standard radio-opaque grid and conventional technique. The physician positioned the needle for insertion with freehand and the error was calculated by the EM tracking system. Then, the angle selection system selected by randomization was used to simulate needle insertion and errors were measured again. The actual biopsy was completed by a second radiologist according to standard technique.

Results: Nine subjects have completed the experimental protocol. Four subjects were assigned to L-NASS, with better accuracy than freehand alignment (angle error 4.3 ± 2.3 degrees vs. 8.6 ± 3.3 degrees, distance error 8.0 ± 2.2 mm vs. 12.5 ± 5.6 mm). Five subjects were assigned to B-NASS which also demonstrated less error than freehand alignment (angle error 2.0 ± 1.3 degrees vs. 5.8 ± 2.1 degrees, distance error 8.6 ± 4.6 mm vs. 10.6 ± 3.4 mm).

Conclusions: Preliminary data suggests that angle selection systems are easy to use for interventional procedures, and more accurate than freehand needle alignment. These systems could potentially improve accuracy for less experienced users, and should be assessed for differences in outcomes in terms of diagnostic yield, needle repositioning, intra-operative risk, radiation exposure, and procedure time.

In vivo treatment of pig liver using steerable needle therapeutic ultrasound with combined imaging and electromagnetic tracking system

Goutam Ghoshal[a], Tamas Heffter[a], Emery Williams[a], Corinne Bromfield[b], Vasant Salgaonkar[c], Laurie Rund[b], John M. Ehrhardt[b], Chris J. Diederich[c], E. Clif Burdette[a]

[a]Acoustic MedSystems, Inc., Savoy, IL, USA
[b]Department of Animal Sciences, University of Illinois, Urbana, IL, USA
[c]Department of Radiation Oncology, University of California, San Francisco, CA USA

Purpose: Extensive surgical procedure or liver transplant still remains the gold standard for treating slow-growing tumors in liver. But only few candidates are suitable for such procedure due to poor liver function, tumors in unresectable locations or presence of other liver diseases. In such situations minimally invasive surgery may be the best therapeutic procedure. The success of minimally invasive procedure depends on accurately targeting the desired region and guiding the entire procedure. The purpose of this study is to use a combined ultrasound imaging and electromagnetic tracking system to accurately place a steerable acoustic needle ablator and multiple temperature sensors in pig liver *in vivo*.

Methods: Catheter based interstitial ultrasound applicator of center frequency of 6-7 MHz was used to ablate *in vivo* pig liver under gas anesthesia. Temperature sensors were placed at eight different locations to estimate thermal distribution in the three-dimensional treated volume. The ultrasound imaging was acquired using a SonixTouch (Ultrasonix, Richmond, BC, Canada) system with an L14-5/38 GPS probe. The in-house software architecture and interface was developed to communicate with the hardware, ultrasound imaging and tracking system.

Results: During therapy a maximum temperature of 60-70 ℃ and dose of 10^4-10^6 equivalent minutes at 43℃ was observed at a radial distance 15-20 mm from the center of the ablation transducer for a treatment time of 7-9 minutes. The dose distribution was analyzed and compared with the gross pathology (Fig.1) of the treated region. Accurate placement of the acoustic applicator and temperature sensors were achieved using the combined image-guidance and the tracking system. Note control of energy direction to avoid other structures.

Conclusions: The experimental results demonstrated that the directionality and shape of the ablation zone can be controlled using catheter based high intensity sectored ultrasound transducers. The 180° sectored transducers helped in creating desired ablation pattern without damaging the nearby vein/vessels in the tissue verified from gross pathology inspection (Fig. 1(a)). Our results suggest that tracked targeting coupled with directionality and shape of the ablated region could accurately control ablation zones using the proposed technology.

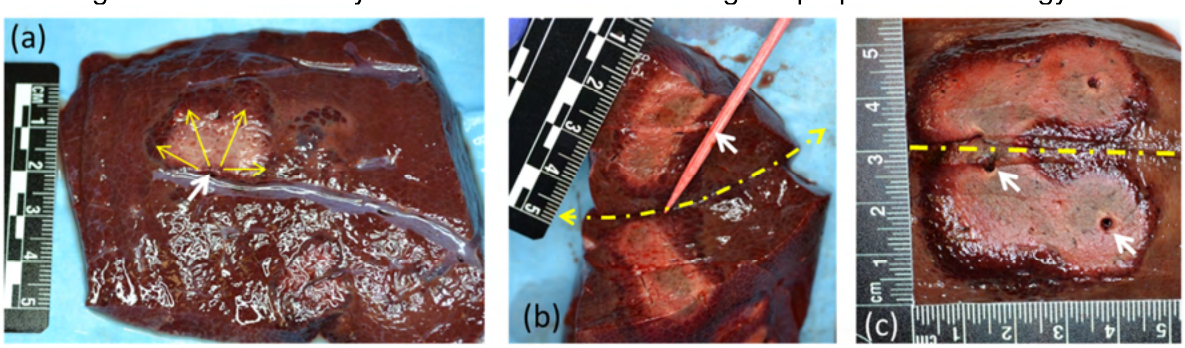

Figure 1: Gross pathology of the ablated pig liver tissue with (a) 180° radiation pattern single needle applicator (yellow solid arrows indicate the beam pattern) avoiding and (b) depth of abated region by 180° pattern applicator for tissue cut along long axis of needle (applicator location indicated by wooden stick), (c) pattern of 360° radiation pattern applicator (white arrows indicate the applicator position, dashed yellow arrow indicates the line of cut for tissue dissection).

Towards a framework for robotically assisted ureteroscopy

Rahul Khare, Kevin Cleary, Linan Zhang, Emmanuel Wilson, Patrick Cheng, Craig Peters
Sheikh Zayed Institute for Pediatric Surgical Innovation, Children's National Medical Center, Washington, DC

Purpose: Existing endoscope designs rely on decades-old manual controls for translation, rotation and tip flexion. Because of the complexity of movements needed for many applications, integration of a robotic control system has the potential to greatly enhance the safety, efficacy, and efficiency of these instruments. Here, we present work towards designing and implementing a robotic control system to control a flexible ureteroscope with the goal of improving the efficiency and precision of tip placement.

Methods: The framework for robotically assisted ureteroscopy (Fig. 1) consists of two parts: a) robotic device; and b) control mechanism. For the robotic device, we designed and fabricated a 3 degrees-of-freedom device allowing one translation and two rotary motions. The endoscope can be mounted on the device and a ball-screw is used for the linear motion. This motion is linked to the insertion and extraction motion of the endoscope. The rotary motions of the robot device are linked to the rotation and flexion/extension of the endoscope. The control mechanism includes a Galil controller interfaced to a computer. Three input devices including a Sixense game controller, a keyboard and foot pedals are used as interfaces for controlling the robot device. The video output from the endoscope processor is also interfaced to the computer and is presented to the user through a dialog-based application on the system display.

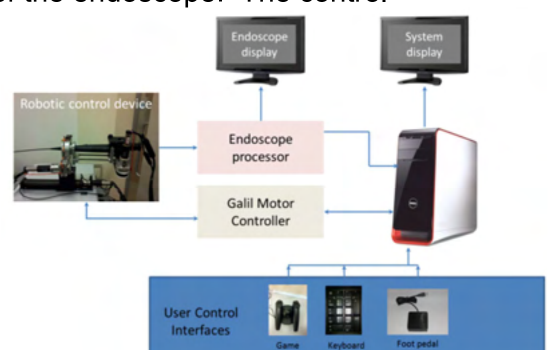

Fig. 1: System setup for robotically assisted ureteroscopy

To control the robot, we developed three user interfaces. In the first interface, six different buttons are linked to each of the six possible motions of the endoscope. In the second interface, the joystick on the game controller controls the insertion/extraction and the rotate left/right motion of the endoscope. Two other buttons on the game controller change the flex/extension of the endoscope. In the third interface, the orientation of the game controller is used to position a cross-hair on the video output of the endoscope and select a point of interest. When a button is pressed on the game controller, the endoscope rotation and flexion is changed to bring the point of interest to the center of the view. Then, the user presses the foot-pedals to insert the endoscope to move closer to the point of interest.

Results: The system was able to smoothly control the motion and flexion of the tip using all three of the user interfaces. Evaluation studies are in progress.

Conclusions: Robotic control for a flexible ureteroscope has the potential to improve procedural efficiency and tip placement precision during procedures such as exploration of the kidney calyxes. The concept presented is also applicable to other endoscopic devices.

Proof of Concept of Wireless Tissue Palpation in Abdominal Surgery

Marco Beccani[1], Christian Di Natali[1], Mark Rentschler[2], Pietro Valdastri[1]

[1]Vanderbilt University, Nashville, TN 37235. [2]University of Colorado, Boulder, CO 80309

Purpose. In minimally invasive and robotic surgery the surgeon has minimal, or no, chance to leverage tactile and kinesthetic sensations in exploring non-visible organ features to detect hidden tumor margins or to prevent accidental tissue damage. Since registration with preoperative imaging is not effective for soft tissues, restoring tactile sensations would be crucial to guide a complete resection of tumoral masses without sacrificing excess normal tissue. One of the main barriers to adoption for laparoscopic instruments with embedded force and/or tactile sensors developed so far can be identified as the need for a dedicated surgical access port for the palpation device. We propose a wireless approach to intraoperative palpation that does not require port space.

Methods. The proposed approach takes advantage of an external magnetic field source and an intraoperative wireless palpation device (WPD). The WPD can be introduced into the peritoneal cavity through a standard trocar and positioned on the target by a laparoscopic grasper. Then, tissue indentation can be achieved by properly modulating the gradient of the external magnetic field. This approach has been assessed on the benchtop, limiting our investigation to vertical motion of the WPD. The WPD is a cylindrical capsule with a diameter of 12.7 mm (compatible with access through a standard trocar for 12 mm instruments) and a length of 27.5 mm. Inside the WPD, a wireless microcontroller transmits the measurements acquired by a triaxial accelerometer and a set of magnetic field sensors. These data are used to derive tissue indentation depth and pressure, thus obtaining the elastic module of the tissue being palpated. The WPD also embeds a permanent magnet that is coupled with an external source of magnetic field that modulate the indentation force. The WPD was used to indent three silicone tissue simulators having different stiffness (elastic modulus ranging from 50 kPa to 93 kPa), and the results were compared with a standard technique for material testing. A second trial aimed to identify differences in elastic modulus due to a lump embedded in a porcine liver.

Results. The maximum relative error on elastic module identification for the three silicone tissue simulators was below 3%. As concerns the ex vivo trial, wireless tissue indentation detected a 21.49 kPa variation in the elastic modulus due to the stiffer material.

Conclusions. The authors have developed a novel platform that does not require physical continuity across the abdominal wall between the palpation probe tip and the user interface. Preliminary experimental data suggest that wireless tissue indentation is effective in a laboratory setting, showing comparable results to well-established indentation techniques. Next step will be to move forward in vivo trials to complement image-guided surgery in resecting tumoral masses buried within soft tissue organs.

MR-guided Focused Ultrasound System for Continuous Breathing Liver Ablation

Andrew Holbrook[1], Pejman Ghanouni[1], Juan Santos[2], Charles Dumoulin[3], Yoav Medan[4], Kim Butts Pauly[1,5,6]

[1]Department of Radiology, Stanford University, [2]HeartVista, [3]Department of Radiology Cincinnati Children's Hospital, [4]Department of Biomedical Engineering, Technion, [5]Departments of Bioengineering, and [6]Electrical Engineering, Stanford University,

Purpose MR-guided focused ultrasound of the liver is hampered by respiratory motion. Forced breathholding under anesthesia is a simple technological solution, but is more invasive for the patient than being able to treat during continuous breathing, which could be done without anesthesia or intubation. The purpose of this work was to put together a complete system for FUS treatment during continuous breathing including liver tracking, transducer tracking, beam steering, and MR-thermometry monitoring. The system was tested in phantoms and in an *in vivo* porcine liver.

Methods The system was developed with a 3.0T GE MRI and an InSightec Conformal Bone FUS system (1000 elements, 550 kHz, 4 incorporated MR tracking coils). GRE Scout, MR-Tracking, MR-ARFI and MR-thermometry sequences were implemented in RTHAWK, which also allowed a customizable user interface to control the MR scanning and display, as well as to control the ultrasound beam steering. Transducer placement was facilitated by projecting pre-acquired images on the animal to visualize underlying anatomy. After placement, ultrasound coupling tests were performed to verify a good connection between the transducer and skin. Liver tracking was done by correlating the diaphragm and user-defined vessels with the bellows information, which was then used in real-time to determine the liver position via a lookup table. Similarly, the transducer position as a function of respiratory phase was determined from MR Tracking. With the liver and transducer positions thus known as a function of the bellows respiratory position, beam steering was performed in real-time by switching between pre-allocated phase tables within 16 ms. MR-ARFI was used for beam localization and calibration. Both MR-ARFI and thermometry were done with a small FOV single shot EPI sequence and thermometry processing was done with hybrid multibaseline/referenceless algorithm.

In phantom experiments, sonications were made while 1) the phantom was moving and the beam steered to keep a consistent location (n=6) and 2) without beam steering (n=4). These results were compared to 3) static sonications (n=6) on the basis of three metrics: area of >10°C rise isotherm, energy required to reach 15°C above baseline, and the average rate of temperature rise during the first 10 seconds of sonication. Subcostal steered *in vivo* sonications (n=15) were compared to breathhold sonications (n=14) on three metrics: the average rate of temperature rise during the first 10 seconds of sonication and length and width of the 5°C rise isotherm at the timepoint where the maximum temperature rise reached 10°C.

Results For the phantom experiments, the area measurements were found to be statistically significantly different ($p \leq 0.003$). However, in the other two metrics, the static and unsteered sonications were not statistically different ($p > 0.9999$). Steered in vivo HIFU ablations were not statistically significantly different from ablations during breathholding.

Conclusions A system for performing HIFU steering during ablation of the liver during continuous breathing motion is presented and shown to achieve results equivalent to ablation performed with breathholding.

Acknowledgements RO1 CA121163

MR-Guided Episcleral Plaque Brachytherapy for Uveal Melanoma

J. Esthappan, Y. Hu, and P. Grigsby

Washington University School of Medicine, Siteman Cancer Center, St. Louis, MO

Purpose: We have developed a magnetic resonance (MR) imaging technique for patient-specific tumor and anatomic definition of the eye, and for three-dimensional (3D) COMS-based isodose planning for episcleral brachytherapy for uveal melanomas. We are developing an MRI-based method for post-implant dosimetric verification of episcleral brachytherapy to verify the radiation doses delivered to the tumor.

Methods: Uveal melanoma patients were prescribed to receive 85 Gy over 96 hours from episcleral plaque brachytherapy using iodine-125 seeds. Traditionally plaque size and prescription depth were based on tumor basal dimensions and apex heights as determined by US and fundus photography. From this information, the source strength (uniform activity per seed) was determined. MR-guided treatment planning was performed prior to plaque implantation. Patients were imaged on a 1.5-T Philips scanner, with head coil in place, yielding T2-weighted (T2W) and T1-weighted (T1W) scans. Images were imported into a brachytherapy treatment planning system. Contouring of the tumor was largely based on the T2W scan, with reference to the standard measurements, but adjusted based on the T1W scan which in most cases provided improved definition of the tumor apex. Optic nerve, globe of the eye, and lens were also contoured on the T2W scan. Anatomic dose points were defined as tumor apex, tumor anterior and posterior edges, macula, optic disk, lens, and retina. Isodoses were computed on the T2W scan, with no inhomogeneity corrections, and point doses as well as dose-volume information were analyzed. Post-implant imaging and dosimetry was performed.

Results: For the T2W turbo spin echo (TSE) sequence, thirty-three 1.5 mm axial slices with no gap were acquired, echo time (TE) was 75 ms, repetition time (TR) was "shortest", flip angle (FA) was 90°, and number of averages was 3. For the T1W 3D magnetization-prepared rapid acquisition with gradient echo (MPRAGE) sequence, eighty-three 1.2 mm slices were acquired. The TE, TR, FA and the number of averages were 4.0 ms, 8.5 ms, 8° and 1, respectively. For both scanning sequences, the in-plane voxel size was 1 mm × 1 mm, and the in-plane field-of-view was nominally 150 mm × 169 mm and adjusted slightly based on patient anatomy. Total scan time was approximately 4-5 minutes per sequence. Post-implant imaging was performed with T2W, T1-weighted (T1W), and balanced steady state free procession (SSFP) techniques.

Conclusions: We have developed and clinically implemented an MR imaging technique for patient-specific tumor and anatomic definition of the eye MR-guided treatment planning, and post-implant dosimetry verification. We believe the implementation of such methods for more accurate dosimetry will be critical for the proper determination of tumor dosing technique and the evaluation of risks associated with treatment-related morbidities.

Intraarterial MR Perfusion Imaging of Meningiomas: Comparison to Digital Subtraction Angiography

Hetts S, Martin A, Dowd C, Halbach V, Higashida R, McDermott M, Saloner D
UCSF Radiology and Biomedical Imaging and Neurological Surgery

Purpose
Meningiomas often benefit from preoperative embolization to reduce operative blood loss and associated morbidity. Intraarterial (IA) administration of contrast into the external carotid artery (ECA) and internal carotid artery (ICA) branches supplying the tumor during the embolization procedure maps out the blood vessels supplying the tumor as well as evaluating which portions of the tumor are successfully devascularized. Whereas IA digital subtraction x-ray angiography (DSA) is the gold standard for embolization guidance, IA perfusion MRI may offer increased sensitivity to residual vascularized tumor.

Materials and Methods
Studies were performed in a combined XMR suite wherein an x-ray angiography unit (Integris V5000, Philips) is coupled in-line to a 1.5 T MR scanner (Intera, Philips), allowing easy patient movement between the two imaging modalities during endovascular procedures. We evaluated 14 patients with IA T2* dynamic susceptibility contrast (DSC) perfusion MR during preoperative embolization. Eight of these patients were also evaluated with intraprocedural IA T1 weighted perfusion MR. IA perfusion was performed with dilute gadolinium injected initially into the ECA and subsequently into the CCA. The selected carotid artery was confirmed to provide vascular supply to the tumor by prior DSA. The portions of the tumor demonstrated to be associated with ECA or ICA supply, based on IA MR perfusion measures, were compared to DSA.

Results
Both T2* and T1 IA perfusion MR techniques were more sensitive than DSA at detecting vascularized tumor prior to or following embolization. The T1 technique (Figure, top row, pre and post embolization) was subject to less susceptibility artifact, and thus performed better than the T2* technique (Figure, bottom row, pre and post embolization) at the skull base. Both IA MR perfusion techniques demonstrated tighter arterial input functions than the IV MRI perfusion technique due to contrast administration directly into cervicocerebral arteries. Similarly, time enhancement curves for the IA MR perfusion methods demonstrated reduced mean transit time (MTT) and lack of a recirculation peak as comparted to the IV MR perfusion method. IA MR perfusion methods were good at differentiating ECA from ICA supply to individual tumors. However, vascular variants such as anterior falx artery or meningohypophyseal artery tumor supply (ICA branches outside the blood brain barrier) presented interpretive challenges for MRI but were readily apparent on DSA.

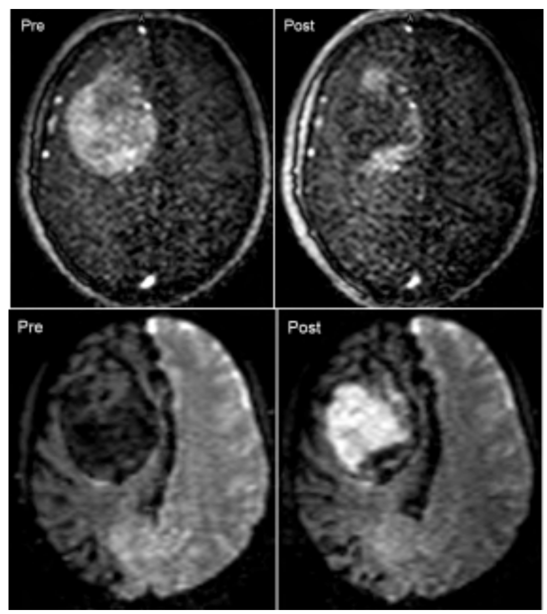

Conclusion
IA MR perfusion techniques appear to be a useful adjunct to DSA in determining tumor vascularity and the source of that blood supply during preoperative embolization procedures.

Systematic Investigation of Convection-enhanced Delivery Infusion Protocols and Catheters Using Real-time MRI

BP Grabow[1], R Raghavan[2] M Brady[2], K Kubota[3], C Ross[4], EK Brodsky[1] J Raschke[3], AL Alexander[1] and Walter F. Block[1]
University of Wisconsin[1], Therataxis[2], Kinetics Foundation[3], and Engineering Resources Group[4]

Purpose Convection Enhanced Delivery (CED) is a neurosurgical procedure for delivering agents related to the treatment of cancer and neurodegenerative diseases in the human brain [1-3] as well as exciting neurological investigations in animal models of optogenetics. A disparate ensemble of catheters, flow rates, and infusions techniques has been employed in an attempt to predict and control the ultimate infusion distribution while minimizing unwanted loss of infusate through a low pressure escape route along the exterior of the catheter, termed “backflow”. We present our latest results to undertake a systematic study of the multiple variables utilized today to mitigate unwanted backflow in CED using MR image-guidance for real-time device manipulation and real-time MR monitoring.

Methods Backflow alters the initial drug delivery point from the catheter tip, which produces a desired spherical drug distribution, to a variable length line, which produces a varied, less predictable cylindrical drug distribution. We investigated three methods which have been previously reported to mitigate backflow with varying success: slow, ramped transitions to peak flow rates, positive flow during catheter insertion, and varying catheter diameters and tip designs in nearly 100 infusions of 2mM gadodiamide suspension in the 26 adolescent pigs.

Rapid device targeting and insertion in the thalamus was accelerated with an in-house developed software plug-in that enables real-time device manipulation [5]. Rapid 2D single-plane monitored backflow during the infusion along the catheter tract.

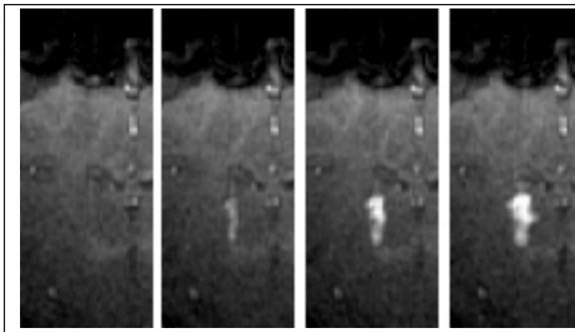

Figure 1 Progression of significant backflow at t=0, 30, 150, 300 seconds with constant flow rate. Catheter tip is located at the lower end of the hyperintense region. Backflow height along the catheter tract is established early in the infusion, while additional infused volume spreads radially from the catheter.

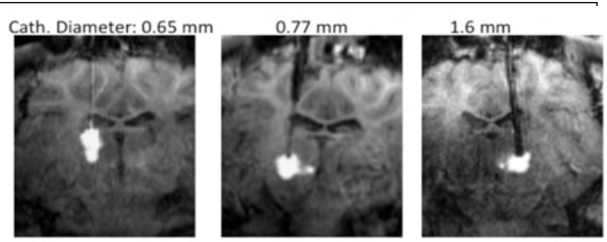

Figure 1 Backflow is significant with 0.65 mm catheter, while not present with larger catheters (center and right). Previously, backflow was thought to worsen with increasing diameter.

Results In comparison to constant flow (control), ramped infusions showed no less likelihood of backflow. Flow rate determined height of backflow along the catheter, independent of the ramping process. The use of 2D real-time imaging along the catheter indicates that backflow occurs at its full length within the first few seconds of an infusion (Figure 1). Previously it was believed to occur gradually. After the initial increase in backflow height, the remaining infused volume increases the radius of the infusion cloud, but not the height. Catheter insertion under positive flow also did not reduce the likelihood of a catheter to experience backflow. Finally, decreasing catheter diameter does not explain differences in backflow performance as seen in Figure 2.

Conclusion Systematic study under real-time MRI is providing new insight into the effects catheter design and infusion protocols have on drug distribution. The design of the catheter tip is likely to be more influential on performance than previously understood.

Referenes [1] R. H. Bobo, et al, “CED in the brain.,” *PNAS*, vol. 91, no. 6, pp. 2076–80, Mar. 1994. [2] M. T. Krauze, et al, *Journal of neurosurgery*, vol. 103, no. 5, pp. 923–9, Nov. 2005. [3] V. Varenika, et al, *Journal of neurosurgery*, vol. 109, no. 5, pp. 874–880, 2009. [4] C. L. Truwit and H. Liu, *JMRI*, vol. 13, no. 3, pp. 452–7, Mar. 2001. [5] E. Brodsky, et al, ,” *Biomedical Sciences and Engineering Conference*, pp. 6–9, 2011.

Single vs. multiple tensor diffusion tractography: which is better correlated with function?

Lauren J. O'Donnell, Jiaolong Cui, Neelan Marianayagam, Kelly Doolin, Isaiah Norton, Yanmei Tie, Laura Rigolo, Alexandra J. Golby
Golby Lab, Brigham and Women's Hospital, Harvard Medical School

Purpose

Diffusion MRI fiber tracking has been widely applied for neurosurgical planning, especially for preoperative assessment of functionally relevant white matter anatomy. However, owing to the well-known inability of traditional diffusion tensor streamline tractography to trace through regions of crossing fibers, potential inaccuracies in the depiction of the tracts pose a challenge for clinical applications. We have performed a clinically motivated validation study to assess the potential of classic versus state-of-the-art multi-tensor streamline tractography to trace crucial structures of interest with reference to subject-specific functional activations.

Methods

In 10 healthy subjects and 10 neurosurgical patients with mass lesions, we compared the performance of typical single tensor (DTI) streamline tractography versus two-tensor unscented Kalman filter (UKF) streamline tractography [1]. The UKF tractography fits the tensor models to the diffusion data during tracking, taking advantage of stabilizing information from the previous tractography steps when fitting the model at the current location. The single tensor method fits the model to all data first, then performs Runge-Kutta order two tracking in 3D Slicer version 4.0 [2]. We tested the ability of the tractography methods to trace critical motor pathways, using clinically acquired diffusion data with a standard b-value and subject-specific functional MRI data for three motor tasks: hand clench, toe wiggle, and lip pursing. fMRI was thresholded for each subject, and the individually determined threshold was chosen that resulted in activation in the anatomical regions known to be associated with each task, producing functional regions of interest (ROIs). These subject-specific fMRI activation maps were used as the functional ROIs for tract selection, using the "AND" operation with structural ROIs in the posterior limb of the internal capsule (PLIC). The PLIC was chosen, rather than an ROI more inferior in the cerebral peduncle, to increase sensitivity in the area of neurosurgical interest superior to the PLIC.

Results

In both controls and patients, the two-tensor UKF tractography found more tractography trajectories connecting the hand and lip motor areas (Figure 1). In some subjects this came at the (relatively minor) expense of some additional false positive or spurious trajectories with this method (Figure 1, right).

Conclusions

The two-tensor method is promising and is better correlated with function.

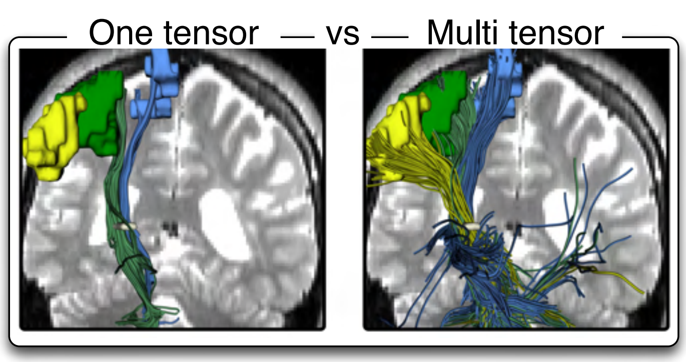

Figure 1. Higher sensitivity of UKF tractography (right) compared to DTI (left). When seeded in the entire brain, DTI tractography was unable to connect to lateral motor activations. Data are from a patient with right frontotemporal and parietal oligodendroglioma.

References

[1] Malcolm, J. G., Shenton, M. E., & Rathi, Y. (2010). Filtered multitensor tractography. Medical Imaging, IEEE Transactions on, 29(9), 1664-1675.
[2] Gering, D. T., et al (2001). An integrated visualization system for surgical planning and guidance using image fusion and an open MR. Journal of Magnetic Resonance Imaging, 13(6), 967-975.

Subminute deformable image registration for image-guided radiation therapy

Wen Li[1], William Plishker[2], Junghoon Lee[3], John Wong[3], Raj Shekhar[1]
1 Sheikh Zayed Institute for Pediatric Surgical Innovation, Children's National Medical Center
2 IGI Technologies, Inc.
3 Radiation Oncology and Molecular Radiation Sciences, Johns Hopkins School of Medicine

Purpose

In intensity-modulated radiotherapy (IMRT), precise patient positioning is imperative to avoid detrimental effects of missing the target volume (TV) while irradiating normal tissue. In IMRT, the prescribed dose is given incrementally in 30-40 daily fractions. The treatment planning, however, is typically performed a week before the treatment begins. For each daily fraction, the patient needs to be repositioned as seen in the planning CT. There are expected to be additional anatomic changes during the treatment. Further study is needed to understand and quantify their effect on planned treatment.

Deformable registration between planning CT (pCT) and daily cone-beam CT (CBCT) is necessary to determine the aforementioned anatomic changes. Accurate deformable registration, however, is usually complex and can take hours to complete. We have accelerated deformable image registration using recent graphic processor units (GPUs) such that it executes in less than a minute, making quantifying anatomical changes practical. In this work, we report the result of applying GPU-accelerated deformation registration to pCT and CBCT of patients who underwent IMRT of the head and neck tumors.

Methods

Archived pCT and 13 of 30 daily CBCT image sets acquired during the IMRT of a head and neck cancer patient were obtained. Couch shifts (i.e., 3D translation) applied to reposition the patient during these fractions were also recorded along with imaging data. The pCT (floating image) was registered to align with daily CBCT (reference image). After preprocessing (resampling, denoising, and window/level rescaling) in the CPU (Intel Core i7-3820@3.60GHz x 8), the image were transferred to the GPUs for registration. Mutual information-based rigid and nonrigid image registration was implemented in two NVIDIA GTX 680 graphic cards installed in a desktop computer (Dell Alienware Aurora R4). The entire registration process was automatic and its output was a voxel-wise displacement map.

Results

For the 13 image pairs, deformable registration, including preprocessing and data resampling, took 53±3 s. For each pair, the displacement vector at the radiation isocenter, through which the central beams pass was used to compare automatic registration with couch shifts in each principal direction: right-left, anterior-posterior, and superior-inferior. The two shifts at the isocenter were subtracted and the residual errors in each direction were averaged over 13 fractions, which were 0.8 mm (right-left), 1.4 mm (anterior-posterior), and 1.3 mm (superior-inferior). The result shows our registration recovers couch shifts with subvoxel accuracy, implying it could be a viable automated method for clinical practice.

As a second metric to evaluate the quality of registration, we computed normalized cross-correlation (NCC) between the pCT and CBCT. To show regional improvement at the isocenter, the NCC was calculated in a 50 mm × 50 mm × 50 mm neighborhood centered at the isocenter. Our results showed a greater improvement in NCC after deformable image registration versus after applying the couch shifts, (7.5% vs. 4.4%, respectively).

Conclusions

With GPU acceleration, we were able to complete deformable registration of pCT and daily CBCT images accurately in less than one minute. This presents the potential of using high-speed deformable registration for daily quality assessment in IMRT. Future directions of this ongoing work include exploring other methods of validation, testing the registration on a larger collection of clinical data, and, eventually, clinical integration.

Development of a Novel Vascular Phantom for Navigation Testing in Interventional MRI

Losey, Aaron D.[1]; Martin, Alastair J. [1]; Lillaney, Prasheel[1]; Yee, Erin J. [1]; Wilson, Mark W. [1]; Saeed, Maythem[1]; Do, Loi[1]; Hetts, Steven W. [1]

[1]Radiology and Biomedical Imaging, University of California, San Francisco, San Francisco, CA, United States.

Purpose: Interventional MRI offers the unique capability to steer catheters by creating a magnetic field near the catheter tip. Efficacy of MR guided navigation must be tested *in vitro* in vascular phantoms that mimic the *in vivo* environment. Previous vascular phantoms have shortcomings including lack of MRI compatibility, artifact creation, non-physiologic stiffness, and high frictional resistance that limits navigation capabilities. We sought to develop a vascular phantom from poly(vinyl) alcohol cryogel (PVA-C) that overcomes these limitations and provides a tool to test our magnetically-assisted remote control (MARC) endovascular catheter.
Methods: Design considerations for the phantom were as follows: MRI compatible, MR relaxation times similar to body tissues, smooth lumen that mimics vessel feel during navigation, compatible with flow, range of navigational difficulty, and the ability to accommodate 6 French catheters. *Phantom Box Construction:* To provide physiologically relevant vessel trajectories, multiple symmetric angles (30-90°) and diameters (3/16-7/8 in.) were designed from Delrin rods connected together and placed in an acrylic box (Figure 1). PVA-C was poured into the phantom box and cross-linked with freeze-thaw cycles. The rods were removed leaving pathways mimicking vessel lumens. *PVA-C Process:* A gel was created using a process previously outlined by Surry, et al. Sevol Grade 165 PVA powder (Sekisui Specialty Chemicals America, Dallas, TX) was used to create 500 ml 10% PVA-C. Four freeze-thaw cycle were performed on the gel. Images were obtained with 1.5 T scanner using b-SSFP, T1, and T2-weighted images, along with quantitative T1 and T2 measurements.
Results: T1 and T2 relaxation times (mean ± SD) for the PVA-C were 1195 ± 36 ms and 189 ± 5 ms. Figure 2 represents a MRI of the PVA-C phantom using a b-SSFE sequence at 1.5T.
Conclusions: The standard deviations show acceptable ranges for homogeneity, and the T1 and T2 values are in an acceptable range for tissue. These initial steps provide the foundation for a human-scale vascular phantom that can be used for testing navigation in our MARC endovascular catheter.

Figure 1: Phantom box with rods

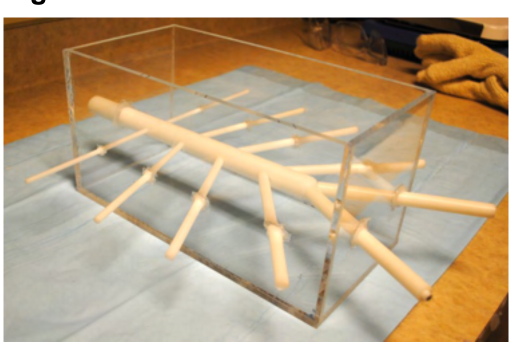

Figure 2: MRI of phantom using b-SSFP at 1.5T

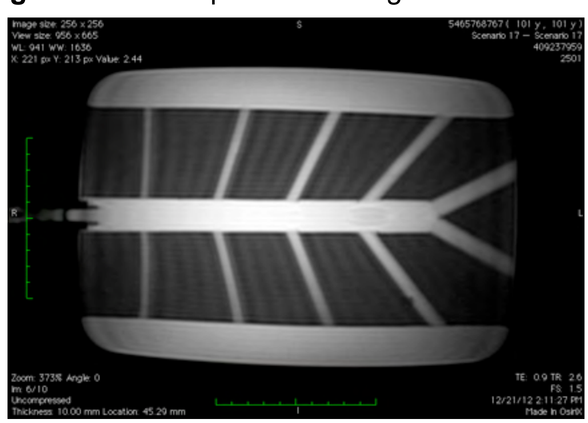

An Evaluation of RF Heating in a Nitinol Braided Endovascular Catheter at 1.5T and 3T

Losey, Aaron D.[1]; Lillaney, Prasheel[1]; Martin, Alastair J. [1]; Wilson, Mark W. [1]; Saeed, Maythem[1]; Do, Loi[1]; Yee, Erin J. [1;] Hetts, Steven W. [1]
[1]Radiology and Biomedical Imaging, University of California, San Francisco, San Francisco, CA, United States.

Purpose: The use of ethylene-vinly alcohol copolymer (Onyx, eV3, Irvine, CA) for liquid embolization of cranial vascular lesions has resulted in microcatheter fragments left in place in patients following procedures performed under x-ray guidance. Undergoing subsequent diagnostic MRI examinations poses a safety concern due to the possibility of RF heating because of the metallic braid incorporated into the catheter. In this study the heating of a nitinol braided catheter commonly used to deliver ethylene-vinvyl alcohol copolymer was assessed in an *in vitro* phantom model.
Methods: A 1.9F nitinol braided catheter (eV3 Echelon, Irvine, CA) was embedded in a head and body gel in the configuration that produced the most heating in a prior experiment. Fluoroptic temperature probes were placed at the device's distal tip and 20cm, 40cm (shoulder), 65cm, and 90cm proximal to the tip along with a background sensor. The phantom was scanned using a test spin echo sequence which allowed for the average specific absorption rate (SAR) to be varied from 0.25 to 4.0 W/kg, while holding other scan parameters constant. Further scanning was performed using short 2-minute clinical scans: T1 FSE, T2 FSE, DWI, T2 FLAIR, 3D-SPGR and b-SSFP. After each 2 minute scan period, the phantom was allowed to cool for 8 minutes. The clinical scan that produced the most heating was repeated over a 15-min acquisition. The catheter was then cut into 9cm, 18cm, 36cm and 72cm fragments and serially embedded in the phantom. Clinical scans from the previous experiment were repeated with temperature probes along the length of the catheter fragments.
Results: The maximal heating for the nitinol braided catheter immersed 93cm occurred at 20cm proximal to the tip using the T1 weighted FSE sequence for 1.5 T. Maximal heating at 3T occurred using the b-SSFP sequence at the same position in the phantom. The maximal temperature rise during a 2-min scan was 0.84°C at 1.5T and 0.45°C at 3T. Figures 1 and 2 show the temperature changes along different points on the catheter during 15-min scans. The same scans for fragment lengths of 9cm, 18cm, 36cm and 72cm produced maximal temperature (°C) rises of 0.68, 0.80, 1.70 and 1.07 at 1.5T, respectively. The temperature changes at 3T for these fragment lengths were 0.66, 0.83, 1.07 and 0.72, respectively.
Conclusions: This study provides information on the magnitude of focal heating induced in a head and body simulating a retained catheter scenario of a patient undergoing clinical scans at a range of SAR levels. Substantial heating of a nitinol braided catheter occurred and is a function of SAR level and geometric considerations. Although the catheter displayed higher heating levels at 1.5T relative to 3T at a given SAR, it should be noted that there are most likely differences between the SAR models on the two scanner interfaces. Furthermore, the 3T scanner used for this study had a wider diameter bore than the 1.5T scanner.

Figure 1

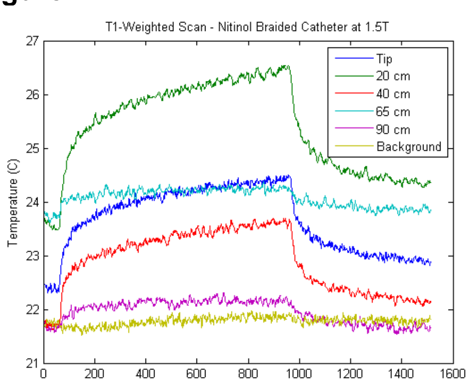

Figure 2

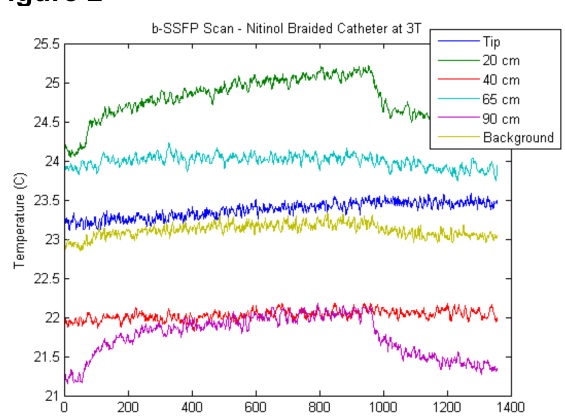

Image-Based Computational Simulations for Patient-Specific Fontan Surgery Planning

Christopher M. Haggerty[1], Maria Restrepo[1], Kirk R. Kanter[2], Timothy C. Slesnick[3], Jarek Rossignac[4], Thomas L. Spray[5], Mark A. Fogel[6], Ajit P. Yoganathan[1]

[1]Wallace H. Coulter Department of Biomedical Engineering, Georgia Institute of Technology and Emory University, Atlanta, GA USA
[2]Division of Cardiothoracic Surgery, [3]Division of Pediatric Cardiology; Department of Pediatrics, Emory University School of Medicine and Children's Healthcare of Atlanta, Atlanta, GA USA
[4]College of Computing, Georgia Institute of Technology, Atlanta, GA USA
[5]Division of Cardiothoracic Surgery, [6]Division of Cardiology; Children's Hospital of Philadelphia, Philadelphia, PA USA

Purpose The total cavopulmonary connection (TCPC) for single ventricle lesions creates adverse hemodynamics that are hypothesized to negatively impact long-term outcomes. Image-based computational modeling provides a novel means to pre-operatively evaluate blood flow characteristics and tailor the surgery to the patient-specific anatomy.

Methods Cardiac magnetic resonance (CMR) images are segmented to create patient-specific vascular models (i.e., bi-directional Glenn or existing TCPC connections) and reconstruct flow information. Then, a specially designed virtual surgery environment is used to mimic the Fontan procedure by simulating baffle placement. Blood flow simulations using computational fluid dynamics characterize hemodynamic metrics (i.e., power loss and hepatic flow distribution) to compare theoretical connection performances and provide input to surgical decision-making.

Results Computer-based surgical planning has been prospectively used for 19 patients, including 8 with a 'failed' existing Fontan connection. The primary indication for most cases was pulmonary arteriovenous malformations, which are believed to form in the absence of hepatic factor in the blood reaching pulmonary arterial segments. Thus, the modeling objective, as demonstrated by the figure below, was to optimally distribute hepatic blood flow to the lungs. Short-term follow-up has shown favorable clinical outcomes and consistency between model predictions and operative results.

Conclusions Computer-based surgery planning is an exciting new paradigm for patients with single ventricle lesions with the potential to deliver patient-specific benefit.

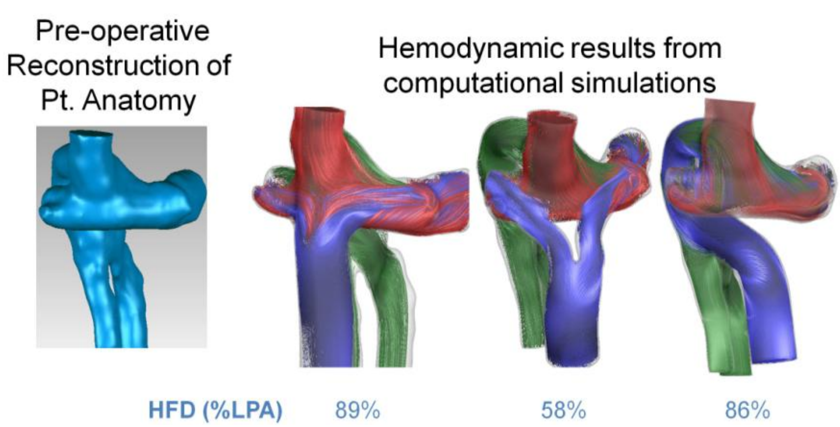

Intra-Arterial MRA based Roadmapping for Magnetically-Assisted Remote Control Catheter Tracking

Alastair J. Martin[1], Prasheel Lillaney[1], Maythem Saeed[1], Fabio Settlecase[2], Lee Evans[1], Mark Wilson[1], Steven Hetts[1]
[1]Department of Radiology and Biomedical Imaging, UCSF, [2]Sunnybrook Health Sciences Centre, Toronto, Canada

Introduction

We have been investigating magnetically-assisted remote control (MARC) endovascular catheters for interventional MRI procedures. MARC catheters contain microcoils on their tips that can be transiently activated by applying DC current [1]. The resulting magnetic moments created by the microcoils generate deflections that enable steering of the catheter into selected vascular structures. These steerable catheters have conductive elements running along their length and produce a magnetic field disturbance around the microcoils and wires when current is applied. While this magnetic field disturbance allows for passive visualization it also obscures the anatomy through which the catheter is being navigated. In this study we developed an alternate tracking approach that capitalizes on arterial access to generate selective intra-arterial angiograms that are used in a "roadmapping" mode to assure that vascular structures are not obscured when catheter deflections are applied. The concept is described and demonstrated in a swine model.

Methods

The technique is based on selective intra-arterial (IA) injections of dilute (1-2mM) gadolinium (Gd) contrast medium (Magnevist,) at the beginning of a dynamic MR angiographic acquisition. The angiogram is a thick slice 2D gradient echo sequence that can be obtained rapidly and requires only brief (~4s) IA Gd infusions (at 1-2cc/s) to highlight the vasculature. The low Gd concentration and short IA angiogram permits exceptionally low contrast doses and makes repeated evaluations practical. The initial angiogram is used as a roadmap that is subtracted from subsequent dynamic acquisitions, similar to conventional DSA practices. Keyhole methods are employed to increase the temporal resolution of the dynamic acquisition above that of the initial angiogram (typically>1fps). Advantages of this approach include the fact that local arterial anatomy is established at the outset and is retained throughout the acquisition period. It also permits very low SAR acquisitions which are necessary when catheters with conductive elements are present to minimize RF heating. Importantly, currents applied for catheter deflection, which produce considerable susceptibility artifact, will not obscure the previously established roadmap. The angiographic sequence is only moderately T_1-weigthed to allow for background signal that will be spoiled during microcoil activation, which will reveal microcoil position on the roadmap. The roadmapping approach was tested in a swine a model in which the carotid artery was accessed with a MARC catheter.

Results

The angiographic imaging protocol (FOV = 200X162mm, voxel dimensions = 1mm x 1mm x 8mm, TR/TE/α = 8.0ms/1.8ms/20^0, BW/pix = 192 Hz, SAR = 0.1 W/kg) was initially acquired in 1.3s while 2mM Gd-based MR contrast was injected at 2cc/s (Fig 1A). Subtraction of all subsequent frames began immediately and a keyhole factor of 60% was employed to achieve a frame rate of 1.33 fps. This balanced our ability to track smaller objects with an acceptable refresh rate. Blood flow rapidly washed out the IA injection (Fig 1B) to reveal the arterial roadmap on subsequent subtracted images (Fig 1, lower row). Activation of the MARC catheter produced a substantial artifact that scaled with applied current and locally obliterated imaging signal (Fig 1, C-E). The artifact created by MARC catheter activation was evident on subtracted images without obscuring the arterial anatomy, permitting catheter tracking during catheter deflection. Low level activation of the MARC catheter (10-50 mA) permitted catheter tracking without substantial deflection. Iterative updating of IA angiogram roadmaps permitted MARC catheter tracking over long distances and tortuous vessels.

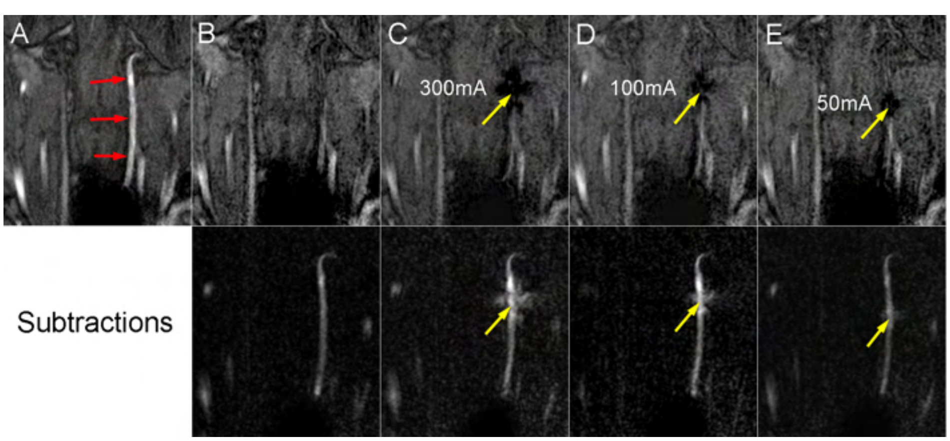

Figure 1: MARC catheter tracking is demonstrated in a swine carotid artery. In the first phase (A) a contrast enhanced MR angiogram is obtained via intra-arterial injection into the carotid to highlight local arterial structure (red arrows) and to create a mask for subsequent dynamics. Subsequent images are subtracted from the mask and reveal just the selected artery once the IA injection washes out (B). Activation of the deflection catheter at different current levels creates an artifact (yellow arrows) that obscures the local anatomy (upper row: C-E). Arterial anatomy is retained on the subtracted "roadmap" images (lower row) upon which the artifact generated by the MARC catheter can also be appreciated and tracked (yellow arrows).

Conclusions

IA MRA roadmapping is a simple, low SAR approach for tracking MARC catheters that allows for high temporal resolution. It requires minimal Gd dose, which allows for frequent roadmap updates, and does not obscure arterial anatomy during catheter deflection. The display is similar to digital subtraction X-ray angiography, which may ease adoption in the clinic.

Reference [1] Settecase F, Sussman MS, Wilson MW, et al. Magnetically-assisted remote control (MARC) steering of endovascular catheters for interventional MRI: a model for deflection and design implications. Med Phys. 2007 Aug;34(8):3135-42.

Catheters for Interventional MR: Fabrication of Micro-Coils for Catheter Tip Deflection

Prasheel Lillaney[1], Vincent Malba[1], Leland Evans[1], Anthony Bernhardt[1], Mark Wilson[1], Timothy Roberts[2], Alastair Martin[1], Maythem Saeed[1], Ronald Arenson[1], Steven Hetts[1]
[1]Radiology and Biomedical Imaging, University of California San Francisco, San Francisco, California, United States, [2]Radiology Department, University of Pennsylvania, Philadelphia, PA, United States

Purpose: Remote MR guidance of catheters for endovascular interventions has been the object of considerable research and development over the past ten years. The purpose of this work was to develop a microfabrication technique for catheter tips that could be utilized to deflect a catheter into targeted small vessels. The approach utilizes the static magnetic field of an MR system to interact with a magnetic moment created by passing an electric current through coils placed at the catheter tip.

Methods: We propose a lithographic technique to manufacture the coils, which we call LaserLathe. This method allows non-planar surfaces such as cylinders to be patterned with feature sizes as small as 5 um. Figure 1a shows a schematic of the LaserLathe apparatus. It consists of three high-precision translation stages (x, y, and z), and one high-precision rotary stage. The axis of the rotary stage is parallel to the translation of the x-stage. The "cutting tool" for the LaserLathe is a 405-nm, 50 mW diode laser. It doesn't actually cut; it is used to expose a positive photoresist. The z-stage is used to focus the beam by moving a microscope objective through which the beam is passing. With precision motion control of the stages provided by a Delta Tau PMAC card, any design can be patterned on the surface of the cylinder.

Results: The typical designs are shown in figures 1b and 1c, which illustrate the solenoid and racetrack coil designs. The single axis racetrack coil was tested in a water bath bifurcation phantom (figure 1 d-f) using a balanced SSFP MR imaging sequence (TR = 5.5 ms TE = 1.6 ms, 30º flip angle, 128 x 128 matrix, 5-6 mm slice thickness) to demonstrate navigation capabilities. Studies related to the heating issue of the activated catheter are underway.

Discussion/Conclusions: We have demonstrated proof of concept of a remote controlled deflectable catheter design that utilizes laser lithography to fabricate the catheter tips. The heat produced by the activated coil is also a concern, and current work focuses on safety issues related to measuring and reducing the heat generated to insure that there are no damaging effects in vivo.

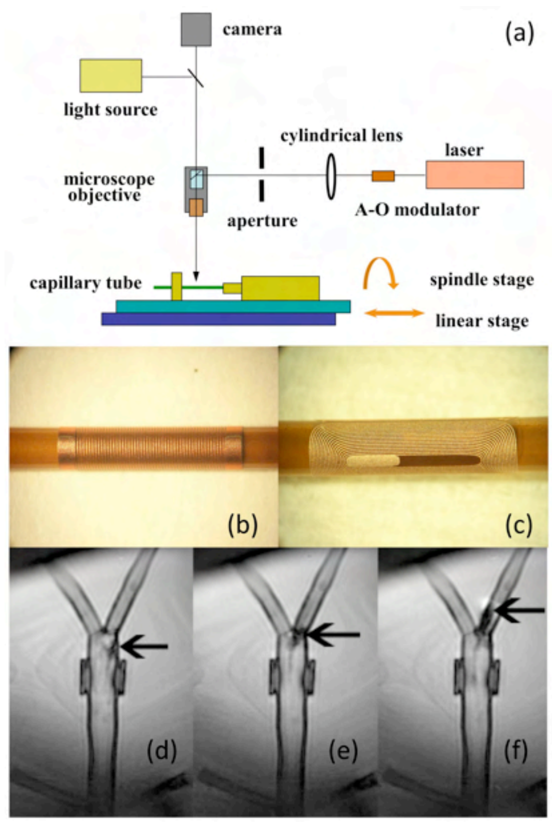

Fig. 1 (a) The LaserLathe apparatus. (b) 50-turn helical coil patterned on a 1.37 mm OD polyimide cylinder. 0.5 mm collars at each end are solder attachment pads. (c) 40-turn racetrack coil. There is a solder attachment pad at the center of the racetrack. (d-f) Frames from bSSFP imaging to test catheter navigation capabilities. A racetrack coil was used and the catheter was deflected towards the right bifurcation. The orientation of the static field vector is inferior to superior.

Feature Tracking for Image-guided Mitral Valve Repair

Martin Rajchl[1,2], Feng P. Li[1,2], John Moore[1], Chris Wedlake[1], Usaf Aladl[1] and Terry M. Peters[1,2]

Purpose: Recently, a guidance interface has been introduced (Moore et al., 2012) to facilitate minimally-invasive trans-apical mitral valve repair. It significantly improves guidance safety during tool navigation in the left ventricle and relies on the manual definition mitral valve hinge points from cross-plane echocardiography images. However, during trans-apical tool manipulation the mitral annulus can undergo substantial organ shift that requires manual re-initialization of the hinge points. We developed an algorithm to automatically update these points used for orientation purposes during tool navigation from the acquired echocardiography images. This paper presents the initial implementation of this algorithm within the navigation guidance platform for mitral-valve repair.

Methods: Our technique employs retrospective gating to identify the optimal cardiac phase and updates the point positions with a patch-based registration procedure. It is implemented on a GPU using CUDA architecture (NVIDIA, Santa Clara, CA) to facilitate rapid computations, thus freeing system resources for the underlying guidance interface.

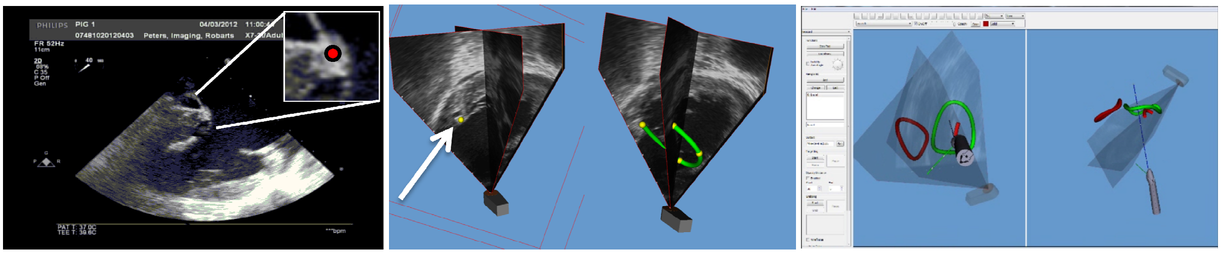

Figure 1: 2D echocardiography image with mitral valve hinge point (left), manual annulus identification and 3D representation via spline interpolation (mid) and the mixed-reality guidance interface described by Moore et al. (right).

Results: As demonstrated in Figure 1, preliminary retrospective studies from porcine ultrasound data indicate our algorithm is able to track mitral valve annulus hinge points effectively. While an extensive validation study has yet to be done, a visual assessment of the automatically updated points by an expert during intervention suggests the tracking error to remain within the clinically acceptable range of 5 mm.

Conclusions: Automated updating of mitral valve annulus points can avoid the need for manual redefinition of features and so reduce the overall required interventional time in minimally-invasive mitral valve repair.

[1]Robarts Research Institute; [2]Biomedical Engineering Graduate Program, Western University, London, ON

JT Moore et al. (2012) *A navigation platform for guidance of beating heart transapical mitral valve repair*, IEEE Trans Biomed Eng. (E-Pub)

Funding for this work was provided by Canadian Foundation for Innovation (20994), the Ontario Research Fund (RE-02-038) and the Canadian Institutes of Health Research (179298). We received additional funding from NeoChord Inc to support the animal laboratory research.

CT-Enhanced Ultrasound for Guidance of Off-pump Beating Heart Interventions

Feng P. Li[1,2], Martin Rajchl[1,2], John Moore[1], Chris Wedlake[1], Terry M. Peters[1,2]

Purpose: Guidance systems for off-pump beating heart interventions must show both cardiac anatomy and tissue motion. Echocardiography (ultrasound), because of its real-time imaging capability, flexibility, non-invasiveness, and low cost, is frequently employed in cardiac surgery as both a monitoring and imaging modality. However, safety concerns exist since it can be difficult for surgeons to appreciate the position and orientation of 2D images relative to a surgical tool, and to keep the tool tip and target in the image plane simultaneously. In our current work, developed to facilitate the repair of mitral valves in the beating heart[1], we employ CT images to provide high-quality 3D context to enhance ultrasound images, providing an enhanced guidance system with very few changes to standard workflow. We have also developed a method to generate synthetic 4D CT images, when dynamic pre-operative CT images are not available.

Methods: We describe an image-based method to register pre-operative CT image to dynamic intra-operative ultrasound using a rapid GPU-based implementation. The registered CT images can be visualized in a variety of ways according to user's requirements (Figure 1). When dynamic CT images are not available, we deform the static CT image, based on motion information extracted from the US images, to create synthetic dynamic CT images (Figure 2).

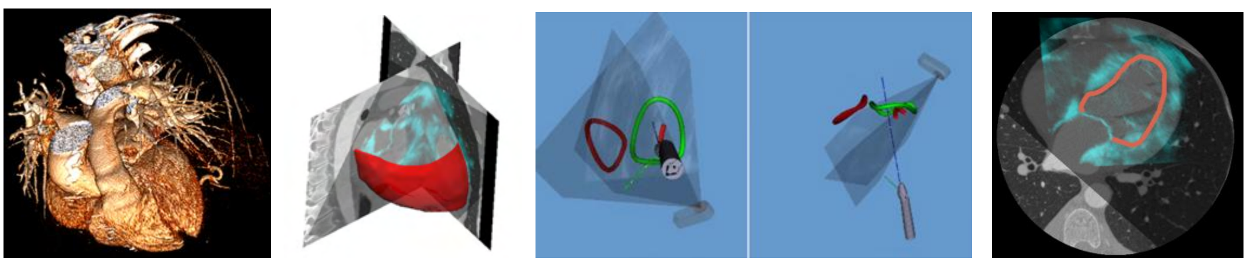

a b c d

Figure 1: Different visualization options: a) volume rendering, b) fused CT, US, and models from CT c) selected anatomy from CT fused with US d) direct overlay of CT and US

Results: Our approach can perform as many as 5-6 registrations per second with less than 5mm target registration errors. The synthetic 4D CT was validated by comparing it to an actual dynamic CT image, resulting in an average Dice metric of 0.82 and an average RMSE of 2.96mm with respect to the surface of the left ventricle.

Conclusions: We have demonstrated the feasibility of real-time registration of a static CT image to intra-operative ultrasound, to provide context for intra-cardiac interventions. In addition, the pre-operative CT can be dynamically updated, based upon motion models derived from the US image, to provide a realistic dynamic CT image as part of the navigation environment.

[1] JT Moore et al. (2012) *A navigation platform for guidance of beating heart transapical mitral valve repair*, IEEE Trans Biomed Eng. (E-Pub)

[1]Robarts Research Institute, [2]Biomedical Engineering Graduate Program, Western University, London, ON. Funding for this work was provided by Canadian Foundation for Innovation (20994), the Ontario Research Fund (RE-02-038) and the Canadian Institutes of Health Research (179298). We received additional funding from NeoChord Inc to support the animal laboratory research.

Interactive *Real-Time* Segmentation for Vertebral Bodies and Intervertebral Discs in Sagittal Planes

Jan Egger, Ph.D., Ph.D.[a,b,c], Tina Kapur, Ph.D.[a], Bernd Freisleben, Ph.D.[b], Christopher Nimsky, M.D., Ph.D.[c]

[a] Dept. of Radiology, Surgical Planning Lab, Brigham and Women's Hospital Boston, MA, USA, [b] Dept. of Mathematics and Computer Science, University of Marburg, Marburg, Germany, [c] Dept. of Neurosurgery, University of Marburg, Marburg, Germany

Purpose – Interactive segmentation approaches like [1, 2] get more and more popular, because automatic segmentation methods are typically only suitable for a specific type of pathology in a specific imaging modality and still fail time-by-time. Moreover, most automatic approaches need precise parameter settings to provide good results. The state of the art or rather clinical practice is in the most medical departments still manual slice-by-slice segmentations which are very time consuming. In this contribution, we present the initial results of an interactive graph-based approach for vertebral bodies and intervertebral discs segmentation that provides *real-time* feedback to the user during the segmentation process. The speed and *real-time* behavior makes this approach even suitable for MR-guided biopsies of vertebral bodies where several planes are used in planning and executing the interventions [3].

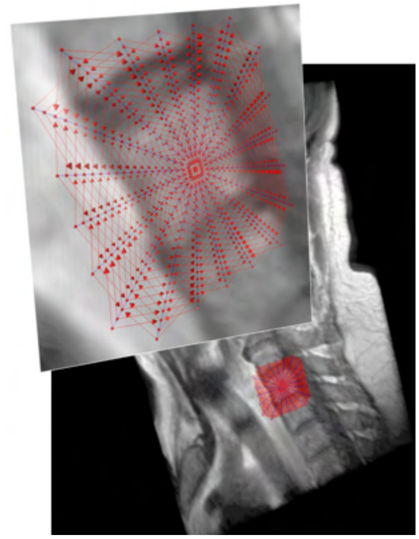

Figure 1 – Graph within a MRI dataset.

Methods – The *Square-Cut* scheme [4] was used and extended for this study. Briefly, the *Square-Cut* algorithm sets up a directed 2D-graph *G(V,E)* in two steps: (I) sending rays through the surface points of a square template and (II) sampling the graph's nodes $n \in V$ along every ray (Figure 1). In addition, a set of edges $e \in E$ is generated, which consists of edges between the nodes and edges that connect the nodes to a source *s* and a sink *t*. After graph construction from a user defined seed in the image (which is the square's center), the minimal cost closed set on the graph is computed via a polynomial time *s-t-cut* [5], which results in the segmentation outcome. For an initial study we implemented a C++ module within the prototyping platform *MeVisLab* (http://www.mevislab.de).

Results – With our interactive segmentation technique the user gets *real-time* feedback of the segmentation result. To demonstrate our technique and for an initial feasibility study we implemented an interactive version to segment vertebrae (discs) in 2D. Therefore, we applied a graph-based method that uses a square template like presented in [4] and made it interactively by allowing the user to move the graph's center point over the image. This could be achieved in *real-time* for a graph consisting of 900 nodes, 870 *z*-edges and 900 (1800) *xy*-edges (template diameter was 35mm, 30 rays, 30 points-per-ray and a delta value of 5). Figure 2 below illustrates – from the left to the right – how the user can interactively move the graph's center point (white dot) to find satisfying segmentations (red dots) by getting on the same time *real-time* feedback.

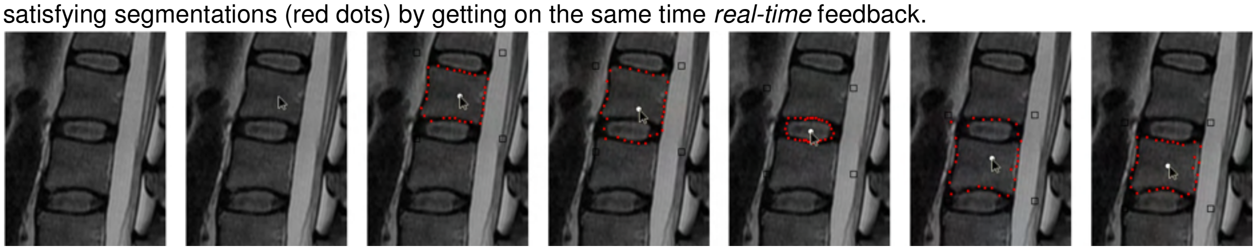

Figure 2 – From left to right: several screenshots from a video demonstrating our interactive *real-time* segmentation for vertebral bodies and intervertebral discs in a sagittal plane of a MRI scan. The white dot is the graph's center point, the black boxes define the corners of the square template and the red dots are the segmentation outcomes.

Conclusions – In this initial study, we showed that the *Square-Cut* scheme can be used as an interactive approach for vertebral body and intervertebral disc segmentation in sagittal planes. However, the presented principle can also be applied to other images and dimensions (e.g. non-medical, color-level, 3D) and potential application examples for different templates in 2D and 3D are presented in [6]. In a next step, we plan to extend the interactive approach to 3D for vertebral body segmentation based on a cubic template [7].

Acknowledgements

The authors would like to thank Fraunhofer MeVis in Bremen, Germany, for their collaboration and especially Professor Dr. Horst K. Hahn for his support.

References

[1] Y. Boykov, et al. Interactive Graph Cuts for Optimal Boundary & Region Segmentation of Objects in N-D Images. ICCV, 105-112, 2001.
[2] S. Steger, G. Sakas. FIST: Fast interactive segmentation of tumors. Abdominal Imaging, Vol. 7029, Springer, pp. 125-132, 2011.
[3] E. Salomonowitz. MR imaging-guided biopsy and therapeutic intervention in a closed-configuration magnet: single-center series of 361 punctures. AJR Am J Roentgenol. 2001 Jul;177(1):159-63.
[4] J. Egger, et al. Square-Cut: A Segmentation Algorithm on the Basis of a Rectangle Shape. PLoS One. 2012; 7(2):e31064.
[5] Y. Boykov, V. Kolmogorov. An Experimental Comparison of Min-Cut/Max-Flow Algorithms for Energy Minimization in Vision. IEEE Transactions on Pattern Analysis and Machine Intelligence, 26(9), pp. 1124-1137, 2004.
[6] J. Egger, et al. *Template-Cut: A Pattern-Based Segmentation Paradigm*. Scientific Reports, Nature Publishing Group, 2(420), 2012.
[7] R. Schwarzenberg, B. Freisleben, R. Kikinis, C. Nimsky, J. Egger. [A Cube-Based Approach to Segment Vertebrae in MRI-Acquisitions]. In: Proceedings of BVM, Heidelberg, Germany, Springer Press, 6 pages, accepted, March 2013.

Osteochodritis dissecans of the knee; MRI guided retrograde drilling at 1.5 T and first clinical outcomes in pediatric patients.

Roberto Blanco Sequeiros MD, PhD , Matti Vähäkari MD, Pekka Kerimaa MD, Risto Ojala MD, PhD, Juha J. Sinikumpu MD, Jussi Korhonen MD, PhD, Osmo Tervonen MD, PhD

Institutions: Oulu University Hospital, Departments of Radiology and Pediatric Surgery, Oulu, Finland.
email:roberto.blanco@oulu.fi

Objective:

The purpose of this study was to evaluate the feasibility and first clinical results of percutaneous high field MRI-guided retrograde drilling for the treatment of juvenile osteochondritits dissecans (JOCD) of the femur.

Introduction:

Femoral osteochodritis dissecans (OCD) is relatively common cause of persistent knee pain in pediatric population. Magnetic resonance imaging (MRI) is invaluable in determining the location and the stability of the lesion, the classification of the lesion is performed using a four step staging system. Operative treatment is standard but more invasive and leads to increased risk of development of early osteoarthritis. For this reason retrograde drilling of the lesion through femoral bone is preferred by some authors. MRI presents as promising tool in intraoperative minimally invasive orthopedic procedures. The purpose of this study was to evaluate the preliminary clinical feasibility of MRI to guide therapeutic retrograde drilling of the JOCD of the femur.

Materials and Methods

7 JOCD lesions of the femur (mean age 12 y) (fig.1A), unresponsive to conservative therapy, were treated with MRI-guided percutaneous retrograde drilling (3 mm drills) (fig.1B). All the patients had limitation of activity due to the OCD related pain. A 1.5 T wide bore MRI scanner (Siemens Espree, Erlangen, Germany) was used. Mean postprocedural follow up time was 14 months.

Results: All the OCD lesions were succesfully drilled without complications. Mean time was 58 minutes. All patients had pain relief, mean pain score declined from 7 to 2. Follow up MRI showed ossification in 5 lesions (fig.1C-D).

Conclusion

MR-guided retrograde drilling is accurate and feasible method in the treatment of the juvenile OCD lesion of the femur.

Figure 1.

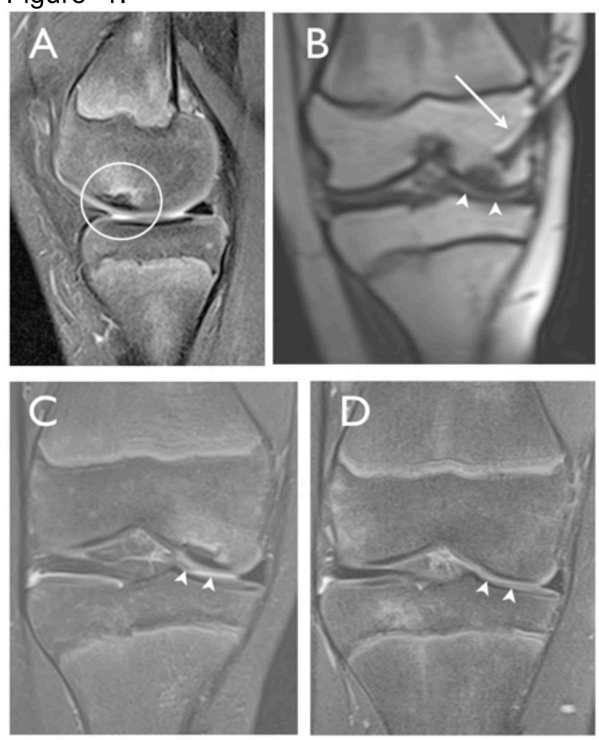

Figure 1 (a) A preoperative sagittal MRI image (1.5 T) depicting medial JOCD lesion (oval) of the femur. (b) A coronal intraoperational MRI (1.5T) image shows MRI guided drilling of the femoral OCD lesion. Drill appears as an oblique signal void (arrow) approaching the lesion with sclerotic margins (arrowheads).
(c) An axial preoperative MRI (1.5T) shows an odematic OCD lesion (d) An axial post-operative MRI at 4 months (1.5T) shows total ossification of the JOCD lesion. The patient was free of any symptoms.

In vivo treatment of spine tumors using needle based therapeutic ultrasound under image guidance with 3D electromagnetic tracking

Goutam Ghoshal[a], Tamas Heffter[a], Emery Williams[a], Corinne Bromfield[b], Serena Scott[c], Laurie Rund[b], John M. Ehrhardt[b], Chris J. Diederich[c], E. Clif Burdette[a]

[a]Acoustic MedSystems, Inc., Savoy, IL, USA
[b]Department of Animal Sciences, University of Illinois, Urbana, IL, USA
[c]Department of Radiation Oncology, University of California, San Francisco, CA USA

Purpose: Spinal metastatic disease and multiple myeloma affects over 600,000 people every year in the United States and cause progressive bone destruction that results in incapacitating pain, fractures, and the inability to walk. Minimally invasive thermal therapies such as RF and ultrasound ablation techniques have proven to be effective for treating tumors outside the spine. The successes of such treatments rely on accurately controlling the direction and shape of the ablated region and avoid damaging anatomical sites such as the spinal cord. The purpose of the present study was to use a high intensity interstitial ultrasound ablator under ultrasound image and electromagnetic (EM) tracking guidance to ablate tissue near the lumber vertebrae in pig.

Methods: Needle/catheter based interstitial ultrasound applicator of center frequency of 6-7 MHz was used to ablate 5 mm away from the dorsal process in the region at intersection of dorsal and transverse process in pig under gas anesthesia. Temperature sensors were placed at two different locations to estimate thermal distribution in the three-dimensional treated volume. The ultrasound imaging was acquired using a SonixTouch (Ultrasonix, Richmond, BC, Canada) system with an L14-5/38 GPS probe combined with EM tracking system to guide the insertion of the applicator (Fig. 1). An in-house software system for image processing and control was developed to communicate with the hardware, ultrasound imaging, tracking system, and treatment control.

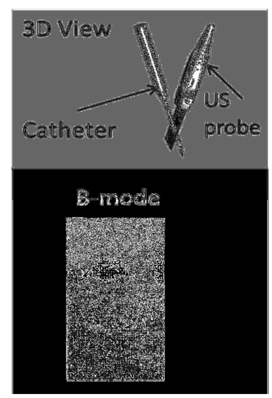

Figure 1: Image guided with EM tracking for applicator insertion.

Results: The ultrasound applicator was successfully inserted as per treatment plan using combined ultrasound imaging EM tracking guidance system. During treatment a maximum temperature of 60-70 ℃ and dose of 10^5-10^7 equivalent minutes at 43℃ was observed at a distance 10 mm from the center of the ablation transducer for a treatment time of 5-7 minutes. The dose distribution was analyzed and compared with the gross pathology (Fig. 2) of the treated region.

Conclusions: The experimental results demonstrated that the directionality and shape of the ablation zone can be controlled using the proposed technology of angularly-sectored tubular ultrasound transducers. This preliminary study shows the feasibility of ablating tissue near the vertebrae and in vertebral body successfully without damaging the spinal cord.

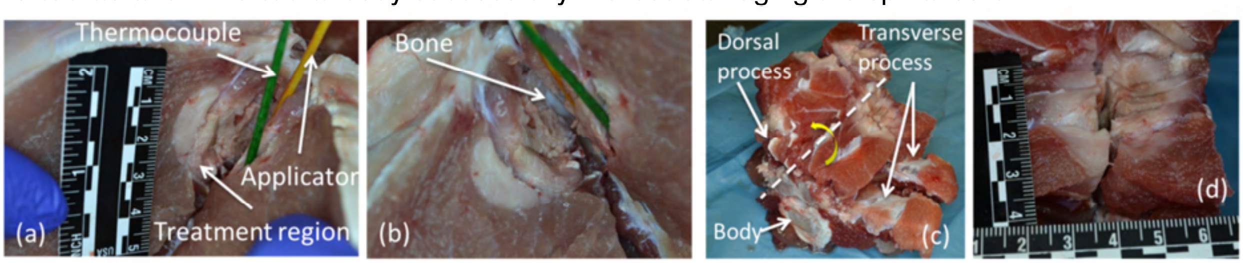

Figure 2: Gross pathology of the ablated muscle tissue near the spine with 360° pattern applicator showing (a) applicator, thermocouple position, and treatment zone, (b) the location of the bone and the ablated region, (c) anatomical sites of the spine and the treatment region (white dashed line indicate the line of cut for the tissue and yellow curved arrow indicate the directions tissue section was parted open to visualize the ablated region), and (d) a 3 cm by 3 cm cross-sectional area of the ablated region.

An integrated ultrasound-guided, magnetic-tracked, spine needle system

Elvis C.S. Chen and Terry M. Peters

Robarts Research Institute, London, Ontario, Canada

Purpose: Several surgical interventions such as lumbar puncture involve the careful placement of a long hollow needle into regions of anatomy containing complex structures. Ultrasound has been shown to be an effective aid to guide these needle insertions, but has yet to receive wide adaptation in the clinical setting due to several technical challenges. An Augmented-Virtuality (AV) needle navigation system is proposed, comprising a magnetic tracking system (MTS), a needle assembly, a needle calibration jig, an ultrasound machine, and the guidance software. Both the ultrasound transducer and needle assembly are tracked and spatially-calibrated using the MTS, and visualized in the guidance software in real-time. Streaming ultrasound images are shown with respect to the ultrasound transducer, providing a 3D context of the anatomy.

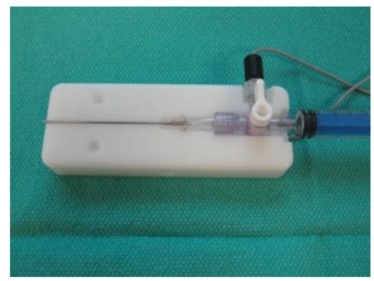

Methods: A commercial MTS (Aurora, NDI, Canada) with 6DOF magnetic sensors was employed to track needle. An US transducer with an integrated 6DOF sensor was calibrated using a line-fiducial phantom. The needle assembly compromises of the metal needle, a surgical syringe, and a Luer-lok™, T-connector with a 6DOF sensor integrated into the male Luer taper. The needle assembly was calibrated using a custom calibration jig. The guidance software employs the real-time tracking information and renders the virtual representation of the US transducer and the needle assembly in a common coordinate space. Streaming US images are displayed with respect to the rendered transducer. A virtual "laser pointer" line is extended along the shaft away from the tip of the needle to indicate the needle trajectory. Two modes of visualization are provided. In the "freehand" 3D mode, the virtual camera can be freely moved to any vantage point, while in the "conventional" 2D mode, the transducer and streaming US image are rendered at a stationary pose. Switching between two modes is triggered by a foot-pedal. The guidance software and the MTS system are integrated into the operating software platform of US machine (Ultrasonix, Canada).

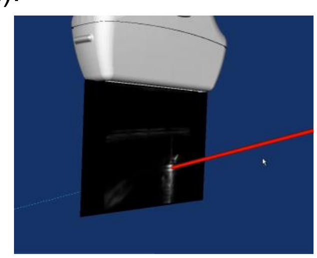

Results: Both junior and senior anesthetists will be recruited and training to use this system. Quantitative measures such as number of attempts, time to completion, and user-preference between 2D/3D modes, will be collected and analyzed.

Conclusions: A fundamental design criterion for this guidance system was to employ standard surgical instruments, thus avoiding the expensive commercial MTS-tracked needle and to allow standard hollow needle to be used. The use of hollow needle is of particular importance for certain surgical techniques where the passage of fluids/air is essential for performing the procedure. A potential limitation of this system is that the bending of the needle shaft and thus the displacement of the needle tip are not accounted for. The advantage is the ability to visualize needle advancement even when the needle is not in the plane of the US image, which can greatly facilitate a targeting task.

The Perk Tutor Training Platform Integrated with Simulated Ultrasound

Laura Bartha, Andras Lasso, Csaba Pinter, Tamas Ungi, and Gabor Fichtinger
Percutaneous Surgery Laboratory, School of Computing, Queen's University, Kingston, ON

Purpose: To aid in the training of ultrasound-guided needle placement techniques, the Perk Tutor (Fig.1) open-source training platform was previously developed (Ungi *et al*. TBME 2012). Until recently, the Perk Tutor was coupled with an ultrasound machine to acquire the images, making Perk Tutor a rather expensive scheme. We propose to simulate real-time ultrasound imaging from a surface mesh model, thereby removing the need for an ultrasound machine. We hypothesize that mesh-based imaging without elaborate simulation of biological speckle is suitable for spinal musculoskeletal applications, where the target is not covered with thick layers of soft tissue. The work presented here integrates the simulated ultrasound with the Perk Tutor.

Methods: The simulated ultrasound is generated using surface meshes to represent all objects, both anatomy and surgical tools, to appear in the simulated image. The pose of the meshes is represented using linear transforms, in this case, originating from a tracker. This simulation is implemented as a part of the PLUS (the Public Library for Ultrasound, www.plustoolkit.org) software package, which the Perk Tutor already employs for ultrasound image acquisition and position tracking data collection. PlusServer, an application within PLUS, is used to connect the video source, being the simulated ultrasound, with the position information originating from the tracker via the OpenIGTLink network protocol (Tokuda *et al.*, Int. J. Med. Robot. 2009). These two pieces of information are sent to 3D Slicer (www.slicer.org) to visualize the training scenario. In 3D Slicer, the OpenIGTLink connection is established with the use of an OpenIGTLink module, and visualization of the simulated ultrasound is made possible using the Volume Reslice Driver, available as an extension to 3D Slicer.

Results: The integration of Perk Tutor and simulated ultrasound was demonstrated on a spinal needle placement training phantom. An electromagnetic tracker, the Ascension trakSTAR, was connected to the computer and provided position information. The ultrasound images were generated at a speed of 50 frames per second, and a resolution of 820 x 616 pixels on a Windows PC with a 3.4 GHz processor. As the tracking tool moved, the virtual transducer on the screen moved smoothly and it generated the ultrasound images in real-time (Fig 2.).

Fig. 1: Perk Tutor in spinal intervention training

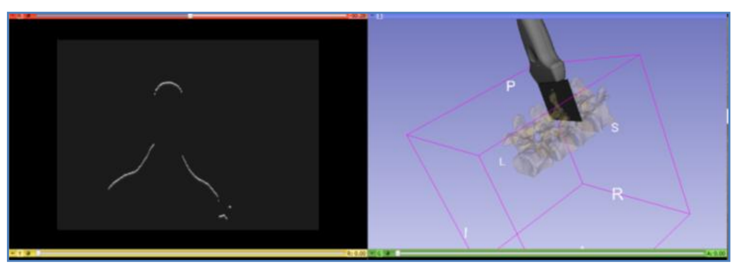

Fig. 2: Simulated ultrasound image of a spine in the Perk Tutor

Conclusion: The Perk Tutor training system has been equipped with simulated ultrasound and is functioning in real-time at 50 frames per second. Real-time simulation and rendering of the surgical tools (such as needles) in the ultrasound image is currently a work in progress. The effectiveness of the simulated ultrasound-enabled needle placement training environment will be determined in the forthcoming human operator performance study. Previous studies with the Perk Tutor (Ungi *et al*., TBME 2012; Moult *et al.*, IJCARS, in press) showed the effectiveness of the Perk Tutor as a training tool in ultrasound-guided spinal needle placement. The forthcoming study will compare the performances of novice trainees in spinal needle placement procedures using the Perk Tutor with real ultrasound versus simulated ultrasound imaging. We expect the simulated ultrasound to be especially suitable for early phase training.

MOBILE IMAGE OVERLAY SYSTEM FOR IMAGE GUIDED INTERVENTIONS

M. Anand[1], T. Ungi[1], T., A. Lasso[1], P. U-Thainual[1], J. Jayender[2], J. Fritz[3], J. A. Carrino[3], F. A. Jolesz[2], G. Fichtinger[1,3]

[1]Queen's University, [2]Harvard Brigham and Women's Hospital, [3]Johns Hopkins University

Purpose: An image overlay guidance system has been proposed previously for aiding needle placement interventions [1, 2]. In this technique, a 2D computer display image is reflected by a semi-transparent mirror, so that the virtual image appears floating inside the patient in correct 3D position. This concept provided accurate transverse image guidance for musculoskeletal interventions of the shoulder, hip and spine [3, 4, 5, and 6]. The previous, static mounting of the system was either fixed to the CT/MR imaging system or on a floor-mounted frame over the patient table. This mounting required careful calibration before each procedure, and was prone to misalignments due to structural deformation or unintended physical contact with the device. Furthermore, the static mount limited the access to the patient and excluded clinically relevant ranges of motions of the tool and the physician. To overcome those limitations, we propose the Mobile Image Overlay System (MIOS).

Methods: The MIOS consists of a 2D image overlay system, similar to the one used in [1] and it is attached to a floor-mounted articulated arm (Figure 1). The physician moves the MIOS freely over the patient. It is equipped with optical markers to report its pose during the entire procedure. Another optical marker is fixed to the patient for co-registration of scanned images and the MIOS. After imaging, the physician performs the surgical planning, and the MIOS is positioned over the target anatomical region. Depending on the tracked position of the MIOS, the software displays the correct image on the overlay monitor. Therefore, the image is virtually displayed inside the patient, providing image guidance to the physician while seeing through the mirror. At any desired position, the MIOS can be locked firmly.

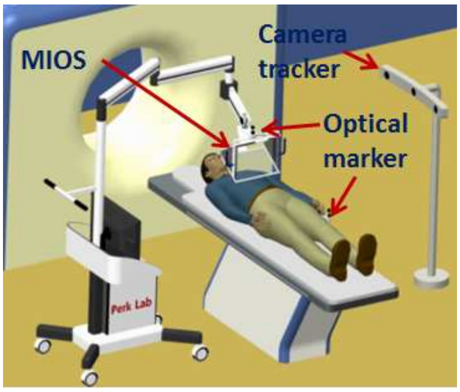

Fig1: MIOS concept

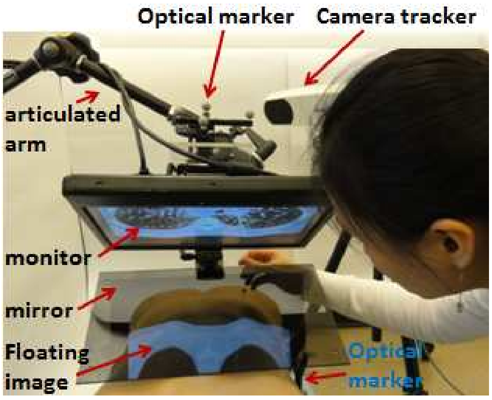

Fig2: MIOS prototype

Results: The MIOS concept is shown in Figure 1 along with the tracker camera. The first prototype developed for demonstrating the proof of concept is shown in Figure 2 and shall be used to conduct phantom experiments and define system ergonomics. For the articulated arm, we plan to mount the image overlay system on an arm similar to the one used in the Calypso system, (Calypso Medical Systems, USA). The following generation of MIOS will be also MRI-compatible.

Conclusion: Based on successful pre-clinical testing of the static image overlay system, the mobile image overlay promises to become a useful tool for image-guided interventions, such as musculoskeletal needle injections, parathyroidectomy, percutaneous nephrolithotomy and percutaneous access to blood vessels.

References: **[1]** Fichtinger *et al., IEEE transactions on biomedical engineering, 52(8), 2005*; **[2]** Weiss *et al., American Journal of Roentgenology, vol.196, 2011*; **[3]** Fischer *et al., Journal of Computer Aided Surgery, 12(1), 2007;* **[4]** Fritz *et al., American Journal of Roentgenology, 198(3), 2012;* **[5]** Fritz *et al., European Radiology, 23(1), 2013*; **[6]** Fritz *et al., Investigative Radiology, 48(6), 2013.* *(This work was jointly funded by the NIH R01 CA118371, the Natural Sciences and Engineering Research Council of Canada and Cancer Care Ontario.)*

Deformable Registration of Prostate MRI using Statistical Deformation Modeling

A.M. Tahmasebi[1], R. Sharifi[1], H.K. Agarwal[1], B. Turkbey[2], M. Bernardo[2], P. Choyke[2], P. Pinto[3], B. Wood[4] and J. Kruecker[1]
1. Philips Research North America, NY, USA.
2. Molecular Imaging Program, NIH, Bethesda, MD, USA.
3. Urologic Oncology Branch, NCI, NIH, Bethesda, MD, USA.
4. Center for Interventional Oncology, NCI and Radiology and Imaging Sciences, Clinical Center, NIH, Bethesda, MD, USA.

Purpose

The introduction of endorectal coils (ERC) in prostate MR imaging provides high-resolution anatomical detailing of the prostate. The integration of MRI into radiation treatment planning has proven to improve the outcome of the treatment by achieving targeted boosted radiation without increasing the radiation to normal tissue. However, the use of ERC in MRI causes deformation of the prostate shape posing a challenge in image registration, e.g. for the purpose of interventional guidance, and in particular for multi-modality registration. In this work, we present a model-based technique for accounting for the deformation of the prostate gland due to ERC.

Methods

The proposed technique consists of a training phase and an estimation phase. In the training phase, a set of deformed (ERC-MRI) and non-deformed (MRI without ERC) prostate image data are used to generate the deformation model of the prostate. Deformation field maps are calculated from intensity-based nonlinear registration of without ERC (w/oERC) to with ERC (wERC) MRI. Principal component analysis (PCA) is then utilized on the resulting deformation fields to extract the statistical mean deformation as well as the most significant modes of deformation for every point of the prostate. Given a new registration problem, first a nonlinear registration is calculated for a limited number of corresponding landmarks in both modalities (such as surface contour points or other anatomical landmarks such as urethra). The deformation field values at the known points are then used to calculate the eigen coefficients corresponding to the deformation modes. Finally, an estimate of the deformation field for every point constituting the prostate gland is computed as the summation of the mean deformation plus a linear combination of the deformation modes with the calculated eigen coefficients.

Results

wERC and w/oERC T2-weighted MRI available from 72 patients were used in this study. The imaging study was approved by the institutional review board of the National Cancer Institute of the National Institutes of Health. In order to validate the accuracy of the proposed technique, two comparisons were performed: First, a leave-one-out (LOO) cross-validation scheme was utilized. Out of 72 datasets, one dataset was excluded at a time and the rest were passed through PCA to generate the eigen deformation modes. The displacement field values at surface points from the excluded data together with the resulting mean displacement field and eigenvectors from the PCA were used to estimate the displacement field at the rest of the voxels. Second, a binary-mask-based BSpline registration was also calculated between every pair of segmented prostate binary images from w/oERC and wERC. As the gold standard for the comparison, the deformation fields from the intensity-based BSpline registration between w/oERC and wERC prostate images were used. The mean estimation error from LOO analysis was 0.99 *mm* for the model-based approach compared to a mean error of 3.5 *mm* for the binary-mask-based registration.

Conclusions

Pure surface-based nonlinear registration of the prostate, as often encountered in interventional multi-modality guidance settings, may suffer from limited accuracy. A novel registration method using statistical deformation modeling more accurately predicts volumetric prostate deformation based on surface registration, and thus improves overall registration accuracy. This approach may prove advantageous in multi-modality registration settings in which direct intensity-based registration is not feasible.

Prospective Evaluation of Simultaneous PET/MRI and PET/CT in Cervical Cancer

P. Grigsby,[1,2] K. Fowler,[2] B. Siegel,[2] F. Dehdashti[2]

[1]Washington University School of Medicine, [2]Mallinckrodt Institute of Radiology

Purpose: The objective of this study was to compare the findings of whole-body FDG-PET/CT to whole-body simultaneously acquired FDG-PET/MRI in patients with cervical cancer.

Methods: A prospective institutional study was performed in which whole-body FDG-PET/CT was obtained for routine clinical evaluation and was then immediately followed by whole-body PET/MRI. We studied 44 patients with cervical cancer: 10 for initial staging, 30 for routine follow-up, and 4 to assess tumor response during the course of initial therapy. Patients underwent a single FDG injection. The administered activity of FDG ranged from 12.1 to 19.3 mCi (mean, 14.9 mCi). PET/CT was performed on either a Biograph 40 HD or a Biograph mCT scanner per our standard clinical procedure after which the patients underwent PET/MRI on a Biograph mMR scanner Attenuation correction was performed with a dual-echo VIBE Dixon sequence that separates water and fat with TE1/TE2 = 1.23msec/2.46 msec, TR = 3.6 msec, left-right FOV = 500 mm and anterior-posterior FOV = 300 mm. A high-resolution DWI acquisition was also performed. Additional high resolution small field of view TSE T2 imaging was performed for the pelvis.

Results: All sites of metabolically active cervical cancer identified on PET/CT were also identified on PET/MRI. No additional sites of disease were identified on PET/MRI. In 3 of 10 patients with a new diagnosis of cervical cancer the PET/MRI significantly clarified the anatomic site of disease visualized on PET/CT. In 2 of these patients there was inability to distinguish on PET/CT whether tumor was in the ovary versus pelvic lymph node, and this was readily clarified on PET/MRI. For the third patient, PET/MRI clarified omental metastases that were not readily localized on PET/CT. Additionally, localization of the metabolically active disease in the cervix was readily identifiable.

Conclusion: Simultaneous PET/MRI is feasible in patients with cervical cancer. PET/MRI findings show all sites of disease seen on PET/CT. PET/MRI has better soft tissue contrast than does PET/CT. Radiation dose to patients is less with PET/MRI than with PET/CT.

Real-Time 3D Needle Shape Tracking Using Fiber Bragg Grating Sensors for Prostate Percutaneous Interventions

Reza Seifabadi[2,1], M.Sc.; Esteban Escobar Gomez[1], B.Sc., Fereshteh Aalamifar[1], M.Sc., Gabor Fichtinger[2], PhD; Iulian Iordachita[1], PhD
[1]Johns Hopkins University, Baltimore, MD
[2]Queen's University, Kingston, Canada

Purpose

During prostate needle insertion, the gland and therefore targets move resulting in targeting inaccuracy. To compensate for this error, in a previous study we proposed robotic bevel-tip needle steering under live MRI. One important drawback is that tracking a flexible (20G) needle under real-time MRI is inaccurate due to the needle artifact and the image update frequency is relatively slow (>200 ms). As an alternative solution, we embedded some FBG strain sensors along the needle shaft at certain locations and reconstruct the needle shape from this information. Compared to the previous study on this topic by others, the following development have been done: 1) this study is extended to needle of higher gauge (thinner), 2) we guarantee below 0.5 mm accuracy at the needle tip for *all insertion depth*, 3) we extended it to bevel-tip needles (through modelling and mathematical formulation), 4) we visualized the 3D shape of the needle in 3D Slicer which is a commonly used planning and navigation software for prostate interventions, 5) our needle tracking is real-time.

Methods

Figure 1 shows an overview of the methodology. In order to estimate the needle 3D shape, the needle curves in *x-y* and *x-z* planes (*x* is the needle axis) should be estimated individually. For this reason, we measure the strain at three certain locations along the needle (x_1, x_2, and x_3) for each plane. Strain has linear relationship with the second derivative of the curve and consequently it is possible to estimate the *x-y* and *x-z* curves. This means two fibers, each with 3 FBGs with different wavelength are required. An identical extra fiber (again with 3 FBGs) is added for temperature compensation (i.e. finally in 120 degree configuration in cross section view - Fig. 1). The fibers were embedded into the inner stylet. The optimum locations of the FBGs were found from mechanical modeling of the beveled needle followed by computer simulations. After building the needle, we connected the fibers to an FBG interrogator to attain wavelength shift for each FBG. Through a novel calibration procedure, the wavelength shift of each FBG was related to the corresponding strain value. We post processed the strain data in MATLAB and generated 3D curve equation for the needle. Eventually, the needle curve equation was sent from MATLAB to 3D Slicer for visualization. The communication of MATLAB and 3D Slicer was established using OpenIGTLink.

For calibration and evaluation, a setup as showed in Fig. 2 was prepared. The needle was held by a pin vise attached to a 2-DOF (linear/rotary) micro-stage (Fig. 2). The stage can translate vertically with 10 µm resolution thus enabling needle-tip deflection with high accuracy. The rotary stage with 1º resolution provided rotation of the needle for enabling deflection in different planes. In order to detect the first moment of starting deflection, a scale with 0.001grams resolution was used. A sharp blade was placed on top of the scale to enable point contact between the scale and the needle. The needle tip was deflected from 0 up to10% of the needle cantilever length. This experiment was repeated for three depths, (27mm, 75mm, 110 mm) and for two angles (θ=0° and 90°, where θ is the needle orientation).

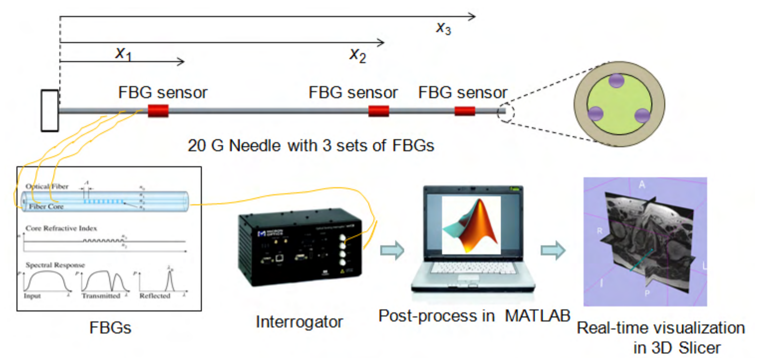

Figure. 1. Real-time needle 3D shape tracking using FBGs and visualization in 3D Slicer

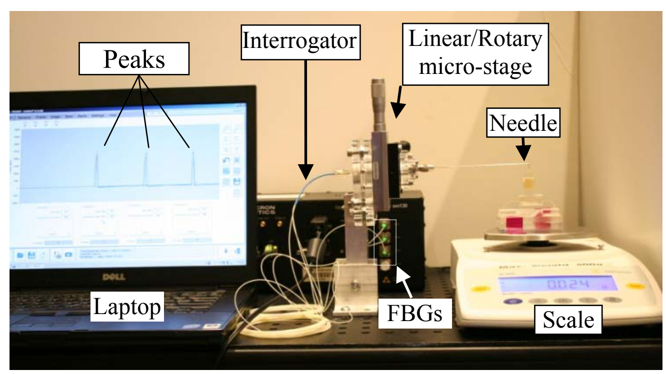

Figure 2. Calibration and experimental setup.

Results

The optimal locations of the sensors were found to be x_1= 30 mm, x_2=79 mm, x_3=99 mm after mechanical modeling of the beveled needle and computer simulations. Three calibration matrices (each 3x2) were found for each location. Based on them, the needle shape and tip location in 3D were estimated. The estimated results then were compared to the actual translation of the micro-stage. The errors were below 0.5 mm for all cases with the exception of depth= 110 mm at 0 degree (max- 0.8 mm).

Conclusions

In this study we developed a needle tracking system using FBG sensors for flexible bevel-tip needles. The needle was specifically designed for a real scenario, i.e. robot-assisted bevel-tip needle steering under MRI guidance for prostate interventions. Results showed needle tip tracking error below 0.5 mm in all insertion depths, covering all clinically relevant insertion depths in transperineal prostate needle placement procedures. These results prove the feasibility of this needle tracking approach.

Transperineal prostate biopsy: update on multireader, multiparametric navigated interventions

Tobias Penzkofer, Kemal Tuncali, Andriy Fedorov, Junichi Tokuda, Sang-Eun Song, Fiona Fennessy, Nobuhiko Hata, Clare Tempany
Surgical Planning Laboratory, Department of Radiology, Brigham and Women's Hospital, Harvard Medical School, Boston, USA

Introduction: Prostate cancer diagnosis and detection remains a clinical dilemma, many indolent cancers are over diagnosed and treated. Transrectal ultrasound is performed without lesion/target guidance. While many cancers detected are of low aggressiveness and can be followed by surveillance protocols, there is still a need to distinguish these from aggressive forms of the cancer. Prostate MRI is the modality of choice to detect and - through precisely targeted biopsies - correctly stratify patients. We have established a MR imaging and targeted in bore biopsy protocol. This involves a joint effort as a multiparametric, multireader workflow for navigated MRI-guided prostate biopsies at NCIGT. We report the current status of this 3T MR guided prostate biopsy program.

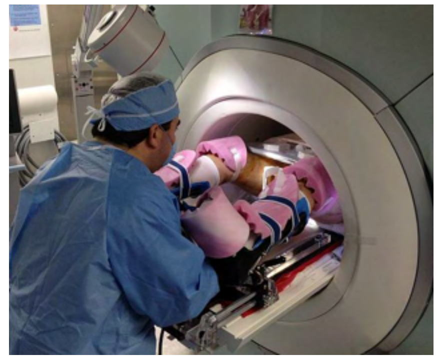

Fig 1: In-bore setup for MR guided prostate biopsies in the AMIGO suite

Materials and Methods: To date we have enrolled 49 men who underwent MRI-guided prostate biopsies. Prior to all biopsies three radiologists analysed all images and identified and rated all suspicious areas within the prostate gland based on pre-procedural 3.0T MRI. On review of our population, there were 30 men referred due to rising PSA levels and at least one negative TRUS biopsy or recent PSA re-elevation after previous prostate cancer treatment (n=19). The images/lesions were rated for the degree of suspicion based on T2-weighted, diffusion-weighted and semi-quantitative as well as quantitative pharmacokinetic maps. In total 204 suspicious lesions were identified, on average 4.2 ± 1.8 per patient. 77% of the biopsies were conducted in the advanced multimodality image guided operation (AMIGO)-suite, 23% in a similar free standing magnet (3.0T wide-bore, Siemens Verio, Germany, Figure 1, top). To ensure accurate and precise mapping of the pre-procedurally defined targets to the intraprocedural imaging space, non-rigid registration was performed initially and in case of apparent prostate or patient motion. All data processing was carried out within the image guided therapy software platform 3D Slicer (www.slicer.org, Figure 2, bottom).

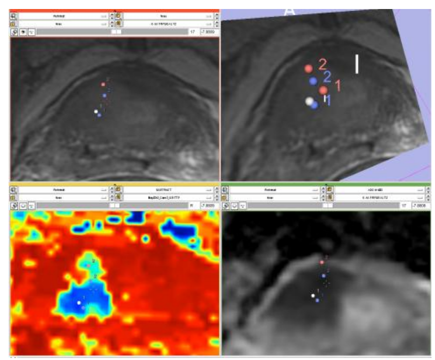

Fig 2: Multireader workflow for prostate MRIs and definition of biopsy plan

Results: All procedures were performed under conscious sedation, using a transperineal approach. They were all successful and without severe adverse effects to the patient, pain during the procedures was rated 0.8 ± 0.6 on a 10 point pain scale and 0.1 ± 0.3 post-procedurally. Sixty-six of the specimens were positive for malignant tissue (35.5%), resulting in prostate cancer diagnoses for 55% (n=27) of the patients. The mean procedure time was 72.6 ± 21 min, with a final needle placement time of 19.8 ± 8.4 min. On average 4.5 ± 2.6 control scans were performed per target.

Conclusions: The proposed workflow is a successful multi-disciplinary effort which has established this in-bore transperineal MR-guided prostate biopsies in a multiparametric, multireader setting applying current diffusion weighted and dynamic contrast enhanced imaging. MR or MR/TRUS guided biopsies are rapidly becoming a common approach to this clinical problem. The protocol is safe and yields a high number of positive histological confirmations in a study population of patients with no successful previous confirmation of prostate cancer.

Acknowledgements: This project was supported by the National Cancer Institute, the National Center for Research Resources and the National Institute of Biomedical Imaging and Bioengineering of the National Institutes of Health through Grant Numbers 1R01CA111288, R01CA124377, 5R01CA138586, 5P01CA067165, P41EB015898, P41RR019703, and U01CA151261; TP receives funding from RWTH Aachen University Hospital.

Preliminary Experience with a Software System to Enable MR-Guided Adaptive Brachytherapy of the Pelvis

Cormack RA[1], Burdette C[2], Neubauer P[2], Hefter T[2],Hata N[3], Song S[3], Tokuda J[3], Nguyen PL[1], Tempany CM[3]
[1]Department of Radiation Oncology, Dana-Farber Cancer Institute and Brigham and Women's Hospital,
[2]Acoustic Medsystems Inc., [3]Department of Radiology, Brigham and Women's Hospital

Purpose: Imaging is widely recognized as essential to the planning, placement and evaluation of interstitial brachytherapy, and MR is the modality of choice to visualize pelvic anatomy. While MR is increasingly used for dosimetric evaluation of prostate and gynecologic brachytherapy, real-time MR guidance of the implant process is not generally available, in part, due to the physical constraints of current 3T magnet designs. Robotic systems are under development to facilitate insertion of trans-perineal interstitial needles and improve implant quality. We report on initial experience with an integrated system for MR image guidance, adaptive brachytherapy treatment planning and robotic needle placement.

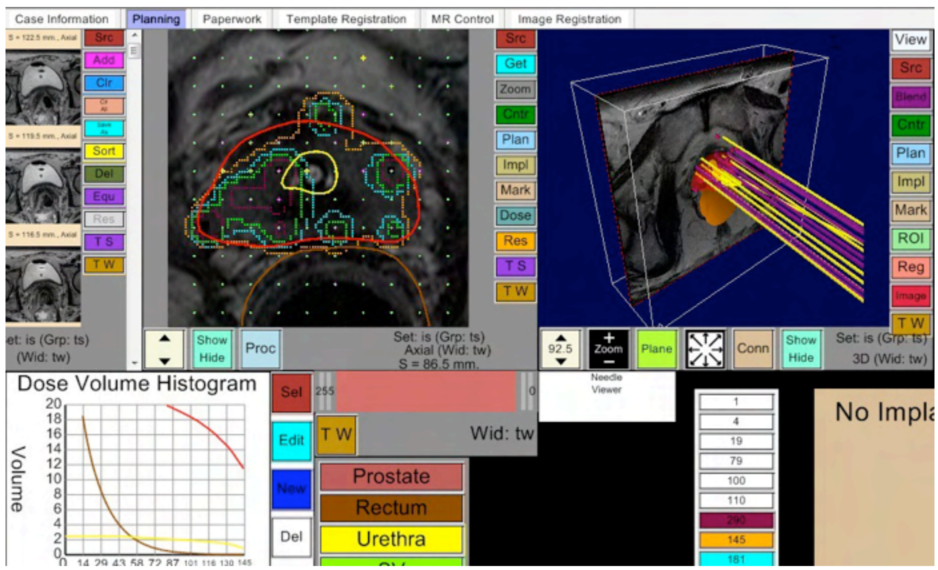

Methods: A collaboration brought together expertise in imaging, brachytherapy, robot design and software development. Brigham and Women's Hospital has active programs in image guided needle placement and brachytherapy of the prostate and cervix in an image guided operative suite with a closed bore 3T MR scanner. John Hopkins and Worcester Polytechnic Institute are developing an MR compatible robotic system for positioning and insertion of interstitial needles. Acoustic Medsystems, Inc. has developed a brachytherapy treatment planning system (Radvision) incorporating MR image guidance and robot control.

Results: The RadVision software provides image guidance and treatment planning functionality appropriate for intraoperative MR brachytherapy procedures. The software uses the OpenIGTLink protocol for communication with both an interventional MR and an MR compatible brachytherapy robot. The software provides a framework for registration of needle guidance templates or robot mechanisms to the MR imaging space. In addition to image based brachytherapy dose calculation, incorporation of real-time imaging of needle placement enables adaptive dose treatment planning allow dosimetric feedback to guide the implant opposed simple geometric feedback. Dose calculation is supported for both high dose rate and permanent implant brachytherapy. These features enable efficient implantation of prostate or cervix in an MR environment.

Conclusions: The Radvision software is an enabling technology for MR guided brachytherapy procedures. While developed for initial use with 125I and 103Pd prostate implants, it also supports treatment of the cervix and can be generalized to other sites. Future efforts will include clinical deployment and evaluation for both manual and robotic brachytherapy.

Support: NCI RO1 CA 111288, P41 EB 015898

Towards Open Source Infrastructure for Joint MRI/TRUS Guided Prostate Interventions

A. Fedorov[1], A. Lasso[2], M. Moradi[3], E. Neubauer Sugar[1], S.-E. Song[1], R. Owen[4], T. Kapur[1], W.M. Wells[1], P. Nguyen[1], G. Fichtinger[2], C. Tempany[1]
[1]Brigham and Women's Hospital, Boston, MA [2]Queens University, Kingston, ON
[3]University of British Columbia, Vancouver, BC [4]BK Medical, Peabody, MA

Purpose Transrectal Ultrasound (TRUS) and Magnetic Resonance Imaging (MRI) are complementary imaging modalities in visualizing anatomy of the prostate and characterizing the tissue for cancer presence. Our goal is to develop a free open-source infrastructure to facilitate image acquisition, visualization, analysis, and joint guidance for prostate interventions using these two modalities. Towards this goal, our initial step was to establish the feasibility and technical setup for research data acquisition of TRUS and TRUS/MRI registration.

Methods *Clinical Setup* TRUS image acquisition was performed during brachytherapy prostate volume studies. Per standard clinical setup, TRUS probe (BK 8848) was attached to a motorized mover (Nucletron EndoCavity Rotational Mover (ECRM)) and mounted on a stepper (Nucletron OncoSelect). Imaging was performed using the sagittal array of the probe rotated by ECRM. *Research setup* Camera link and OEM research interfaces of the BK ProFocus US scanner (BK Medical) were used to collect radiofrequency (RF) TRUS concurrently with the clinical image acquisition. Spatial sensor (Phidget Spatial) was attached to the handle of the probe to track sagittal array orientation during motorized sweep. Synchronous collection of the RF and tracking data was performed using Public Library for UltraSound research (PLUS)[1] on a workstation equipped with a camera link interface (Dalsa X64 CL Express). *Post-processing* We used PLUS for brightness and scan conversion, and 3D reconstruction from the tracked data. Reconstructed volumes were aligned with the T2-weighted MRI images, and the prostate gland was contoured in both volumes using 3D Slicer (http://slicer.org). Distance transform was applied to the gland contours. The distance maps were registered non-rigidly using BRAINS module of 3D Slicer. The resulting transforms were applied to the MRI dataset.

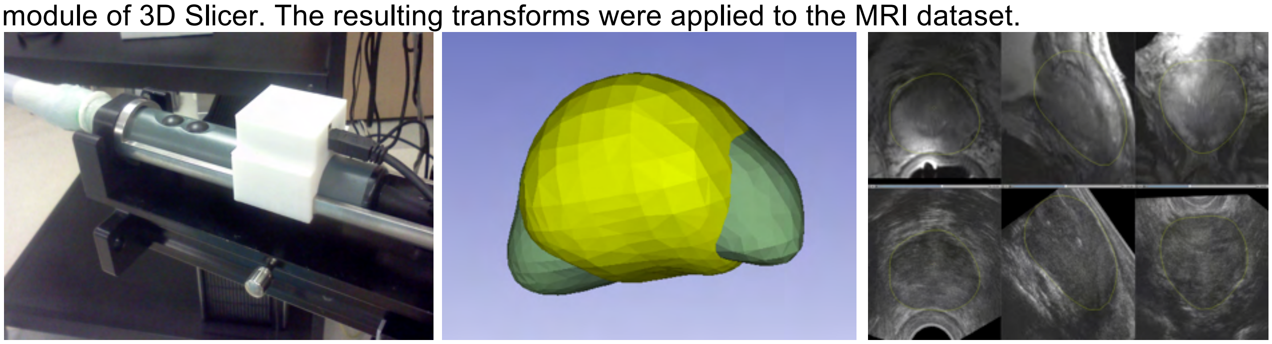

Fig. 1: Left: transrectal probe setup with the tracking device attached. Middle: Rendering of the prostate gland surfaces recovered from MRI (green) and reconstructed TRUS (yellow) after rigid alignment. Right: Reformats of the T2w MRI and 3D TRUS after non-rigid registration.

Results The described approach was applied in an cohort of clinical patients (n=10). Our setup was compatible with the clinical workflow and did not introduce delays or complications during the procedure. Based on the initial analysis (n=2), deformable registration was feasible and qualitative assessment deemed the results satisfactory.

Conclusions We demonstrated the feasibility of tracked acquisition of TRUS RF data during conventional prostate volume study procedures, and established the post-processing workflow for joint visualization of TRUS and MR imaging data. Our approach requires availability of US research interface, but otherwise relies on publicly available software and tracking components.

Acknowledgments Partial support by U.S. NIH CA111288 and Cancer Care Ontario, Canada.

---

[1] *Public Library for UltraSound research (PLUS):* http://www.plustoolkit.org/

Development of a Passive Master-Slave System for MRI-Guided Interventions

Santhi Elayaperumal[1], Mark Cutkosky[1], Bruce Daniel[2]

[1]Department of Mechanical Engineering and [2]Department of Radiology, Stanford University

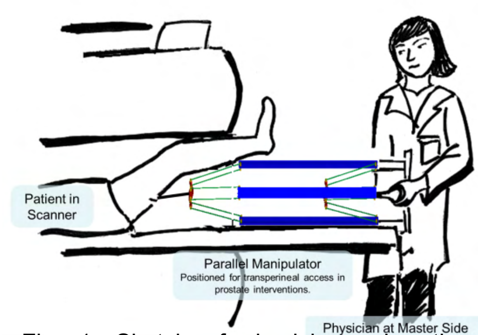

Fig. 1. Sketch of physician using the passive master-slave system to manipulate a biopsy needle for an MR-guided biopsy in the prostate.

Purpose: To design a passive master-slave mechanism allowing a physician standing just outside the bore of an MRI scanner to intuitively manipulate an interventional tool, such as a biopsy needle, inside the bore (Fig. 1). The primary intended applications are for transperineal MR-guided prostate biopsy, brachytherapy and cryotherapy. The manipulator will be used in conjunction with an interactive imaging system, which relays real-time information about instrumented tools, such as their 3D shape and interaction forces. The system provides physicians access to the patient, even in close-bore MRI machines, and could be integrated with advanced systems[3]. **Methods:** The original concept uses a double Delta mechanism with two platforms supported by six legs, coupled via prismatic sliders. To match the geometry of an MRI scanner, the mechanism was modified to take an "upside-down" isosceles form. To evaluate the optimal design, kinematic and quasistatic force analysis was performed. Several prototypes were built and tested in MRI scanners to evaluate its workspace. Additional work focused on the design and testing of a sensing system with MR tracking using fiducial markers embedded in the slave platform of the manipulator to provide position and orientation information of interventional tools. Future work will enable counter-balancing and braking. **Results:** The manipulator workspace was evaluated by employing modified dexterity and isotropy measures[4,5]. The measure of isotropy on various designs showed that isotropy is improved in the isosceles design (Fig. 3), in lieu of a traditional equilateral Delta mechanism. Modeling of the input to output force transmission ratio showed that when there is even a small amount of friction in the sliders, there is a significant loss of forces at the slave platform. Hence, friction was minimized in the prismatic joints by the use of roller bearings. **Conclusions:** We successfully analyzed and built a passive manipulator for MR-guided transperineal interventions. Because the mechanism does not use powered actuators or electronic components, it is low-cost and provides less safety and regulatory concerns.

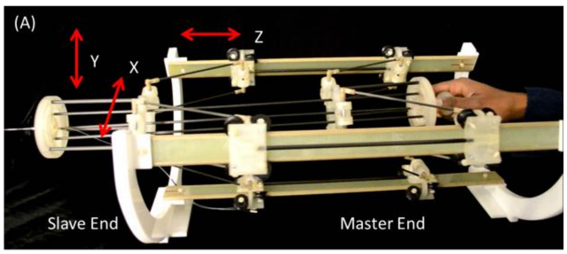

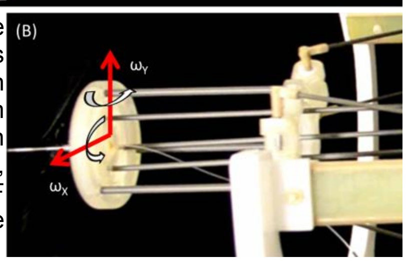

Fig. 2. The mechanism has (A) 3DOF in translation from the Delta with prismatic joints, and (B) 2DOF in rotation due to the gimbal.

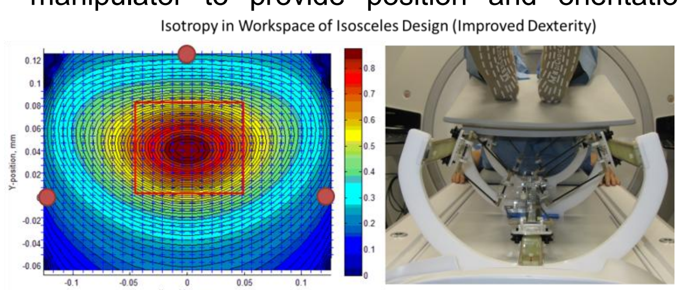

Fig. 3. Isotropy in the XY workspace improved with longer struts, a larger platform, and inner angles of 45°-45°-90°. The small circles represent slider locations, and the red square indicates the regional workspace of interest (±4 cm from the centroid formed by the sliders as vertices). Reachable workspace expands ±10 cm from the centroid.

[3]J. Tokuda et al, DOI: 10.1016/j.compmedimag.2009.07.004
[4]J.-O. Kim and P. Khosla, DOI: 10.1109/IROS.1991.174572
[5]J. P. Merlet, DOI: 10.1115/1.2121740

Acknowledgements: This work was made possible by grants from the National Institutes of Health (NIH P01 CA159992 "Magnetic Resonance Imaging Guided Cancer Interventions") and Intuitive Surgical (Sunnyvale, CA).

Evaluation of force, torque, and range of motion exhibited during abdominal ultrasound exam of phantom and human subjects to set requirements for robot-assisted ultrasound

Jim Goldie [1], Kristen LeRoy [1], Brendan LaBrecque [1], Kevin Cleary[2], Katherine P. Davenport [2], Emmanuel Wilson [2], Daniel Swerdlow [3]

[1] Vivonics, Inc, Waltham Massachusetts, USA, [2] Sheikh Zayed Institute for Pediatric Surgical Innovation, Children's National Medical Center, Washington DC, USA, [3] Department of Radiology, Georgetown University Hospital, Washington DC, USA

Purpose: The purpose of this research was to ascertain the range of applied forces, torques, and range of motion by the sonographer during typical US exams. This data was used to determine system requirements for a robotically-assisted, teleoperable ultrasound system consisting of a high bandwidth parallel mechanism and a lower bandwidth serial arm. Robotic-assisted ultrasound can both (1) empower the nonspecialist to administer an ultrasound exam while treating the trauma patient and, more generally, (2) eliminate the ultrasound practitioner from having to manually perform cumbersome movements and/or deliver large, potentially self-injurious forces/torques to the patient during an ultrasound scan.

Methods: This study utilized a simulated right upper quadrant (RUQ) portion of the Focused Abdominal Sonography in Trauma (FAST) exam. To measure the forces and torques applied during the scan, a commercial force/torque sensor was used (Mini45, ATI Industrial Automation, Apex, NC). In order to enable the operator to manipulate the ultrasound probe (Terason Ultrasound System 128 with a 4C2 curvilinear probe, Teratech Corp, Burlington, MA) while the forces and torques applied were being measured, a custom-designed grip was designed and built. An optical tracking system with passive markers (Vicra, Northern Digital Inc., Waterloo, Canada) was used to track the position of the US probe assembly. The Paracentesis phantom from Blue Phantom (Redmond, WA) was used for the phantom study.

Results: For the phantom study, each of three operators performed a FAST examination, repeated three times. The average of the maximum forces recorded over all three operators (and three trials each) was 36.7 N (range 21.9–54.4 N). The average maximum torque applied was 1.33 N-m (range 0.53-1.92 N-m) about an axis contained in the interface plane of the force/torque sensor. The range of motion (ROM) for the exam was measured: the average X ROM was 929.7 mm (range 900-949), average Y ROM was 508.7 mm (range 375-667), and average Z ROM was 410.3 mm (range 397-434).

For the human study, ten subjects participated, ranging in age from 17 to 57, with an average BMI of 23.8 kg/m^2 (range 20.4-31.1). The average maximum force applied at the time of optimal hepatorenal interface localization was 26.4 N (range 14.6-34.9 N). The average maximum torque applied at this time was 1.36 N-m (range 0.78-2.06 N-m). The range of motion (ROM) for the entire RUQ exam was measured: the average X ROM was 399 mm (range 285-520), average Y ROM was 328.2 mm (range 205-422), and average Z ROM was 262.9 mm (range 210-324). There appears to be no clear relationship between a subject's BMI and the force, torque, or range of motion required to obtain a high quality US image.

Conclusions: Evaluation of the US force, torque, and motion tracking proved feasibility of this measurement accessory and supplied ranges of 'normal' values exhibited during a standard RUQ FAST exam of human subjects. Knowing the requisite force, torque, and ROM to perform an acceptable exam, we were able to estimate the output torque requirements for the motors that drive the parallel mechanism, and determine the ROM specifications for the serial robot arm.

Acknowledgements: Funding for the measurements taken with phantoms was provided by the US Army TATRC/USAMRAA under Contract #W81XWH-10-C-0190, entitled Actively Compliant Parallel End-Effector Mechanism for Medical Interventions, on which Vivonics is the prime. Funding for the human study was internally provided by Children's National Medical Center.

Integrated and teleoperated system for wireless Robotic Natural Orifice Transluminal Endoscopic Surgery (R-NOTES)

Azizi Koutenaei B.[1,2], Kojcev R.[3], Wilson E.[2], Gary K.A.[4], Navab N. [1], Cleary K. [2]

[1]*TU Munich, Computer Aided Medical Procedures (CAMP), Munich, Germany* [2]*Children's National Medical Center, The Sheikh Zayed Institute for Pediatric Surgical Innovation, Washington, DC* [3] *University of Bern, Institute for Surgical technologies and Biomechanics, Bern, Switzerland* [4]*Arizona State University, Department of Engineering, Mesa, AZ*

Purpose. To reduce the number of incisions, new techniques such as single port surgery and Natural Orifice Transluminal Endoscopic Surgery (NOTES) have been proposed. In this work, the system architecture for a novel Robotic NOTES (R-NOTES) concept is described. As a step towards implementation, a small circular printed circuit board for motor control and wireless communication based on the ZigBee protocol was developed. This board was incorporated in a three Degree Of Freedom (DOF) robotic module called the MicroBot. The prototype system was tested in a swine animal study.

Methods. Wireless robot control seems to be a natural mode for NOTES applications as this could eliminate the need for communication wires. A proposed solution for an integrated and teleoperated R-NOTES is presented in Fig 1. This system consists of two robotic components: a gross positioning robot, the KUKA lightweight 7 DOF robot, and the other component is the small MicroBot we are prototyping. There are two human computer interaction devices in our implementation, a SpaceNavigator mouse and a Phantom Omni haptic device. The gross positioning component consists of the KUKA robot and the Magnetic Anchoring and Guidance System (MAGS) to hold the MicroBot. The first prototype of the MicroBot has 2 rotational DOF, and a gripper as an end effector as shown in Fig 2a. The MicroBot communicates wirelessly over ZigBee to the Master Control Station (MCS). The MCS should also monitor the status of hardware components and provides error handling actions (Fig. 2b).

Results. A non-survivable swine animal study was conducted under an approved protocol at Children's National Medical Center to test various components of the R-NOTES and MAGS. By watching the laparoscopic video camera, it could be observed that the MicroBot inside the body mimicked the movement of the external MAGS coupling as shown in Fig. 2c. The last part of the study was to test the capability of using the Zigbee protocol to wirelessly control the MicroBot. For this test the gripper module was inserted into the abdomen through the hand port. The SpaceNavigator on the MCS was able to open and close the gripper jaws using the Zigbee link, and some sample pieces of tissue were grasped.

Conclusions. This paper described our concept for teleoperated and integrated R-NOTES, including an overall architecture, system concept, and the result of our initial animal feasibility study. Though the initial test has been done, extensive evaluation of the algorithm is still needed, along with user evaluation studies. However, we hope that this system and concepts presented here can be one step closer toward enabling R-NOTES procedures in the future.

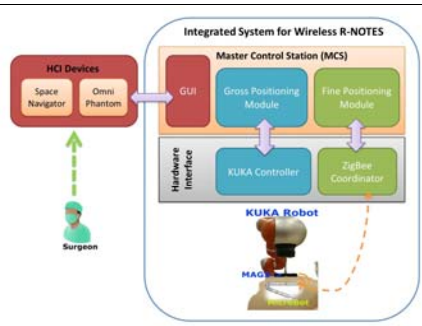

Fig 1. Proposed solution for an integrated and teleoperated R-NOTES.

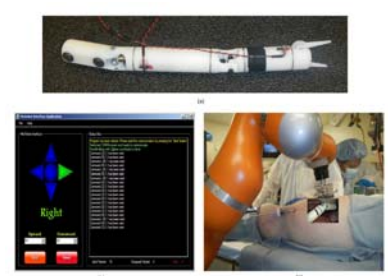

Fig. 2 Miniaturized MicroBot with two rotational DOF and one gripper (a). Screenshot of Master Control Station (MCS) application (b). Swine animal study of wireless R-Notes (c).

NEW DEVELOPMENTS IN ROBOTIC NAVIGATION AND GUIDANCE FOR IMAGE-GUIDED INTERVENTIONS

Yilun Koethe[1,2], Sheng Xu[1], Gnanasekar Velusamy[3], Bradford J. Wood[1], Aradhana M. Venkatesan[1]
[1]National Institutes of Health, Center for Interventional Oncology, Bethesda, MD, USA [2]Duke University School of Medicine, Durham, NC [3]Perfint Healthcare Pvt. Ltd, Chennai, India

Purpose: Robotic needle guidance has the potential to reduce inter-operator variability and procedure time, with the potential to not only simplify complex spatial relationships for the interventional radiologist, but potentially improve lesion targeting & patient care. A review of this technology is presented, including recent results concerning set-up of a novel robotic navigation platform. The impact of these results is discussed, with an emphasis on their impact on healthcare outcomes and ease of integration into standard clinical workflow.

Methods: A mobile interventional radiology (IR) assistance platform is highlighted (MAXIO, Perfint, Chennai, India). This platform has not been previously evaluated in the United States. The system includes an electromechanical robotic guide arm that provides 180-degrees range of motion with five degrees of freedom, a computer console for receiving CT images and calculating coordinates, and an interface for data communication between the guide arm and computer console. After the physician operator selects skin entry and target points, the apparatus positions itself over the patient and aligns its needle guide accordingly. The needle is subsequently inserted via the guide by the operating physician.

Results: The IR assistance platform successfully obtained DICOM formatted images from the host CT, accurately depicted the CT table position, executed needle trajectory planning, and moved its robotic guide arm, accounting for planned needle angles and depth, thus permitting operator single-pass needle insertion.

Conclusions: Percutaneous needle placement with use of a novel robotic interventional radiology assistance platform is feasible, readily integrated into standard workflow without the need for registration with each use, and does not require needle modifications. Additional prospective randomized phantom and clinical studies in the future are anticipated to further define the specific benefits of this technology, in terms of impact on needle tip accuracy, mean needle repositionings, verification scans and procedure time.

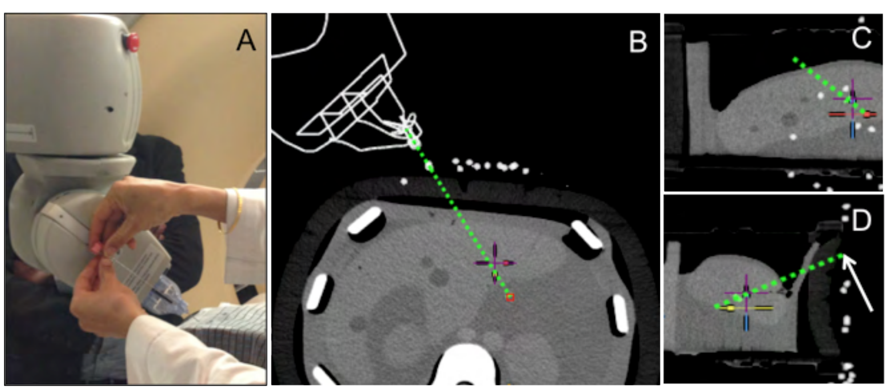

Figure 1. Physician inserts the needle through needle guide at the end effector of the robotic arm (1A). Graphical user interface of IR assistance platform provides multiplanar display of planned needle trajectory (1B-D). The point target is delineated by a red square on axial CT (1B). Skin-entry point (solid arrow), though out of plane in the axial (1B) and coronal view (1C), is delineated in the sagittal plane (white arrow) (1D).

Preliminary Observations on MRI-guided Targeted Prostate Biopsy using a Smart Template

Sang-Eun Song, Kemal Tuncali, Junichi Tokuda, Andriy Fedorov, Tobias Penzkofer, Clare Tempany, Nobuhiko Hata

National Center for Image-Guided Therapy, Department of Radiology, Brigham and Women's Hospital, Harvard Medical School, Boston, MA 02115, USA

Purpose In order to overcome the constraints of limited needle insertion accuracy and human communication error in the use of a conventional needle guidance template in MRI-guided prostate interventions, we developed a motorized MRI-compatible needle guidance template (Smart Template) that allows automated needle guidance without position restriction in a 3-Tesla MRI scanner.

Methods We are conducting engineering evaluation studies to ensure the safety and functionality of Smart Template [1]. To implement Smart Template in clinic, we performed a number of full-staff dry-runs to establish the safety and procedural workflow. Subsequently, Smart Template has been deployed in clinical practice for preliminary assessments in an image guided intervention suite (AMIGO) at BWH.

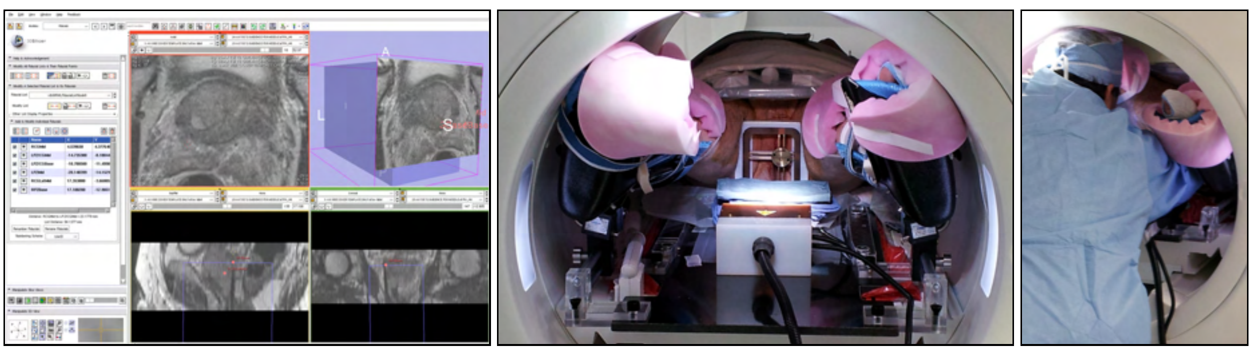

Fig. (from left) a screenshot of the planning software, 3D Slicer ProstateNav module, a scanner rear view of the intervention setup at imaging position showing a typical access space, and a view of clinician's needle insertion.

Results Early observations include: 1) Smart Template is very acceptable and integrates easily into the procedural workflow of the existing MRI-guided prostate biopsy procedure, 2) detachable sterile parts i.e. needle guide and perineum-contacting covers allow quick and easy setup and resterilization, and 3) unrestricted needle positioning can help clinician's expectation of reaching any location within the prostate.

Conclusions Smart Template has been clinically deployed in patient trials in preliminary clinical feasibility study. As designed, human error in target information communication between navigation software and in-bore insertion site has been eliminated. Early clinical trials demonstrate that the use of Smart Template's automated and unrestricted needle guidance can provide greater utility than the use of a conventional template and may improve the efficacy of MRI-guided targeted prostate biopsy.

[1] Song S, Tokuda J, Tuncali K, Tempany CM, Zhang E, Hata N. Development and Preliminary Evaluation of a Motorized Needle Guide Template for MRI-guided Targeted Prostate Biopsy. IEEE Trans Biomed Eng. 2013. DOI: 10.1109/TBME.2013.2240301 - In Process

This project was supported by the National Cancer Institute, the National Center for Research Resources and the National Institute of Biomedical Imaging and Bioengineering of the National Institutes of Health through Grant Numbers 1R01CA111288, R01CA124377, 5R01CA138586, 5P01CA067165, P41EB015898 and P41RR019703; New Energy and Industrial Technology Development Organization Grant; Center for Integration of Medicine and Innovative Technology Grant 11-325; RWTH Aachen University Hospital.

Smart Tissue Anastomosis Robot (STAR)

Simon Léonard, Yonjae Kim, Carolyn Cochenour, Kyle Wu, Peter Kim and Axel Krieger
Sheikh Zayed Institute for Pediatric Surgical Innovation, Children´s National Medical Center

Introduction Although teleoperated robots improve the ergonomics and increase the dexterity of surgeons, there is no clear evidence that such systems reduce operative time and intraoperative complications. We address these challenges for the specific task laparoscopic suturing by developing a supervisory control system for robotic assisted surgeries. Our main contributions are two folds. First, we develop an actuated laparoscopic suturing tool that is mounted on a robot manipulator. Second, we propose a vision-guided system that enables a surgeon to specify the placements of sutures by clicking on intraoperative images. The selected placements determine where the robot ties a knot and executes a running suture. Our results demonstrate that STAR can execute a planar suturing task on a training pad faster and with greater consistency than experienced surgeons executing the same task with state of the art master-slave surgical robots.

Methods The STAR hardware is composed of a Kuka LWR (Kuka, Germany), an actuated laparoscopic suturing tool and a camera. We modified an Endo360° (EndoEvolution, MA) laparoscopic suturing tool with two actuators: one motor (Maxon, Switzerland) for actuating the circular needle and the other for actuating the pitch axis. The STAR software is composed of a graphical user interface (GUI), visual tracking, trajectory generation with a virtual remote center of motion and force control. The GUI enables the surgeon to select the suture placements by clicking on the intraoperative images. These image coordinates are tracked and transformed into the coordinate system of the robot by the computer vision system. At the first placement, the robot executes a knot tying routine followed by visiting the subsequent positions. Initially, the system pulls a sufficient length of thread based on the estimated measured distances between the sutures. After each suture, the robot adjusts the tension in the thread by pulling until it measures a sufficient force. We compared the performance of STAR (n=6) to the performances of standard 5mm laparoscopic (n=4), manual Endo360° (n=4), and robot-assisted suturing (n=4; DaVinci, Intuitive Surgical, CA). Experienced surgeons were asked to perform suturing procedures involving one knot followed by 9 stitches on 3D phantoms (3-DMed, OH). After the fourth suture, the phantom was rotated by 45° during which the desired placements were tracked by STAR. Speed, consistency, and quality of the stitches were measured based on the duration of execution (minutes), variations in suture spacing (mm), depth (mm) and displacement (mm) under 0.2 Newton normal force. Statistical analysis was performed using MannWhitneyWilcoxon Test (SigmaStat 3.5).

Results and Conclusions Results are reported in Table 1. In conclusion, we present a novel supervised control robotic system for laparoscopic suturing. Our system embraces the broad claim that a surgeon knows "what" to do and a robotic system with a specialized knows "how" to do it. This claim was supported by our experiments where STAR was faster and more consistent to execute a planar suturing task than experienced surgeon using current state of the art technologies.

The authors would like to thank Craig Peters MD, Aaron Martin MD, Kelly Swords MD, and Amy Burns MD for their participation.

Table 1: Performance of STAR.

	Duration (p value)	Spacing	Depth	Displacement (p value)
STAR	1.03 ± 0.01	0.85	0.70	0.42 ± 1.09
DaVinci	5.71 ± 3.77 ($p = 0.01$)	1.24	1.10	1.08 ± 1.26 ($p < 0.01$)
Laparoscopic	9.34 ± 4.31 ($p = 0.01$)	1.55	1.09	1.56 ± 2.12 ($p < 0.01$)
Endo360°	4.79 ± 1.29 ($p = 0.01$)	1.55	1.38	1.22 ± 1.84 ($p < 0.01$)

Interactive Initialization for 2D/3D Intra-Operative Registration using the Microsoft Kinect

Ren Hui Gong, Özgür Güler, Ziv Yaniv

Sheikh Zayed Institute for Pediatric Surgical Innovation, Children's National Medical Center, Washington, DC

Purpose: All anatomy-based 2D/3D rigid registration, X-ray/CT or X-ray/MR, algorithms are iterative, requiring an initial estimate of the 3D image pose. Current initialization methods have limited applicability in the OR setting, due to the constraints imposed by this environment or due to insufficient accuracy. In this work, we use the Microsoft Kinect device to allow the surgeon to interactively initialize the registration using gestures, avoiding the need for physical contact with an input device.

Methods: To perform initialization, the X-ray images and 3D image are loaded into our program and displayed. The X-ray images are used as references to guide the initialization process. The user selects a specific X-ray and the 3D image is rendered using the known parameters of this X-ray acquisition. The user iteratively modifies the current 3D image pose so that it becomes visually similar to the reference X-ray. This process is repeated for all X-rays until all rendered images are similar to the corresponding X-rays. To obtain the initial 3D image pose we align the center of the 3D image with the point defined by the average intersection of the principal rays of all X-ray cameras. Interaction with our program is done using the Kinect, both to initiate actions via gestures and to modify the 3D image pose via arm motions. We use gestures for selecting a reference X-ray image, switching manipulation mode between rotation and translation, and selection of the rotation axis. Modifying the translation and rotation of the 3D image is done by tracking hand motions. To obtain intuitive visual feedback in response to user interaction, pose modification of the 3D image is indirectly achieved by moving the camera.

Results: Our method was evaluated using three publically available reference data sets for 2D/3D registration. We performed manual initialization using two interaction modes, our gesture-based approach and the conventional mouse-based approach. We analyzed the performance of both approaches in X-ray/CT and X-ray/MR registration. Experiments showed that, with initial target registration errors of 117.7±28.9mm, a user was able to achieve final errors of 5.9±2.6mm within 158± 65 sec using our gesture-based approach, compared to 4.8± 2.0mm and 88± 60sec when using the mouse for interaction.

Conclusions: We conclude that initialization using our gesture-based interaction results is sufficiently accurate for initialization of X-ray/CT and X-ray/MR registrations in the OR. The initialization error and time depend both on user's experience with our tool and user's spatial perception of the anatomy. For users that have no prior experience using the Kinect, half an hour of training is sufficient to master the gesture-based interaction method.

Dynamic Tracking with Electromagnetic Systems Using Particle Filters

H.Tutkun Şen, Peter Kazanzides

Johns Hopkins University, Baltimore, MD/USA

Purpose: Tracking systems play a crucial role in mapping actual patient anatomical information to preoperative and/or intraoperative images for many computer assisted interventions. This study presents a particle filter to improve the dynamic tracking performance of a coil array electromagnetic tracking (EMT) system, even when transmit coils are driven sequentially and/or receive coils are not sampled simultaneously. Experiments are performed on a custom EMT system, Fig.1, consisting of a transmitter coil array and one or more receiving coils, to demonstrate the dynamic tracking performance at different velocities.

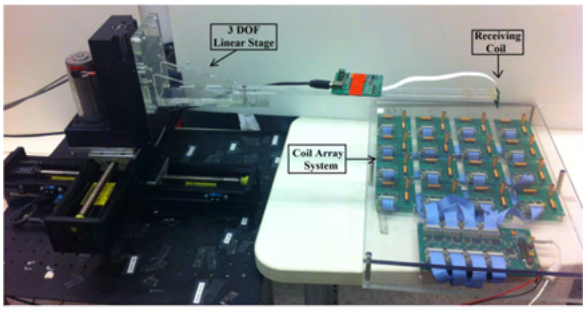

Fig. 1 System Setup

Methods: For low-cost systems that acquire data sequentially, rather than simultaneously, recursive filters, such as particle filters (PF), are good candidates to achieve convergence. Recursive filters have a prediction stage and an update stage. In this study, we used a constant velocity model for the prediction stage. For the update stage (the measurement stage), we used a dipole field approximation to describe the near field seen by the receiving coil. To eliminate field distortions due to nearby metal objects, we attached the receiving coil to the tip of a Plexiglass beam. In the experiments, we moved the linear stage at various velocities on a single axis, while measuring the receiving coil voltage and estimating its position and orientation.

Results: The PF position and velocity estimates can be seen in Fig. 2. In Fig.3, the 3D position error at various velocities is shown. (Error is defined as the minimum distance between a calculated point and the ground truth line after converging to the linear path.)

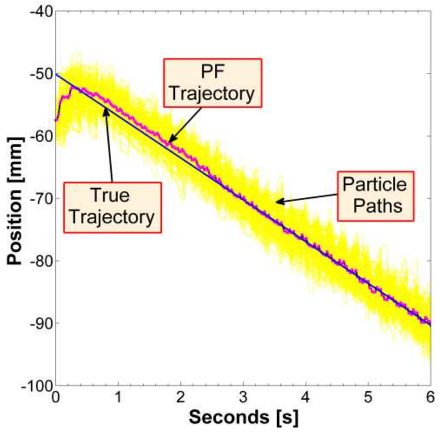

Fig. 2 X Axis Position vs. Time at V=9.9 mm/s

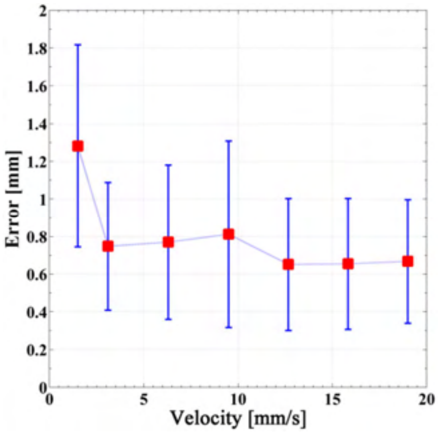

Fig. 3 Mean Position Error vs. Velocity

Conclusions: The contribution of this paper is to show that a particle filter can provide dynamic tracking accuracy that is equivalent to the static tracking accuracy, even for simple, low-cost tracking systems that cannot provide synchronized measurements. The results (Figs. 2-3) show that the dynamic tracking accuracy appears to be nearly independent of the velocity. The overall accuracy of our EMT, under best case conditions, is on the order of 0.8 - 1 mm.

Prototyping image-guided therapy applications using the SlicerIGT platform

Tamas Ungi[1], Junichi Tokuda[2], Adam Rankin[1], Andras Lasso[1], Gabor Fichtinger[1]
[1]*Laboratory for Percutaneous Surgery, Queen's University, Kingston, ON, Canada*
[2]*Surgical Planning Laboratory, Brigham and Women's Hospital, Boston, MA*

Purpose: Interventional navigation systems require high quality and reusable software for rapid incremental development. Development of such software demands significant expertise from research teams. Our goal was to provide an open-source, configurable software toolkit.

Methods: The SlicerIGT software platform is based on the PLUS library [1] and the 3D Slicer application framework (www.slicer.org). SlicerIGT provides all components of a typical image-guided navigation system (Figure 1). The following main functions are implemented in the SlicerIGT toolkit: (1) Calibration of tracked tools using arbitrary tracked reference coordinate system. (2) Registration and fusion of images, including tracked ultrasound. (3) Various visualization options for all components of the navigation system in 2D and 3D (Figure 2). (4) Recording of tracked tool trajectories.

Results: SlicerIGT enabled rapid prototyping of multiple translational applications for navigated interventions, including regional anaesthesia [2], musculoskeletal injections, orthopaedic surgery, and urology. SlicerIGT is accessible to users from the 3D Slicer extension manager. Most applications do not require programming. If the functionality of the SlicerIGT extension needs to be changed, the source code is available with BSD-style license that allows modifications without restrictions on use from www.slicerigt.org.

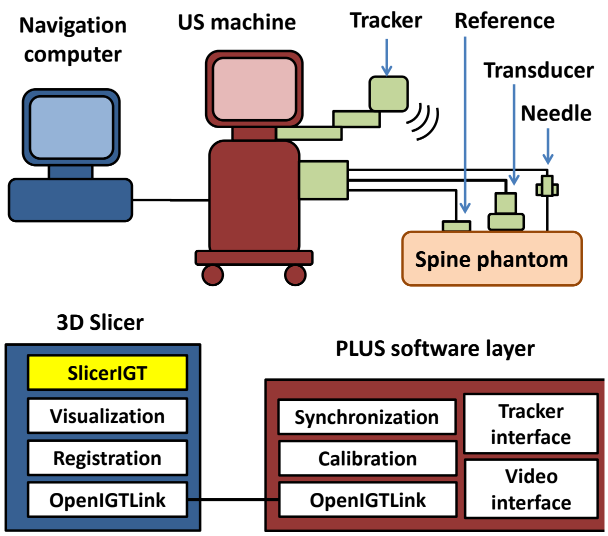

Fig. 1: Hardware and software components of a typical SlicerIGT system configuration

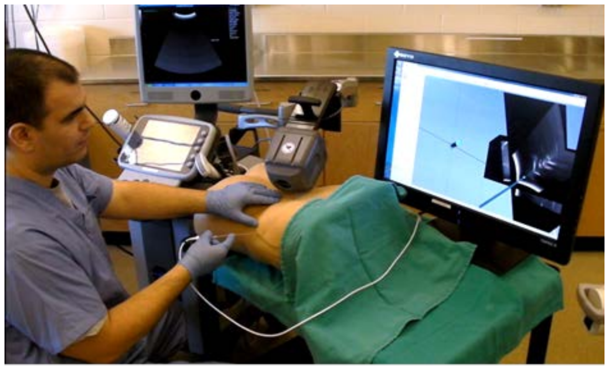

Fig. 2: Ultrasound-guided nephrostomy navigation system built from SlicerIGT platform components.

Conclusions: SlicerIGT enables rapid prototyping of translational applications for image-guided navigated interventions and can be easily adapted to new clinical scenarios and workflows.

Acknowledgements: This work was jointly funded by Cancer Care Ontario, NIH P41EB015898, R01CA111288, R01CA124377, R01CA138586, P01CA067165, and CIMIT 11-325. T. Ungi is an Ontario Ministry of Research and Innovation Postdoctoral Fellow.

References:

[1] Lasso A., et al. MIDAS Journal. 2012 Jul 16. http://hdl.handle.net/10380/3367

[2] Ungi T., et al. IEEE Trans Biomed Eng. 2012 Oct;59(10):2766-72.